

THE DETERMINATION OF PREFERRED ORIENTATION
IN ROLLED ELECTRICAL STEELS USING
SINGLE DIFFRACTION OF NEUTRONS

by
Manuel R. Eugenio

Thesis submitted to the Faculty of the Graduate School
of the University of Maryland in partial fulfillment
of the requirements for the degree of
Doctor of Philosophy
1963

C.1

APPROVAL SHEET

Title of Thesis: The Determination of Preferred Orientation
in Rolled Electrical Steels Using Single
Diffraction of Neutrons

Name of Candidate: Manuel R. Eugenio
Doctor of Philosophy, 1963

Thesis and Abstract Approved:

Dick Duffey
Dr. Dick Duffey
Professor of Nuclear
Engineering

Date Approved:

26 June 1963

2771
2 pp only

64-6341
M R Eugenio
Eng, Metal
U of Maryland

ABSTRACT

Title of Thesis: The Determination of Preferred Orientation
in Rolled Electrical Steels Using Single
Diffraction of Neutrons

Manuel R. Eugenio^{ornado}, Doctor of Philosophy, 1963

Thesis directed by: ^{Sup.} Professor Dick Duffey

Preferred orientation in rolled electrical steels has been determined using single diffraction of neutrons from the University of Maryland pool-type nuclear reactor (UMR) operating at 10 KW thermal.

X-rays are used extensively to determine preferred orientations in metallic wires and rolled sheets, but X-rays suffer the disadvantage of high absorption and cannot be used effectively on thick samples without chemical or mechanical treatment which ultimately results in the destruction of the samples. The use of reactor neutrons for this purpose is believed to offer particular advantages such as the use of thicker samples and wider beams. To this end, neutrons from the UMR were scattered directly from metallic sheet samples to obtain diffraction patterns from which preferred orientations of the crystallographic axes could be deduced.

The neutron diffraction data were obtained in the form of : 1) Maxwellian curves; and 2) rocking curves.

To obtain the first type of curve, the sample and neutron detector were rotated at a 1-to-2 angular ratio, respectively, and the diffraction pattern was essentially the Maxwellian neutron energy distribution. From the maximum of the Maxwellian curve, the crystallographic plane mainly responsible for the reflection was calculated; from this, the main orientation was deduced. For the second type of curve, the sample was rocked back and forth, with the neutron detector fixed, and the resulting pattern was used to infer the variation of a given crystallographic direction about its main orientation.

The results of this study, particularly on grain-oriented and cube-textured silicon-iron (Si-Fe) alloy sheets demonstrate that single diffraction techniques can be used to determine preferred orientation in highly oriented materials. The results on Si-Fe sheets described as non-oriented indicate the possibility that these techniques may be applicable to ordinary rolled metallic sheets which are not highly oriented.

ACKNOWLEDGEMENTS

The author wishes to thank his adviser, Dr. Dick Duffey, who suggested the investigation of preferred orientation in metals using neutron diffraction techniques and directed the ensuing thesis research.

The author also wishes to express his gratitude to Dr. Donald T. Bonney, Dr. Joseph Silverman, and Dr. A. Gomezplata for their encouragement and kind interest in this work.

Thanks are also due to: Dr. Melvin R. Meyerson of the National Bureau of Standards for suggesting the investigation of transformer sheets; Armco Steel Corp. and Westinghouse Electric Co. for supplying the materials used in this study; Mr. Chieh Ho for maintaining the operational status of the reactor and scheduling its use; Mr. Thomas McWilliams, Jr. for helping the author set up the X-ray diffraction apparatus; Mr. Arthur Loeb for machine-shop work on the goniometer; Dr. S. Lakshmanan, Mr. Richard Farman, Mr. Francisco Cheng, Mr. Gil Ugiansky, and Lieut. Paul Roberts for their kind patience in helping to obtain data; and to all those who, in one way or another, helped towards the completion of this thesis.

TABLE OF CONTENTS

| Chapter | Page |
|---|------|
| ACKNOWLEDGEMENTS | ii |
| I. INTRODUCTION | 1 |
| II. REVIEW OF THE LITERATURE | 4 |
| A. X-Ray Diffraction Methods | 4 |
| B. Neutron Diffraction | 5 |
| C. Electrical Sheets | 12 |
| III. CRYSTAL DIFFRACTION THEORY | 20 |
| A. The Laue and Bragg Equations | 20 |
| B. The Crystal Structure Factor | 23 |
| C. The Effect of Crystal Reflectivity on Neutron Diffraction Intensities | 29 |
| IV. EXPERIMENTAL APPARATUS | 35 |
| A. Nuclear Reactor | 35 |
| B. Neutron Beam Collimator | 36 |
| C. Goniometer | 37 |
| D. Nuclear Instrumentation | 39 |
| E. X-Ray Spectrometer | 39 |
| V. PROCEDURES AND MATERIALS | 41 |
| A. Data Taken | 41 |
| B. Materials Investigated | 44 |
| VI. EXPERIMENTAL RESULTS | 47 |
| A. Sodium Chloride (NaCl) Single Crystal | 47 |

| Chapter | Page |
|---|------|
| B. Grain-Oriented Silicon-Iron Electrical Sheets | 50 |
| 1. M-5 Reflection Diffraction Curves | 50 |
| 2. M-5 Transmission Diffraction Curves | 54 |
| 3. M-6 Curves | 55 |
| 4. Oriented Thin Steel (OTS) Curves | 56 |
| C. Cube-Textured Silicon-Iron Electrical Sheets | 57 |
| D. Non-Oriented Electrical Sheets | 58 |
| E. Nickel-Iron (Ni-Fe) Alloys, 48% Ni | 59 |
| VII. SUMMARY AND CONCLUSIONS | 61 |
| A. Advantages of Neutron Diffraction over X-Ray Diffraction | 61 |
| B. Advantages and Disadvantages of Single Diffraction | 62 |
| C. Sodium Chloride (NaCl) Single Crystal | 62 |
| D. Preferred Orientation in Grain-Oriented Materials | 63 |
| E. Non-Oriented Materials | 63 |
| F. General Conclusions | 64 |
| G. Recommendations | 65 |
| H. Proposed Future Studies | 65 |
| APPENDIX A - PHOTOGRAPHS | 103 |
| APPENDIX B - PHOTOMICROGRAPHS | 107 |
| REFERENCES | 108 |

LIST OF FIGURES

| Figure | Page |
|---|------|
| 1. The "Cube-on-edge" and "cube-textured" Orientations | 68 |
| 2. One-dimensional Lattice of Scatterers | 69 |
| 3. Two-dimensional Lattice of Scatterers | 69 |
| 4. The Body-centered-cubic Unit Cell | 70 |
| 5. University of Maryland Reactor Core Arrangement | 71 |
| 6. Plan View of the Reactor Showing Positions of Beam Ports and Through Tube | 72 |
| 7. The Neutron Beam Collimator | 73 |
| 8. Sketch of the Neutron Diffractometer (Goniometer) | 74 |
| 9. Schematic Diagram of the X-Ray Spectrometer | 75 |
| 10. Diagram Showing Sample Positions | 76 |
| 11. X-Ray Diffraction Patterns of "Cube-on-edge" M-5 and "Cube-textured" Sample | 77 |
| 12. X-Ray Diffraction Patterns of ^{48}Ni and Orthonik Nickel-Iron Alloys | 78 |
| 13. NaCl Ingle Crystal Rocking Curve at $2\theta' = 60^\circ$ ($\theta = 13.5^\circ$) | 79 |
| 14. NaCl Single Crystal Maxwellian Curve | 80 |
| 15. NaCl Single Crystal Maxwellian Curve (Calculated curve based on real crystal formula) | 81 |
| 16. M-5, 4 Sheets, Cross-rolling Direction (C.R.D.) | 82 |
| 17. M-5, 4 Sheets, C.R.D. | 83 |

| Figure | Page |
|--|------|
| 18. M-5, 4 Sheets, C.R.D. | 84 |
| 19. M-5, 4 Sheets, Rolling Direction (R.D.) | 85 |
| 20. M-5, 4 Sheets, 3" x 3" Rocking Curves | 86 |
| 21. M-5, 4 Sheets, R.D. | 87 |
| 22. M-5, 1 Sheet, R.D. | 88 |
| 23. M-5, 1 & 2 Sheets, R.D. | 89 |
| 24. M-5, 1 & 8 Sheets, R.D., Transmission Diffraction | 90 |
| 25. Maxwellian Curves, M-5, 8 Sheets, Transmission Diffraction | 91 |
| 26. Maxwellian Curves, M-5, 8 Sheets, Transmission Diffraction, Corrected for Geometrical Effect | 92 |
| 27. M-6, 1 Sheet, R.D., Rocking Curve | 93 |
| 28. "Laue Curve," M-6, 1 Sheet, R.D., Reflection Diffraction | 94 |
| 29. Maxwellian Curves, OTS, 28 Sheets, Transmission Diffraction | 95 |
| 30. Maxwellian Curves, 1 Sheet OTS, Reflection Diffraction | 96 |
| 31. 16 Sheets, 6-mil Cube-Textured Silicon-Iron Reflection Diffraction | 97 |
| 32. 16 Sheets, 6-mil Cube-Textured Silicon-Iron Reflection Diffraction, Rocking Curves at $2\theta' = 19^\circ, 33^\circ, \text{ and } 50^\circ$ | 98 |
| 33. 16 Sheets, 6-mil Cube-Textured Silicon-Iron, Transmission Diffraction, Maxwellian Curves | 99 |
| 34. M-22, 1 & 5 Sheets, R.D., Reflection Diffraction | 100 |
| 35. Maxwellian Curves, M-22, 5 Sheets; M-19, 5 Sheets; Reflection Diffraction, R.D. | 101 |

Figure

Page

36. Maxwellian Curves, 48-Ni & Orthonik,
Reflection Diffraction, R.D.

102

CHAPTER I

INTRODUCTION

According to Boas¹, a material with a marked degree of preferred orientation of its constituent crystals shows the anisotropy characteristic of a single crystal of the same material. Such being the case, a highly oriented material should behave somewhat like a single crystal as far as neutron diffraction properties are concerned.

Polychromatic or "white" radiation can be diffracted from single crystals because, from among the different wavelengths present in "white" radiation, a single wavelength can generally be found which will satisfy Bragg's Law (to be discussed later) and radiation of this particular wavelength will be coherently scattered from the single crystal. Therefore, if "white" radiation is used on a material with a measurable degree of preferred orientation, the diffraction pattern should approach that of a single crystal,--the approach should be closer, the greater the degree of preferred orientation.

The diffraction of polychromatic radiation directly from a given sample is called single diffraction, to differentiate it from the method of double diffraction

(or double crystal diffraction) wherein a monochromatic beam is produced by diffraction from a single crystal monochromator and subsequently diffracted from the given sample.

Briefly stated, this thesis deals with the determination of preferred orientation in rolled electrical steel alloys by means of single diffraction with neutrons from the University of Maryland nuclear reactor (UMR), licensed for operation at 10 KW thermal.

Preferred orientation is important in electrical sheets because metal crystals are anisotropic with respect to magnetic properties, i.e., magnetic permeabilities are greater in certain crystallographic directions, such as the $[100]$ direction (Using the notation of Miller indices) in pure iron or in silicon-iron (Si-Fe) alloy, 3% silicon. Specially oriented materials such as grain-oriented Si-Fe alloys and nickel-iron (Ni-Fe) alloys are now being manufactured on a large commercial scale, and recently, the advent of cube-textured Si-Fe sheet promises further advances in the technology of transformers and similar electrical equipments.

Two ways of determining preferred orientation are:

1) The orientation of individual grains can be determined; or,

2) The average orientation of a large number of grains can be measured at once to give the statistical

distribution of the crystal axes. It is this statistical average which was measured in this investigation rather than the orientation of individual grains. This was made possible primarily because of the relatively large area covered by the neutron beam, and also because of the penetrating character of neutrons.

CHAPTER II

REVIEW OF THE LITERATURE

A. X-Ray Diffraction Methods². There are three principal methods used in X-ray diffraction studies:

1) The Laue Method, wherein a beam of polychromatic, or "white", radiation (also called general radiation) is diffracted from a single crystal, resulting in a pattern of spots which is usually recorded on a photograph;

2) The Rotating Crystal Method, wherein a monochromatic beam of X-rays is incident on a single crystal which is made to rotate, or else made to "rock" back and forth, resulting in a pattern of spots which is usually recorded on photographic film placed at a distance around the crystal target; and

3) The Debye-Scherrer Powder Method, in which a monochromatic beam of X-rays is scattered by a powdered sample giving rise to concentric rings which may also be photographed. The diffraction rings are due to the presence of crystals which are oriented at just the right angle so as to satisfy the Bragg condition for a given (h,k,l) plane; h,k,l are the Miller indices.

As an alternative to the use of photographic film, a spectrometer may be used, consisting essentially of a detector for ionizing radiation which can be rotated about the crystalline sample to show diffraction peaks where a spot or part of a ring would show correspondingly on a photograph.

B. Neutron Diffraction. In 1936, neutron diffraction was demonstrated by Mitchell and Powers³ with a Radon-beryllium (Rn-Be) source of about 600 millicurie strength⁴ and sixteen magnesia (MgO) single crystals. The source was encased in a paraffin howitzer, and thermal neutrons were reflected by the MgO crystals at a Bragg angle of 22° into an ion chamber which was boron trifluoride filled in the first run and boron carbide-lined in the second and third runs. When the crystals were tilted away by about 25° , the observed count rate was significantly lower, by about 10%.

Halpern, Hamermesh, and Johnson⁵ discuss the theory of neutron scattering from crystalline material, as well as the effects of magnetization on neutron scattering. According to them, neutron scattering may be coherent or incoherent. Coherent scattering is that wherein the wave character of the scattered radiation bears definite phase relationships with one another and hence, undergo constructive or destructive interference which results in diffraction. For incoherent scattering no such phase

relationships exist.

The results of Whitaker and Beyer^{6,7} on neutron scattering from single crystal and polycrystalline iron are also explained by Halpern, Hamermesh, and Johnson. The measured total scattering cross section from single crystal iron (Fe) is smaller than that from polycrystalline iron ($\sigma_{\text{single crystal}} = 7$ barns compared with $\sigma_{\text{polycrystal}} = 12$ barns); this is because only those neutrons of the Maxwellian distribution whose wavelengths satisfy Bragg's Law were coherently scattered from the single crystal. These form but a small fraction of the total number of neutrons; hence, most of the scattering from the single crystal is incoherent. For both single crystal and polycrystal, $\sigma = \sigma_{\text{coherent}} + \sigma_{\text{incoherent}}$, but σ_{coherent} for the single crystal is very small, while σ_{coherent} for the polycrystal is relatively large; therefore, the difference $\sigma_{\text{polycrystal}} - \sigma_{\text{single crystal}} = 5$ barns represents the coherent scattering cross-section of iron.

In a study by Nix, Beyer, and Dunning⁸ who used neutrons from a Rn-Be source in a paraffin howitzer, it was found that the difference in neutron transmission through fully annealed and quenched nickel-iron (Ni-Fe) alloys shows a broad hump at a composition of 75% Ni (corresponding to Ni_3Fe) indicating a high degree of order at this composition. Cold-working decreased the neutron

transmission, which is consistent with the interpretation that cold-working destroys ordering in the alloy.

A Radium-beryllium (Ra-Be) source (200.5 mg of radium and 8.0 mg of beryllium) was used by Nix and Clement⁹ to measure the effect of grain size on total scattering cross section by transmission. The metals studied were copper and iron, the grains of both of which were randomly oriented. It was observed that the cross section decreased with increasing grain size. This was believed due to the higher number of crystallites reflecting neutrons when the grain size is small, resulting in more coherent scattering.

In 1944, a single crystal monochromator was built by Zinn¹⁰ for use with the University of Chicago, Argonne National Laboratory heavy water reactor. The neutrons were reflected from the (100) planes of a large calcite (CaCO_3) single crystal and detected by a boron trifluoride (BF_3) proportional counter enriched in B^{10} , 5 in. in diameter and 60 cm. long at a pressure of 40 cm. Hg, with an efficiency of nearly 100%. Spectra of the thermal column beam and the direct reactor beam were obtained and compared with theoretical Maxwellian curves calculated by Goldberger and Seitz¹¹. Their equation for the integrated intensity of neutrons reflected from a thick crystal is:

$$\frac{N_R}{N_I} = \frac{\pi/a_K/}{k^2 \sin^2 \theta_B} \left(\frac{\epsilon}{k_0 T}\right)^2 e^{-\epsilon/k_0 T} \quad (1)$$

where N_R = net neutron flux per unit time reflected from the crystal;

N_I = net intensity of incident neutron beam, neutrons per second;

a_K = crystal structure factor;

k = wave number;

θ_B = Bragg angle;

ϵ = neutron energy;

k_0 = Boltzmann's constant;

T = neutron temperature.

The neutron temperature of the direct reactor beam was calculated to be $T = 400^\circ\text{K}$.

Sturm¹² used a single crystal monochromator system, similar to that of Zinn¹⁰, to measure cross sections of different materials. He assumed that his neutron detector had a $1/v$ sensitivity and used the following theoretical equation to fit the Maxwellian spectrum:

$$R_n = c/a_n/nK_1 \csc^3 \theta \exp[-\alpha_n^2 \csc^2 \theta] \quad (2)$$

where R = crystal reflectivity (reflected intensity);

n = order of reflection;

θ = glancing angle;

c = arbitrary constant;

$$K_1 = 2\pi/d_n$$

$$a_n = \sum_j f_j \exp[-2\pi i(h_1 x_j + h_2 y_j + h_3 z_j)]$$

$$\alpha_n^2 = \frac{h^2(2\pi/d_n)^2 n^2}{8mk_0 T}$$

d_n = interplanar distance;

m = mass of neutron;

σ_s^j = scatt. cross section of the j th atom in the unit cell;

k_0 = Boltzmann constant;

T = average neutron temperature;

h_1, h_2, h_3 = Miller indices;

x_j, y_j, z_j = coordinates of the j th atom in the unit cell, in multiples of the lattice constant, a_0 .

The (100) planes of a large calcium fluoride (CaF_2) crystal were used by Fermi and Marshall¹³ to monochromatize neutrons coming from the Argonne Laboratory heavy water reactor through a 1/2 in. wide by 1-1/4 in. high collimator. The monochromatic beam was used to determine the sign of the scattering amplitudes of different elements by diffracting neutrons from alternate monoatomic crystal planes, e.g., (111) planes of sodium chloride (NaCl). The scattering amplitude is related to the scattering cross section, thus¹⁴:

$$\sigma_s = 4\pi f^2$$

(3)

where σ_s = scattering cross section;

f = scattering amplitude.

Given a crystal consisting of two atoms A and B, if the sign of the scattering amplitude of A is the same as that of B, then the even orders of diffraction from alternate planes of A and B will show strong reflection and the odd orders will show weak reflection. This is because in the former case, the net amplitude will be equal to the sum of the two amplitudes, in the latter case, the net amplitude will be equal to the difference of the two amplitudes.

Fermi, Sturm, and Sachs¹⁵ measured the scattering cross sections of polycrystalline beryllium (Be) and beryllia (BeO) as a function of the neutron energy with a mechanical velocity selector (slow chopper) and a lithium fluoride crystal spectrometer. The collimated neutron beam was $3/4$ in. x 3 in. with a Maxwellian peak at about 0.04 ev. The scattering cross-section varied as λ^2 between cut-offs (where the cross-section drops down abruptly to a lower value) at $\lambda = 2d$, where λ = wavelength and d = inter-planar distance, in agreement with the theory for Debye-Scherrer diffraction. The peak intensities showed that the scattering amplitudes for beryllium (Be) and oxygen (O) have the same sign.

Values of scattering amplitudes were obtained by Schull and Wollan¹⁶ for different elements and nuclides

from Debye-Scherrer patterns of powdered crystal samples of elements or compounds. Scattering amplitudes were also measured by mirror reflection or by comparison with ordinary hydrogen (H^1) whose scattering amplitude is known. The scattering cross sections so obtained were compared with calculated values of potential scattering cross sections and deviations from these were attributed to the presence of resonances at higher energies. The potential scattering cross section is given by¹⁴:

$$\sigma_{pot.} = 4\pi R_N^2 \quad (4)$$

where R_N = radius of the scattering nucleus.

Lowde¹⁷ describes the use of single diffraction to obtain better resolution in single crystal studies. The disadvantages of the Debye-Scherrer powder method, which is a double diffraction method, are poor resolution and a high incoherent background which may be larger than the significant counting rate. In single crystal studies using double diffraction, a high intensity of the monochromatic beam is required because of the appreciable extinction in single crystals. According to Bacon and Lowde¹⁸, extinction is the reduction of the incident intensity due to diffraction.

Rocking curves of small crystals of sodium chloride (NaCl) and naphthalene (obtained by rotating the crystal

sample with the detector fixed) are given by Lowde¹⁷ and according to him, the intensities obtained were about ten times what would normally be obtained from powdered samples of the same material. For the NaCl, (200)-plane rocking curve, the angular resolution was slightly less than 1.5° (width at half maximum).

Comprehensive surveys of different applications of neutron diffraction are given by Wollan and Schull¹⁹, McReynolds²⁰, Sidhu, Heaton, and Mueller²¹, and Hastings, Elliott, Corliss, and Hamilton²².

Neutron diffraction has been applied to the investigation of preferred orientation in a bar of uranium by Laniesse, Merrill, and Englander²³. A cylindrical metallic uranium specimen of about 5 cm.³ was used to diffract a monochromatic beam of neutrons from the EL-3 reactor at the Saclay Laboratory, Paris, France. A specimen extruded in the alpha (α)-phase showed a marked $[110]$ texture in the direction of extrusion; a similar annealed specimen in the beta (β)-range showed only a weak degree of preferred orientation.

C. Electrical Sheets. The use of silicon iron in transformer sheets was reported by Gumlich²⁴ in 1912. Studies at that time showed that silicon alloys possess high electrical resistance which results in lower eddy current losses as well as lower hysteresis loss and

higher permeability in low magnetic fields as compared with ordinary iron. Gumlich found, however, that these properties are not in direct proportion to the silicon content and that the improvement in such properties cease at about 4% silicon content.

Goss²⁵, in 1935, reported on the development of a 3-3.5% silicon strip with superior magnetic and electrical properties for use as electrical sheet. This was produced by a combination of cold rolling and heat treatment, in the following sequence: a slab of 3% silicon iron was hot-rolled to strip form, heat-treated at around 1600°F either by box annealing or by heating in a continuous electric roller hearth furnace, cold-rolled to an intermediate gage, given a rapid heat treatment at 1600-1800°F, and then cold-rolled to gage, usually 0.0125 in. Finally, the strip was given a rapid heat treatment at about 2000°F in an electric roller hearth furnace. After cutting to proper size for use in electric machinery, it was given a stabilizing heat treatment which improved the electrical and magnetic properties and prevented aging of the material.

Goss examined his material with X-rays using the Laue method and concluded that it was fine-grained and randomly oriented. This conclusion was disputed by Ruder²⁶ who found preferred orientation and fairly large

grain size in the Goss material. Ruder believed that the X-ray method was not reliable because of the large grain size.

Subsequent X-ray examination of the Goss strip by Bozorth²⁷ showed that it had a predominantly $(110)[\bar{0}01]$ preferred orientation; i.e., (110) planes parallel to the rolling plane, $[\bar{0}01]$ direction parallel to the direction of the rolling, and the $[\bar{1}10]$ direction parallel to the cross-rolling direction. This orientation is also referred to as the "cube-on-edge" orientation, and the grains as "Goss-textured," "singly-oriented," or "grain-oriented." On the other hand, grains with $(100)[\bar{0}01]$ orientation are referred to as "cube-textured", "cube-oriented," or "double-oriented." In cube-oriented grains the (100) planes are parallel to the rolling plane, and the $[\bar{0}01]$ direction is parallel to the rolling direction. The "cube-on-edge" and "cube-textured" grain orientations are illustrated in Fig. 1.

Bozorth employed the Debye Scherrer method, using characteristic molybdenum $K-\alpha$ X-rays of 0.710 Angstrom (\AA) wavelength. The grain size of the specimens examined was not very small compared with the X-ray beam cross-section; hence, composite data were obtained from several photographs. From the lengths of the Debye-Scherrer arcs so obtained, it was concluded that the

normal to the (110) planes deviated as much as 8° toward the rolling direction and as much as 15° toward the cross-rolling direction.

According to Bozorth, Goss misinterpreted his X-ray data because the latter did not rotate (or "rock") his specimen. Goss' X-ray procedure was to move his specimen by translation in order to get a composite picture.

Burwell²⁸ also examined the Goss electrical sheet by means of Laue X-ray diffraction using unfiltered "white" radiation from a molybdenum target tube operated at 37 Kilovolts (KV). Pole figures², which are topographical drawings indicating the relative frequency of the crystallographic directions in different orientations, showed a $(110)\sqrt{001}$ preferred orientation with most of the crystals deviating from the rolling direction by less than 11° and from the cross-rolling direction by not more than 20° .

Decker and Harker²⁶ have presented a theory to explain the predominantly $(001)\sqrt{110}$ preferred orientation in grain-oriented silicon steels after cold-rolling and the $(110)\sqrt{001}$ orientation after subsequent annealing. They differentiate between "lamellar" deformation and "complex" deformation of grains during rolling. In the former type of deformation, the grains rotate without breaking; in the latter type of deformation, the grains

fragment under pressure of rolling.

According to their theory, "complex" deformation occurs during rolling in those grains whose slip planes are symmetrically placed with respect to the rolling plane and rolling direction; i.e., those grains in the $(001)\langle 110 \rangle$ and $(110)\langle 001 \rangle$ orientations. Most of the grains which are not symmetrically oriented will deform lamellarly into the $(001)\langle 110 \rangle$ orientation. When "complex" deformation takes place, grains in the $(110)\langle 001 \rangle$ or "magnetic" orientation will receive more energy than grains in other orientations because the $(110)\langle 001 \rangle$ grains are less favorably positioned with respect to the plane of greatest shear stress (which is 45° to the rolling plane). Hence, upon annealing, nuclei will form first from the remnants of such grains, and eventually grow into large grains at the expense of their less strained neighbors. This growth process has come to be known as secondary recrystallization.

According to Dunn³⁰, grain boundary energy plays an important role in the growth of secondaries. Impurities such as manganese, nitrides, and silica are believed to affect the grain boundary energy and hence, influence the relative growth of the oriented grains^{31,32,33}.

Silicon-iron single crystals have also been rolled and attempts made to correlate the initial orientation

with the recrystallized orientation. Walter and Hibbard³⁴ observed that if the crystal's cube plane, i.e., the (100) plane, was originally within 30° of being parallel to the rolling plane, then the recrystallized texture tended to be (100)[001], but if the (110) plane was nearly parallel to the rolling plane, then the recrystallized grains were most likely to be (110)[001]-oriented.

As mentioned previously, preferred orientation is important in electrical sheets because of the resulting effect on their magnetic properties. Single crystals show marked anisotropy with respect to magnetic properties³⁵. Magnetization is easiest in certain crystallographic directions and more difficult in others. For example, the magnetization curve (magnetization M in gauss vs. magnetic field strength H in oersteds) for iron is highest in the [100] direction which is parallel to the cube edge. The [110] direction, parallel to a face diagonal, is a more difficult magnetization direction, and the [111] direction, parallel to the space diagonal, is the most difficult. In nickel, the order of magnetizing ease is the [111], [110], and [100] direction.

The directions of magnetizing ease in single crystals of 3.85% Si-Fe were investigated by Williams³⁶ who showed the marked anisotropy of a single crystal even at low magnetizations. He cut single crystal specimens in the

form of hollow parallelograms oriented along the different crystal axes, wound each specimen with primary and secondary coils, and measured the resulting flux. As in pure iron, the direction of easy magnetization in Si-Fe is along the cube edge.

Nickel-iron (Ni-Fe) alloys of approximately 50% Ni composition are finding increasing use as transformer laminations, particularly in high frequency applications and in high-fidelity equipment³⁷. When specially processed, such alloys develop a cube texture, and a rectangular hysteresis loop.

Sachs and Spretnak³⁸ obtained X-ray diffraction patterns of a 36% Ni-Fe alloy and inferred a cubic texture from $[\bar{1}11]$ and $[\bar{2}00]$ pole figures. Spring³⁹ reported the development of a 2-mil cube-textured 50% Ni-Fe alloy at Allegheny Ludlum Steel Corp., based on a modified German process. According to Seymour and Harker⁴⁰, the $(112)[\bar{1}11]$ and $(110)[\bar{1}12]$ orientations predominate in cold-worked 2-mil 50% Ni-Fe, but after recrystallization at 500°C, the $(001)[\bar{1}00]$ cube-texture developed, with a maximum spread of 10° from the rolling plane and rolling direction. Littman^{41,42} reported on the cube texture of primary recrystallized Armco 48 Orthonik in thicknesses of 1-mil, $\frac{1}{2}$ -mil, and $\frac{1}{4}$ -mil, as observed from $[\bar{2}00]$ and $[\bar{1}11]$ pole figures.

Lattice spacings of 50% Ni-Fe are given by Phragmen⁴³ and Bradley⁴⁴: the lattice constant, or side of a cubic unit cell, $a_0 = 3.58$ A. The structure is face-centered cubic at this Ni-Fe composition.

The lattice constants for different compositions of body-centered cubic Si-Fe are given by Greiner, Marsh and Stoughton⁴⁵. At 3.5% Si, $a_0 = 2.857$ A. Most silicon steels contain about 3% Si. The lattice constant for pure Fe at 20°C is given by Sutton and Hume-Rothery⁴⁶ as $a_0 = 2.8604$ A.

CHAPTER III

CRYSTAL DIFFRACTION THEORY

A. The Laue and Bragg Equations. If, as shown in Fig. 2, a beam of coherent radiation is incident upon a one-dimensional lattice (a line) of scattering points at an angle α_0 , the scattered radiation from the different scattering points will interfere with each other such that constructive interference, or reinforcement, will occur at angles α according to the following equation⁴⁷:

$$m_1 \lambda = a_0 (\cos \alpha - \cos \alpha_0) \quad (5)$$

where $m_1 =$ a constant;

$\lambda =$ radiation wavelength;

$a_0 =$ distance between scattering points.

This phenomenon of interference between scattered radiation is known as diffraction.

For a two-dimensional lattice (a plane) of scattering points, such as the square lattice shown in Fig. 3, the following equations hold:

$$m_1 \lambda = a_0 (\cos \alpha - \cos \alpha_0) \quad (6-a)$$

$$m_2 \lambda = a_0 (\cos \beta - \cos \beta_0) \quad (6-b)$$

where m_1 and $m_2 =$ constants;

$a_0 =$ distance between scatterers;

α_0 and β_0 = angles of incidence of the radiation
with respect to the x and y directions;

α and β = angles of reflection of the radiation
with respect to the x and y directions;

and for a three-dimensional lattice of scatterers, such
as a cubic crystal:

$$m_1 \lambda = a_0 (\cos \alpha - \cos \alpha_0) \quad (7-a)$$

$$m_2 \lambda = a_0 (\cos \beta - \cos \beta_0) \quad (7-b)$$

$$m_3 \lambda = a_0 (\cos \gamma - \cos \gamma_0) \quad (7-c)$$

where α_0 , β_0 , and γ_0 = angles of incidence with respect
to the x, y, and z directions;

α , β , and γ = angles of reflection with res-
pect to the x, y, and z directions.

These are known as the Laue equations.

Squaring the three Laue equations and adding them
together results in:

$$(m_1^2 + m_2^2 + m_3^2) \lambda^2 = a_0^2 \left[(\cos^2 \alpha + \cos^2 \beta + \cos^2 \gamma) - 2(\cos \alpha \cos \alpha_0 \right. \\ \left. + \cos \beta \cos \beta_0 + \cos \gamma \cos \gamma_0) + (\cos^2 \alpha_0 + \cos^2 \beta_0 + \cos^2 \gamma_0) \right]. \quad (8)$$

The different cosines are, in effect, the direction
cosines of the incident and scattered radiation; hence:

$$\cos^2 \alpha + \cos^2 \beta + \cos^2 \gamma = 1 \quad (9)$$

and, $\cos^2 \alpha_0 + \cos^2 \beta_0 + \cos^2 \gamma_0 = 1 \quad (10)$

Eq. (8) therefore reduces to:

$$(m_1^2 + m_2^2 + m_3^2) \lambda^2 = a_0^2 [2 - 2(\cos \alpha \cos \alpha_0 + \cos \beta \cos \beta_0 + \cos \gamma \cos \gamma_0)] \quad (11)$$

From vector algebra, we know that

$$\cos \alpha \cos \alpha_0 + \cos \beta \cos \beta_0 + \cos \gamma \cos \gamma_0 = \cos 2\theta \quad (12)$$

where 2θ = the angle between incident and scattered radiation. Therefore,

$$(m_1^2 + m_2^2 + m_3^2) \lambda^2 = 2 a_0^2 (1 - \cos 2\theta) \quad (13)$$

But

$$\cos 2\theta = 1 - 2 \sin^2 \theta \quad (14)$$

whence,

$$(m_1^2 + m_2^2 + m_3^2) \lambda^2 = 4 a_0^2 \sin^2 \theta \quad (15)$$

If m_1 , m_2 , and m_3 have a common factor n , we have

$$n^2(h^2 + k^2 + l^2) \lambda^2 = 4 a_0^2 \sin^2 \theta \quad (16)$$

where h , k , and l are integers; or,

$$n \lambda = \frac{2 a_0}{\sqrt{h^2 + k^2 + l^2}} \sin \theta \quad (17)$$

Eq. (17) is Bragg's equation:

$$n \lambda = 2 d \sin \theta \quad (18)$$

with

$$d = \frac{a_0}{\sqrt{h^2 + k^2 + l^2}} \quad (19)$$

To relate d with the distance between successive planes in a crystal, we note that the equation of a plane

with intercepts $\frac{a_0}{h}$, $\frac{a_0}{k}$, and $\frac{a_0}{l}$ is given by:

$$hx + ky + lz = a_0; \quad (20)$$

h , k , and l are called Miller indices.

The distance between such a plane as given by Eq. (20) and a plane parallel to it and running through the origin of the coordinate system is:

$$d = \frac{a_0}{\sqrt{h^2 + k^2 + l^2}} \quad (21)$$

which is identical with Eq. (19).

Hence, for radiation of a given wavelength λ , we can calculate the Bragg angle of diffraction (or reflection) from planes with the Miller indices (h, k, l) .

B. The Crystal Structure Factor. The intensity of incoherent scattering from a disordered group of atoms (or nuclei, in the case of neutron scattering) may be expressed in terms of the scattering cross section:

$$I = I_0 N \sigma_s \quad (22)$$

where I = intensity of scattered radiation;

I_0 = intensity of incident radiation per unit area;

N = number of atoms;

σ_s = scattering cross section.

Analogous to Eq. (22), we have for the case of coherent scattering from a crystal, the relationship⁴⁸:

$$I_r R^2 = I_0 \mathcal{N}_C^2 F^2 \quad (23)$$

where I_r = reflected intensity at distance R;
 I_o = incident intensity;
 N_c = number of unit cells in the crystal;
 F = crystal structure factor.

Eq. (23) assumes negligible extinction; the effects of extinction will be treated later. As stated previously, extinction is the attenuation of the incident intensity due to reflection by successive planes. The effects of imperfections in the crystal and a finite spread in the wavelength λ are also neglected in Eq. (23).

The crystal structure factor F , which relates the coherent scattering from a unit cell to the contributions from each individual atom, or nucleus, in the unit cell, will now be derived.

The scattering from an atom at the position x, y, z is related coherently with that from an atom at the origin by the phase factor^{47,48} $e^{i\Phi}$:

$$\Phi = \frac{2\pi s}{\lambda} \quad (24)$$

where s = difference in path length between radiation scattered from an atom at x, y, z and that scattered from the origin;

λ = wavelength of scattered radiation.

The distance s can be shown to be⁴⁷:

$$s = 2r \sin\theta \cos\phi \quad (25)$$

where r = distance from the origin to the atom at x, y, z ;

θ = Bragg angle;

ϕ = angle between r and the perpendicular from the origin to the plane (h, k, l) passing through x, y, z .

Also,
$$r = \sqrt{x^2 + y^2 + z^2} \quad (26)$$

Substituting Eqs. (18), (19), (25) and (26) in Eq. (24):

$$\Phi = 2\pi n \frac{\sqrt{h^2 + k^2 + l^2}}{a_0} \sqrt{x^2 + y^2 + z^2} \cos \phi \quad (27)$$

But

$$\frac{\sqrt{h^2 + k^2 + l^2}}{a_0} \sqrt{x^2 + y^2 + z^2} \cos \phi = \left(\frac{l}{d}\right) \cdot \vec{r} \quad (28)$$

and

$$\left(\frac{l}{d}\right) \cdot \vec{r} = (h\vec{i} + k\vec{j} + l\vec{k}) \cdot (x\vec{i} + y\vec{j} + z\vec{k}) \quad (29)$$

or

$$\left(\frac{l}{d}\right) \cdot \vec{r} = hx + ky + lz \quad (30)$$

Write: $x = a_0 x'$ (31-a)

$y = a_0 y'$ (31-b)

$z = a_0 z'$ (31-c)

to obtain, finally:

$$\Phi = 2\pi n [hx' + ky' + lz'] \quad (32)$$

Let E_0 be equal to the amplitude of the radiation

incident on the j th atom, and E_j be equal to the amplitude of the radiation scattered from the same atom, as measured at point R. Then⁴⁸,

$$\frac{E_j}{E_0} = \frac{f_j e^{i\bar{\phi}_j}}{R_j} \quad (33)$$

where f_j = scattering amplitude of the j th atom;

$$\bar{\phi}_j = 2\pi n [hx'_j + ky'_j + lz'_j]$$

R_j = distance from j th atom to the point where the scattered amplitude E_j is measured.

Note that if the scatterer were situated at the origin, Eq. (33) would reduce to:

$$\frac{E}{E_0} = \frac{f}{R} \quad (34)$$

The resultant amplitude, E_c , due to scattering from the unit cell will be given by:

$$E_c = \sum_j E_j \quad (35)$$

or, substituting Eq. (33):

$$E_c = E_0 \sum_j \frac{f_j e^{i\bar{\phi}_j}}{R_j} \quad (36)$$

Assuming that the distance R_j is very large relative to the dimensions of the unit cell, we can re-write the above equation as:

$$E_c = \frac{E_0}{R} \sum_j f_j e^{i\bar{\phi}_j} \quad (37)$$

or,

$$\frac{E_c}{E_o} = \frac{F}{R} \quad (38)$$

Where F = crystal structure factor. Compare Eq. (38) with Eq. (34) which was derived for the case of a single atom located at the origin of the coordinate system.

From Eqs. (37) and (38):

$$F = \sum_j f_j e^{i\phi_j} \quad (39)$$

and using Eq. (32):

$$F = \sum_j f_j e^{2\pi i n [hx'_j + ky'_j + lz'_j]} \quad (40)$$

The crystal structure factor F is thus equal to the sum of the different scattering amplitudes multiplied by their respective phase factors.

Using Eq. (40), the following rules can be easily derived^{1,47}:

a) For body-centered-cubic monoatomic crystals, $F = 2f$ for scattering from planes in which $n(h \neq k \neq l)$ is an even number,--such as the (110), (200), and (211) planes; and $F = 0$ otherwise;

b) For face-centered-cubic monoatomic crystals, $F = 4f$ for scattering from planes in which $h, k,$ and l are all odd numbers or all even numbers,--such as the (111), (200), and (220) planes; and $F = 0$ otherwise.

These two rules also hold for substitutional alloys

in a disordered state. Rule (a) will be illustrated by means of the silicon-iron alloy (3% Si and 97% Fe) used in this investigation.

The body-centered-cubic unit cell consists of two atoms located as follows (See Fig. 4):

$$\text{atom 1: } x_1 = 0, y_1 = 0, z_1 = 0$$

$$\text{atom 2: } x_2 = \frac{a_0}{2}, y_2 = \frac{a_0}{2}, z_2 = \frac{a_0}{2}$$

$$\text{Therefore, } x_1^i = y_1^i = z_1^i = 0 \quad (41-a)$$

$$x_2^i = y_2^i = z_2^i = \frac{1}{2} \quad (41-b)$$

Substituting these values in Eq. (40):

$$F = 0.97 f_{\text{Fe}} e^{2\pi i n [0]} + 0.03 f_{\text{Si}} e^{2\pi i n [0]} \\ + 0.97 f_{\text{Fe}} e^{2\pi i n [\frac{h}{2} + \frac{k}{2} + \frac{l}{2}]} + 0.03 f_{\text{Si}} e^{2\pi i n [\frac{h}{2} + \frac{k}{2} + \frac{l}{2}]} \quad (42)$$

where f_{Fe} and f_{Si} are the scattering amplitudes of iron and silicon respectively.

Eq. (42) simplifies to:

$$F = (0.97 f_{\text{Fe}} + 0.03 f_{\text{Si}}) (1 + e^{\pi i n [h+k+l]}) \quad (43)$$

from which it can be seen that $F = 2(0.97f_{\text{Fe}} + 0.03f_{\text{Si}})$ when $n(h + k + l)$ is an even number, -- such as the (110)

(200), (211) planes; and $F = 0$ otherwise.

Slow neutron scattering is isotropic,-- the nuclear dimension is very small compared with the neutron wavelength. This is not so for X-rays which are scattered from the atomic electrons whose distances with respect to each other (or with respect to the nucleus) are comparable in magnitude to X-ray wavelengths usually employed. Hence, the scattering amplitude for X-rays (which is always positive and is a monotonic function of atomic number Z) must include the "atomic form factor" which is tabulated or graphed for different elements as a function of $\sin\theta/\lambda$.

C. The Effect of Crystal Reflectivity on Neutron Diffraction Intensities. The neutron density in the reactor core is described by the Maxwell-Boltzmann distribution:

$$M(v) = \frac{dn}{dv} = C_1 v^2 e^{-(v/v_0)^2} \quad (44)$$

where $M(v) = dn/dv =$ neutron density per unit velocity interval;

$v =$ neutron velocity;

and v_0 , the most probable velocity is given by:

$$1/2 mv_0^2 = kT \quad (45)$$

where $m =$ mass of the neutron;

$k =$ Boltzmann constant;

T = neutron temperature.

According to Hughes⁴⁹, the intensity of neutrons incident on a crystal sample is proportional to the neutron flux $\phi = nv$, where n = neutron density, neutrons/cm³ and v = neutron velocity, cm/sec. Therefore, the flux distribution incident on the crystal is given by:

$$\phi(v) = \frac{d\phi}{dv} = C_2 v^3 e^{-(v/v_0)^2} \quad (46)$$

In terms of wavelengths, since

$$\lambda = \frac{h}{mv} \quad (47)$$

where λ = wavelength associated with the neutron;

h = Planck's constant;

m = mass of the neutron;

v = neutron velocity

we have

$$\phi(\lambda) = \frac{d\phi}{d\lambda} = C_3 v^5 e^{-(v/v_0)^2} \quad (48)$$

where $\phi(\lambda)$ = neutron flux intensity per unit wavelength interval, neutrons/cm³-sec.

The neutron distribution reflected from the crystal is^{11,50}:

$$I_r = \phi(\lambda) R^\lambda \quad (49)$$

where I_r = reflected intensity, neutrons/sec;

R^λ = crystal reflectivity (integrated reflection), cm³.

The neutron count-rate as measured with a BF₃ proportional counter is modified by the sensitivity of the counter. Assuming a $1/v$ sensitivity,

$$C.R. = C_4(v_0/v)\phi(\lambda)R^\lambda \quad (50)$$

where C.R. = count-rate, neutrons/sec; and all the other quantities are as defined previously.

For a small, single crystal oriented at the proper Bragg angle, the crystal reflectivity is given by Zachariasen⁴⁸ as:

$$R^\lambda = Q \delta V \quad (51)$$

where R^λ = crystal reflectivity, cm³;

Q = crystallographic quantity defined below, dimensionless;

δV = volume of the small, single crystal.

For the Laue method:

$$Q = \frac{N_c^2 F^2 \lambda^4}{2 \sin^2 \theta} \quad (52)$$

where N_c = number of unit cells per unit volume of crystal, cm⁻³;

F = crystal structure factor, cm;

λ = neutron wavelength, cm;

θ = Bragg angle.

Substituting Eq. (18) in Eq. (52):

$$Q = 2 N_c^2 F^2 \lambda^2 (d/n)^2 \quad (53)$$

Hence, for a small, single crystal, the neutron count-rate should be:

$$C.R. = C_5 v^2 e^{-(v/v_0)^2} \quad (54)$$

where C.R. = neutron count-rate, neutrons/sec;

$C_s =$ a constant.

For a large, perfect crystal, the crystal reflectivity has been theoretically derived by Darwin^{51,52}:

$$R^\lambda = QV \frac{\tanh \frac{mq}{m}}{mq} \quad (55)$$

where $Q =$ crystallographic quantity given by Eq. (52)

or (53);

$V =$ volume of crystal irradiated;

$m =$ number of reflecting planes in the crystal;

and q is the reflectivity of a single plane of unit cells:

$$q = \frac{N_c F \lambda d}{\sin \theta} \quad (56)$$

where $N_c =$ number of unit cells per unit volume;

$F =$ crystal structure factor;

$\lambda =$ wavelength;

$d =$ interplanar distance;

$\theta =$ Bragg angle

Eq. (55) can also be written as

$$R^\lambda = 2 N_c F \lambda (d/n)^2 A \tanh \left(\frac{N_c F \lambda t_0}{\sin \theta} \right) \quad (57)$$

where $A =$ area of crystal intercepting radiation beam;

$t_0 =$ crystal thickness.

However, Eq. (55) underestimates the reflected intensity because single crystals are not perfect, but can be considered as consisting of blocks misoriented at small

angles with respect to each other. The phenomenon of extinction is therefore not too severe with real crystals. Experimentally, it has been found^{18,53} that for large crystals, the reflectivity is proportional to the square root of QV :

$$R^\lambda = C_5 \sqrt{\frac{\gamma Q t_0}{\sin \theta} \left(\frac{2d \cos \theta}{n} \right)} \quad (58)$$

where γ = mosaic spread, which is a measure of the degree of misorientation of the crystal blocks;

t_0 = crystal thickness.

Therefore, the neutron count-rate for a large, real crystal is:

$$\text{C.R.} = C_L v^{3.5} e^{-(v/v_0)^2} (\cos \theta)^{0.5} \quad (59)$$

The experimental neutron count-rates can be plotted and the maximum point of the resulting neutron distribution can be correlated with the maximum of the theoretical Maxwell-Boltzmann velocity distribution in the following manner: since the cosine factor in the foregoing equation does not vary much over the angular positions involved, the count-rate can be assumed to be, approximately:

$$\text{C.R.} = C v^n e^{-(v/v_0)^2} \quad (60)$$

where the exponent $n = 3.5$ for a large crystal, such as the NaCl single crystal used in this investigation.

For small crystals, $n = 2$.

By differentiating Eq. (60), the following relationship can be seen to hold at the maximum:

$$\frac{v_{\max}}{v_0} = \sqrt{\frac{n}{2}} \quad (61)$$

or in terms of wavelengths:

$$\frac{\lambda_0}{\lambda_{\max.}} = \sqrt{\frac{n}{2}} \quad (62)$$

In a given reactor core, operating at a given temperature, λ_0 is fixed. Hence, the wavelength $\lambda_{\max.}$ corresponding to the maximum in the plotted neutron count-rate distribution (Maxwellian curve) depends on the exponent n . The angular position of the Maxwellian curve maximum therefore depends to some extent on the size of crystal, or crystal grain in the case of metals. For small-grained materials where Eq. (54) is applicable, the maximum would be expected to shift by a few degrees to the low energy (long wavelength) side, relative to that for large-grained materials.

CHAPTER IV

EXPERIMENTAL APPARATUS

A. Nuclear Reactor. The neutron beam from the East beam port of the University of Maryland pool-type reactor (UMR) licensed for operation at 10 KW (thermal) was used in these experiments. Between the reactor core and the beam port are 3 in. of graphite reflector, 1/2 in. of water moderator, and 1/4 in. of aluminum plate. The present fuel loading of the UMR⁵⁴ consists of 19 fuel elements with a fuel content of 2.7 kg. of U-235. The fuel elements are distributed as follows:

- a) three 6-plate special elements holding the control rods;
- b) thirteen 10-plate elements;
- c) one 5-plate element containing the "glory hole" for irradiation at the center of the reactor core where the neutron flux is highest;
- d) one 4-plate element at the front side of the core among the graphite reflector pieces; and
- e) one 9-plate element in position C-4 near the "glory-hole."

The exact positions of the fuel elements are depicted in Fig. 5. Each fuel plate contains about 16 g. of

U-235 except for the 5-plate ("glory hole") element, the 4-plate element, and a 10-plate element at the southeast corner of the core, which contain about 18 g. of U-235 per plate.

The estimated thermal-epithermal neutron flux⁵⁴ is 3×10^{11} neutrons/cm²-sec. in the "glory hole" at the center of this core, and the epithermal flux, as measured with aluminum foil, is approximately 10^{10} neutrons/cm²sec. at the same position.

The thermal neutron flux at the inner face of the East beam port^{55,56} is approximately 5×10^{10} neutrons/cm²-sec.

Photographs of the reactor core, the control console, and other equipments used in this thesis research are shown in Appendix A. See also Fig. 6.

B. Neutron Beam Collimator. The neutron beam was collimated by two beam port plugs, one of wood and the other of paraffin, with a 2 in.-diameter hole running through the middle. The wooden plug, 7-3/4" in diameter x 31" in length, consisted of a block of 2" planks glued together, which was then turned in a lathe. At the start of this thesis research, the wood was tested for induced radioactivity and this was found to be mainly due to Mn-56 with a half-life of 2.6 hrs. The paraffin plug, 8-1/4" in diameter x 31" in length, consisted of paraffin poured into a casing of aluminum with 2 in.-dia. aluminum

tube set in the middle.

Outside of the two plugs, the neutron beam was collimated by lead bricks, each 2" x 4" x 8", with an aperture 1/2-in. wide and 2-in. high. The lead brick-collimator was surrounded by solid concrete blocks, each block 3-3/4" x 7-3/4" x 15-1/2". See Fig. 7.

A pedestal of lead bricks with a total thickness of 16 in., sitting on concrete blocks, was placed in front of the main beam to serve as shielding for the neutrons coming directly from the reactor.

The neutron beam intensity was measured directly at the start of this study and found to be equal to 10^7 counts per minute as counted by the boron trifluoride detector and scaler to be described below.

C. Goniometer. The goniometer consisted of an X-ray goniometer base which was modified by adding a set of differential gears such that its two arms could rotate at a 2-to-1 ratio. One arm was able to move along a scale which was fixed to the goniometer base. This scale had an accuracy of 5 minutes of arc. To the other arm was attached a 7"-dia. cylinder of paraffin, 14" long, with a 1"-dia. hole through the middle for holding a 1"-dia. BF_3 neutron detector. This detector arm had its own scale, with an accuracy of 1° of arc, but an additional scale was attached to the metal floor of the goniometer and a pointer was attached to the wheel assembly holding

up the paraffin cylinder. A sketch of the goniometer is shown in Fig. 8.

The goniometer could be used in either of three ways:

1) The detector could be held fixed at a given angular position with respect to the neutron beam from the reactor, and the sample rotated independently of the detector. Experimental results obtained in this manner are designated as "rocking curves."

2) The sample could be locked on to the detector at any sample position, and the sample and detector rotated together at a 1-to-2 ratio. In this manner, the detector angle with respect to the main neutron beam could be held at twice the Bragg angle of the reflecting planes of the sample. Results obtained thus are designated as "Maxwellian curves."

3) The sample could be held fixed with respect to the main beam, and the detector rotated about the sample to give what are herein designated as "Laue curves."

The maximum rotation for the sample arm was about 45° . For greater ease in taking measurements, the goniometer was placed in such a position so that the main neutron beam fell at a scale reading of 43.5° . Therefore, Bragg angles are obtained by subtracting the scale reading, from 43.5° , thus:

$$\theta = 43.5^\circ - \theta' \quad (63)$$

D. Nuclear Instrumentation. An RCL Model 10502 BF_3 proportional counter was used to detect neutrons. This detector was filled with 96%-enriched B^{10}F_3 at a pressure of 12 cm. of Hg and had an active volume 1 in. in diameter and 6 in. in length. According to Price⁵⁷, such a detector has a counting efficiency of about 22% for thermal neutrons coming in through the end.

The BF_3 detector was connected to a Nuclear Chicago Ultrascaler Model 192-A operated at an input sensitivity of 2 millivolts and a high voltage of 1450 volts previously set by counting plateaus.

A Nuclear Chicago Model 1620 Geiger tube radiation monitor was placed beside the shield of concrete blocks. The radiation intensity as measured by this monitor was approximately 1 mr/hr. with the reactor at 10 KW.

E. X-Ray Spectrometer. A Norelco Philips Model No. 42321 X-ray spectrometer was also used to verify lattice spacings and compare X-ray diffraction measurements of preferred orientation with those obtained by neutron diffraction. In this X-ray apparatus, the sample holder and counter were set to rotate at a 1-to-2 ratio, through a Bragg angle range of about 45° . A copper target tube was used with a nickel filter to give a monochromatic beam of 1.54 Angstrom (A) $\text{K}-\alpha$ X-rays. To cut down unwanted fluorescent radiation from the steel samples being investigated, thin aluminum foils ~~were~~ placed in front

of the Geiger tube counter which was connected to a Honeywell Brown Electronik Model No. Y153X(58) 30-mv. recorder. See Fig. 9.

CHAPTER V

PROCEDURES AND MATERIALS

A. Data Taken. According to Boas¹, preferred orientation in a given material is fully specified if (a) the main orientation and (b) the extent of scattering of the crystallographic axes about the main orientation are indicated. If monochromatic radiation were used, the main orientation can be found by adjusting the positions of the sample and detector until a diffraction peak occurs. By adjusting the detector position, the value of the Bragg angle is found which corresponds to the radiation wavelength for the particular planes being reflected from, and by adjusting the sample position, the reflecting planes are placed in just the right position for Bragg reflection.

However, if polychromatic or "white" radiation is used, the detector can be placed at any angular position and only the sample orientation need be adjusted because there will always be a particular wavelength which will satisfy Bragg's condition for diffraction, provided wavelengths are present which are shorter than $2d$, where d is the interplanar spacing.

In the case of neutron diffraction, the low energy neutrons in the reactor core are distributed in energy following the Maxwell-Boltzmann distribution law. According to Hughes⁴⁹, the neutrons coming from the reactor core should have a Maxwellian flux distribution, which is equal to the Maxwellian velocity distribution multiplied by the neutron velocity, v . Neutrons diffracted from a rotating crystal, or from a material that is oriented, should follow closely the Maxwellian distribution, though modified by the reflectivity of the sample which may be a function of neutron velocity.

Essentially then, if the sample is oriented with respect to the detector such that the angle which the incident neutrons make with the reflecting planes is equal to the angle of reflection, and the sample and detector are rotated at a 1-to-2 ratio, neutrons of particular wavelengths will be Bragg-reflected at the corresponding angles, and the angular distribution of the diffracted neutrons will follow the Maxwellian distribution, suitably modified by sample reflectivity. Measurements obtained in this manner are shown in the form of Maxwellian curves.

If the maximum in the Maxwellian distribution of neutrons from the reactor can be determined by means of a single crystal of known orientation, then the main orientation of any given sample can be determined from

the position of the maximum in that sample's Maxwellian curve.

On the other hand, the scatter, or variation, about the main orientation can be obtained by keeping the detector fixed at twice the Bragg angle for the estimated maximum of the Maxwellian distribution and then rotating the sample, or "rocking" it about the Bragg angle. If the sample were a single crystal, such a "rocking curve" would consist of a single diffraction peak. For highly oriented materials, the rocking curve would consist of several peaks grouped about the main orientation.

If the sample is kept fixed at a given angle, and the detector were rotated, the curve obtained would consist of a single peak occurring at twice the Bragg angle for the particular orientation of the sample. Such a curve, herein designated as the "Laue curve," would correspond somewhat to the Laue Method of X-ray diffraction. However, as far as the determination of preferred orientation is concerned, its main disadvantage lies in the fact that the wavelength responsible for the peak in the Laue curve is not known, and recourse must still be made to the Maxwellian curve to determine this wavelength.

The average orientation of a selected crystallographic axis is determined relative to some important directions of the specimen. In the case of the rolled sheets, these important directions are: (a) the rolling plane,

or alternatively, the direction perpendicular to the rolling plane; (b) the direction parallel to the rolling direction, R.D.; and (c) the cross-rolling, or transverse, direction, C.R.D., which lies on the rolling plane, perpendicular to the rolling direction.

The samples used in this investigation were positioned relative to these important specimen directions and to the incident and reflected neutron beams in the manner depicted in Fig. 10, with the designations as labelled in the figure.

B. Materials Investigated. A sodium chloride (NaCl) single crystal was used to determine the Maxwellian distribution of neutrons from the reactor. The NaCl single crystal, from Isotopes Inc., was 2" x 6" x 1/2", cut so that the (100) planes were parallel to the reflecting face.

The major portion of this study dealt with Si-Fe electrical sheets obtained from Armco Steel Corp. and Westinghouse Electric Co. The following table lists the different Si-Fe electrical sheets investigated for preferred orientation:

Table I

Characteristics of Si-Fe Electrical Steels

| <u>AISI</u> <u>Designation</u> | <u>Nature</u> | <u>Thickness</u> | <u>Si Content</u> | Core Loss at 60 cps and <u>15 Kgauss</u> |
|-----------------------------------|----------------|------------------|-------------------|--|
| M-5 | Grain-oriented | 11 mils | 3% | 0.58 watts/lb. |

Table I (continued)

| <u>AISI Designation</u> | <u>Nature</u> | <u>Thickness</u> | <u>Si Content</u> | <u>Core Loss at 60 cps and 15 Kgauss</u> |
|-------------------------|-------------------------------------|------------------|-------------------|---|
| M-6 | Grain-oriented | 14 mils | 2.96% | 0.64 watts/lb. |
| M-19 | Non-oriented, cold-reduced | 25 " | 2.94% | 2.35 " |
| M-22 | Non-oriented, hot-rolled | 25 " | 2.86% | 2.63 " |
| | | | | <u>Core Loss at 400 cps and 15.5 Kgauss</u> |
| O.T. | Thin, oriented | 4 mils | 3.09% | 6.85 watts/lb. |
| O.T.S. | Thin, oriented, specially processed | 4 " | 3.07% | 7.40 " |

(AISI stands for American Iron and Steel Institute).

Nickel-iron (Ni-Fe) alloys with the following characteristics were also examined for preferred orientation by neutron diffraction:

Table II

Characteristics of 48% Ni-Fe Electrical Sheets

| <u>Designation</u> | <u>Nature</u> | <u>Thickness</u> | <u>Ni-content</u> | <u>Si-content</u> |
|--------------------|---------------------------------------|------------------|-------------------|-------------------|
| 48-Ni | Oriented, fine-grained | 14 mils | 48.4% | 0.47% |
| Orthonik | Oriented, cube-textured, fine-grained | 13.5 " | 48.2% | 0.46% |

The cube-textured silicon-iron (Si-Fe) electrical

sheet used in this investigation was supplied by Westinghouse Electric Co. Detailed characteristics of the material are not available, except for the sample thickness which was 6 mils.

CHAPTER VI

EXPERIMENTAL RESULTS

A. Sodium Chloride (NaCl) Single Crystal. Initial experiments were made with the NaCl single crystal to obtain the Maxwellian distribution of the neutrons from the reactor core. Fig. 13 shows the rocking curve obtained with the BF_3 detector fixed at an angle of 27° with respect to the main beam of neutrons from the reactor. The angular resolution, as given by the width of the peak at half the maximum height, is approximately 2° which is approximately equal to the angular resolution obtained by Lowde¹⁷. The peak-to-background ratio is about 10-to-1, the background being partly due to incoherent scattering from the crystal.

The NaCl single crystal was locked on to the detector at the center of the peak and the Maxwellian curve was obtained by rotating the detector, with the crystal following at a 1-to-2 ratio. Fig. 14 shows the Maxwellian curve so obtained and is compared with the calculated Maxwellian velocity distribution curve and the calculated flux distribution curve.

According to Hughes⁴⁹ and Bacon and Thewlis⁵⁰, the

neutron flux leaving the core and impinging on the sample should have a Maxwellian velocity distribution multiplied by the velocity v .

From the theory of crystal diffraction, the integrated reflection from a thick, perfect crystal should be proportional to the neutron wavelength λ . (See Eq. (57) on page 32). If the detector has a $1/v$ sensitivity, then the count-rate should be proportional once again to the flux distribution. The complete derivation of these relationships is given in Section C of Chapter III. The final result is:

$$\text{C.R.} = C v^3 \exp[-(v/v_0)^2] \quad (64)$$

where C = a constant

v = neutron velocity

$$1/2mv_0^2 = kT$$

v_0 = most probable velocity

T = neutron temperature

k = Boltzmann's constant.

This is the same result arrived at by Goldberger and Seitz¹¹, Sturm¹², and Bacon and Thewlis⁵⁰. (For Sturm's expression, see page 8 of this thesis).

The experimental Maxwellian curve shown in Fig. 14 has its maximum at a Bragg angle $\theta = 13^\circ$ ($\theta' = 30.5^\circ$). From Bragg's equation $n\lambda = 2d\sin\theta$ with $n = 2$ and $d = a_0 = 5.64$ A for the 2nd order reflection from the NaCl (100) planes, the neutron wavelength at the Maxwellian peak,

$\lambda_{\max} = 1.3 \text{ \AA}$ is obtained. The wavelength corresponding to a neutron energy of 0.025 eV is 1.8 \AA .

By matching the calculated flux distribution curve given by Eq. (64) to the experimental curve at the maximum, a neutron temperature of approximately 100°C is obtained. On the other hand, by matching the calculated velocity distribution curve, Eq. (44) to the experimental curve, a much higher neutron temperature of approximately 280° is obtained.

The velocity at the maximum of the flux distribution curve given by Eq. (64), $v_{\max.}$, is related to the most probable velocity v_0 by:

$$v_{\max.} = \sqrt{3/2} v_0. \quad (65)$$

From this relationship, and the deBroglie formula:

$$\lambda = h/mv, \quad (47)$$

using $\lambda_{\max.} = 1.3 \text{ \AA}$, the most probable wavelength of the core neutrons is found to be $\lambda_0 = 1.6 \text{ \AA}$.

The use of Eq. (64) presupposes that the NaCl single crystal is a perfect crystal, which is not true. According to Bragg, Darwin, and James⁵⁸, NaCl is far from being a perfect crystal. Only a few crystals, such as diamond, tend to approach the characteristics of a perfect crystal.

As shown in Section C of Chapter III, the correct expression to use for a large, real crystal would be Eq.

(59) which is repeated here:

$$C.R. = C_L v^{3.5} e^{-(v/v_0)^2} (\cos\theta)^{0.5} \quad (59)$$

Using this equation, the calculated neutron distribution is plotted in Fig. 15 together with the experimental data. Substituting the value of the exponent $n = 3.5$ and $\lambda_{\max.} = 1.3 \text{ \AA}$ in Eq. (62) on page 34, λ_0 is then calculated to be 1.7 \AA . This corresponds to a neutron temperature of 61°C . In the ensuing computations, the value $\lambda_0 = 1.7 \text{ \AA}$ will be used.

B. Grain-Oriented Silicon-Iron Electrical Sheets.

1. M-5 Reflection Diffraction Curves. Fig. 16

shows the rocking curves of 4 sheets of grain-oriented M-5 taken at $2\theta' = 36^\circ$ and $2\theta' = 46^\circ$. As designated in the figure, the cross-rolling, or transverse, direction was in the plane of the incident and reflected neutron beams. See Fig. 10.

A few prominent peaks can be observed in Fig. 16. These are apparently due to large grains, and it can be seen that the reflecting planes giving rise to these prominent peaks are very nearly parallel to the rolling plane of the sample as indicated by the angle $\phi = 0^\circ$ in the figure. A photomicrograph of an M-5 sample taken at a magnification of about 100x is shown in Appendix B.

The dotted curve in Fig. 16 is the Maxwellian curve obtained by centering the sample on the highest peak of

the lower rocking curve. The maximum of the Maxwellian curve is close to $\theta' = 25^\circ$ which corresponds to Bragg angle $\theta = 18.5^\circ$.

For large crystal grains, $\lambda_{max.}$ may be calculated from Eq. 62 with $n = 3.5$ and $\lambda_o = 1.7 \text{ \AA}$:

$$\lambda_{max.} = \sqrt{\frac{2}{3.5}} (1.7)$$

from which the value $\lambda_{max.} = 1.3 \text{ \AA}$ is obtained.

From the Bragg formula:

$$n \lambda = 2d \sin\theta \quad (18)$$

where $d = \frac{a_o}{\sqrt{h^2 + k^2 + l^2}}$

$a_o =$ lattice spacing $= 2.86 \text{ \AA}$ for b.c.c. Fe

$h, k, l =$ Miller indices,

the 1st order reflection from the (110) planes is calculated to occur at $\theta = 18.5^\circ$ ($\theta' = 25^\circ$) for a neutron wavelength of 1.3 \AA .

Fig. 17 is another rocking curve for the same M-5 sample conditions as in Fig. 16. The spectrum is slightly broader and the highest peaks slightly lower than in Fig. 16. From the left side of the spectrum, it can be seen that the maximum spread of the rocking curve is about 15° ; i.e., the maximum deviation of the reflecting planes from the rolling plane of the sample is about 15° . This agrees with the findings of Bozorth²⁷ and Burwell²⁸ mentioned previously in Chapter II of this thesis.

Fig. 18 is similar to Figs. 16 and 17. Several points on the right-hand peak of the upper curve demonstrate the reproducibility of the data.

The rocking curve for a 4-sheet M-5 sample in the rolling direction; i.e., rolling direction of the sample in the plane of the incident and reflected neutron beams, is shown in Fig. 19. The curve is narrower than the 4-sheet C.R.D. sample, and the peaks are higher. However, the increased height is partly due to the rectangular shape of the sample, 3 in. in the R.D. and 4 in. in the C.R.D., the collimator opening being $1/2$ in. wide and 2 in. high.

To correct for this geometrical effect, a square sample 3 in. x 3 in. consisting of 4 sheets was rocked at the same Bragg angle, and the high points for the R.D. and C.R.D. positions were compared. The results are shown in Fig. 20. Evidently, the peaks for the R.D. sample are still higher than the peaks for the C.R.D. sample, though now in the ratio of 5-to-4 instead of 2-to-1.

Fig. 21 shows the rocking curve (solid line) for 4 sheets of M-5 in the R.D. The lower dotted line is the background counting rate when the sample was removed. The upper dotted line is the Maxwellian curve for the prominent peak. However, the rocking curve peak is most probably not due to diffraction from a single large grain, but is due to several grains with very close orientations.

The maximum point of the Maxwellian curve occurs at the Bragg angle for diffraction of 1.3 Å neutrons from (110) planes, $\theta = 18.5^\circ$, or $\theta' = 25^\circ$.

A rocking curve and a Maxwellian curve for 1 sheet of M-5. R.D. sample are shown in Fig. 22. The maximum count-rate is approximately half the maximum count-rate for 4 sheets of M-5 in the same position. This is in agreement with the conclusion of Bacon and Lowde¹⁸ that the reflection from non-absorbing real crystals is proportional to the square root of the sample thickness. (See Eq. (58) on page 33).

The rocking curve in Fig. 22 also shows that the maximum deviation of the reflecting planes from the rolling plane is about $8-10^\circ$ in the rolling direction, in agreement with the results of Bozorth²⁷ and Burwell²⁸. As in Fig. 21, the Maxwellian curve maximum occurs at the Bragg angle $\theta = 18.5^\circ$ ($\theta' = 25^\circ$).

One important advantage of neutrons over X-rays in metal diffraction work is the greater penetrating power of neutrons because of their lower absorption in most materials. This is shown in Fig. 23 which is a superposition of rocking curves for two M-5 sheets diffracted separately and diffracted together. The uppermost rocking curve is very nearly proportional to the sum of the two lower curves, demonstrating that neutrons diffracted from the second sheet, in a sandwich of two sheets, can

pass through the first sheet because of the low absorption coefficient. These curves again display a maximum deviation of the reflecting planes of less than 10° from the rolling plane mentioned previously in connection with Fig. 22. The dotted curve in Fig. 23 is the Maxwellian curve for the two sheets diffracted together, and it indicates a (110) preferred orientation.

2. M-5 Transmission Diffraction Curves. To determine completely the main orientations of the unit cell, or cube, with respect to the sample, rocking curves were taken for 1 and 8 sheets of M-5 by transmission diffraction in the R.D. position. (Fig. 24). The detector was placed at $2\theta' = 33^\circ$ which corresponds to a Bragg angle of $\theta = 27^\circ$ at which angle diffraction should take place from (200) planes for neutrons of 1.3 Å wavelength. Alternatively, one may consider 2nd order diffraction as taking place from (100) planes for the same wavelength.

The rocking curve for the single sheet shows several faint peaks while the upper curve for 8 sheets shows a gradual accumulation of diffraction peaks due to reflections from (200) planes oriented perpendicularly to the rolling plane, with the $[200]$ direction parallel to the rolling direction. Indeed, the Maxwellian curves for transmission diffraction in Fig. 25 taken together with the previous Maxwellian curves for the M-5 sample in reflection diffraction, clearly demonstrate the (110)

[001], or "cube-on-edge" orientation of the M-5 sample. The Maxwellian curves for reflection diffraction showed that the reflecting planes parallel to the sheet surface, or rolling plane, were predominantly (110) planes, while the transmission Maxwellian curves show that the reflecting planes perpendicular to the rolling direction were predominantly (001) planes.

The sample used in taking the data for Fig. 25 was 3 in. in the R.D. and 4 in. in the C.R.D. As mentioned before, the rectangular shape gives rise to a geometrical factor which makes the count-rate in the R.D. about twice what it should really be. If the ratio of 5-to-4 found previously (see Fig. (20)) is used, then the R.D. data in Fig. 25 should be corrected by a factor of approximately 5-to-8 which should bring down the R.D. Maxwellian curve relative to the C.R.D. Maxwellian curve, as shown in Fig. 26.

3. M-6 Curves. Fig. 27 shows the rocking curves for a single sheet of M-6 sample in the R.D. position, reflection diffraction at three different positions of the BF_3 detector, corresponding to the Bragg angles for reflection from the (211), (200), and (110) planes, indicating a predominantly (110) orientation parallel to the rolling plane. The maximum deviation of the reflecting planes from the rolling plane is again less than 10° . Presumably, the differences in heights

cannot be due to angular variation of the crystal structure factor because neutron scattering at these low energies is isotropic. In the case of X-rays, the atomic form factor, which varies with the angle θ , has to be taken into account.

Fig. 28 shows "Laue curves" of the same M-6 single sheet sample in the R.D. position. The curves were taken with the sample fixed at a given angle and the counter rotated to obtain the diffraction peak. The peaks so obtained are quite clear but the curves do not provide any new information because the wavelength responsible for a peak cannot be inferred from the data without the additional information provided by a Maxwellian curve. According to Lonsdale⁵⁹, ". . . Laue photographs . . . will not give the size of the unit cell, only its shape, because it gives a measure of angles only, not of spacings."

4. Oriented Thin Steel (OTS) Curves. Fig. 29 shows Maxwellian curves for 28 sheets of 4-mil specially processed oriented thin steel (OTS) taken by transmission diffraction. Note the close similarity of these two curves to those in Fig. 26. As with the M-5 sample, a $\langle 110 \rangle$ orientation in the cross-rolling direction and a $\langle 200 \rangle$ orientation in the rolling direction are indicated, although the relatively flat shape of the R.D. curve towards the low energy region indicates, the pos-

sibility that other components, notably $[211]$, are present in the rolling direction.

Maxwellian curves by reflection diffraction for single sheets of OTS in the R.D. and C.R.D. positions are shown in Fig. 30, indicating a (110) orientation parallel to the rolling plane. These OTS curves, together with the transmission curves in Fig. 29 demonstrate the (110) $[001]$ main orientation of the OTS electrical sheets.

C. Cube-Textured Silicon-Iron Electrical Sheets.

In contrast with the (110) orientation of the OTS rolling plane, the Maxwellian curves for a cube-textured sample in the cross-rolling direction are shown in Fig. 31, exhibiting the (200) orientation of its rolling plane. The production of cube-textured silicon-iron electrical sheet has been reported^{60,61,62,63} but details of the manufacturing process are not known.

The (200) orientation of the cube-textured sample is even more clearly pronounced in Fig. 32 which shows rocking curves at the Bragg angles for 1.3 Å reflections from (110), (200), and (211) planes. The θ_{110} peak is very evidently depressed relative to the θ_{200} peak, which is in direct contrast with the M-6 rocking curves of Fig. 27. The cube-textured sample is strongly (200)-oriented relative to the rolling plane. However, a (211) component is also prominent in the cross-rolling direction. To complete the determination of its main orientations,

Maxwellian curves for the other sample positions were taken. See Fig. 33. While the presence of a (211) component is indicated by the C.R.D. Maxwellian curves, the R.D. curves show that the grains are predominantly (200)-oriented with respect to the rolling direction. In Fig. 33, the OTS Maxwellian curve for the rolling plane orientation is plotted for comparison. X-ray spectra of the M-5 and cube-textured samples are shown in Fig. 11. According to Fig. 11, the M-5 sheet surface is predominantly (110)-oriented, while the sheet surface of the cube-textured sample is predominantly (200)-oriented.

D. Non-Oriented Electrical Sheets. In the next figure, (Fig. 34), are rocking curves for 1 and 5 sheets of 25-mil M-22, which is classified as non-oriented Si-Fe electrical steel by the manufacturer. These curves were taken by reflection diffraction, and the relatively smooth shape and lower counting rates do indicate that the material is not "grain-oriented" as are the M-5 and M-6 samples. Note the similarity of these curves to the M-5 transmission diffraction rocking curves. The lack of prominent peaks indicates small grain-size for the M-22 sample. A photomicrograph of an M-22 sample taken at a magnification of about 100X is shown in Appendix B.

Maxwellian curves for M-19 and M-22 samples are compared in Fig. 35. Both M-19 and M-22 samples consisted of 5-sheet sandwiches, and both were cut to exact-

ly the same size and shape. The Maxwellian curve for the M-19 sample is more peaked than that for the M-22 sample, indicating a greater degree of preferred orientation of the former.

The peak of the Maxwellian curves occurs slightly to the left of the expected angular position for the Bragg scattering of 1.3 Å neutrons from (110) reflecting planes. This is most probably due to the fine-grained nature of the M-19 and M-22 materials which would then make the case of diffraction from small crystals applicable. As shown in Section C of Chapter III, the count-rates for diffraction from small crystals should have a maximum which is displaced slightly towards the low energy side relative to that from large crystals.

These curves also indicate that there is some degree of preferred orientation present in "non-oriented" electrical sheet. Indeed, there is usually some degree of preferred orientation present in most cold-worked or annealed metals; just as, in the opposite extreme, preferred orientation is never perfect, -- there is always some scatter about the main orientation.

E. 48% Ni-Fe Alloys. The last figure (Fig. 36) displays the Maxwellian curves for 8 sheets of 14-mil 48-Ni and 13.5-mil Orthonik which are 48% (by weight) alloys of nickel and iron. According to the literature^{43,44} 48% Ni-Fe is face-centered-cubic in structure, with a lat-

tice spacing of 3.58 Å. Using this value, the Bragg angles for (220) and (200) reflections are found to be $\theta_{220} = 31^\circ$ and $\theta_{200} = 21^\circ$ for 1.3 Å neutrons. Fig. 36 then indicates that 48-Ni contains both (220) and (200) orientations parallel to the rolling plane, while Orthonik is mainly (220)-oriented with respect to the rolling plane. X-ray diffraction patterns of these two materials support the above findings; the X-ray spectrometer data (See Fig. 12) shows peaks of approximately equal height at the 220 and 200 Bragg positions of the 48-Ni sample; with the Orthonik sample, the 200 peak is depressed and the 220 peak either increased slightly or remained the same. These findings show that the Ni-Fe samples investigated were not cube-textured. This is because they had not yet undergone the annealing process which results in the "cube-on-face" or (100) $\langle 001 \rangle$ -orientation.

CHAPTER VII

SUMMARY AND CONCLUSIONS

A. Advantages of Neutron Diffraction over X-Ray Diffraction. In the study of preferred orientation in metals, neutrons possess the advantage of being weakly absorbed in most materials. Hence, they can pass through greater thicknesses of sample than can X-rays. With neutrons, it is therefore not necessary to diffract a large number of thin samples to obtain a statistically significant result²³.

With X-rays, the diffraction patterns obtainable are limited to sample thicknesses of about 5 mils. A thickness of 1 mil of iron will have reduced the X-ray beam intensity by a factor of 1/100. On the other hand, neutron absorption is practically negligible (the half-thickness of iron for neutron absorption is about 500 mils) and the sample thickness is limited by the phenomenon of extinction. For real crystals, the reflectivity varies approximately as the square root of the sample thickness, due to extinction. Therefore, the inner sections of a sample will still be able to make their contributions to the diffraction pattern though not as much as the sections

near to the surface facing the neutron beam.

B. Advantages and Disadvantages of Single Diffraction. The use of single diffraction in studying preferred orientation is limited to materials with simple structure. If the material has a fairly complex structure, then a monochromatic beam is required to produce a diffraction pattern which can be interpreted. On the other hand, for simple structures, such as body-centered-cubic iron, the diffraction patterns are limited to certain reflections, such as the reflections from the (110), (200), and (211) planes. The angular separations between these reflections are wide enough so that the resulting pattern obtained with a polychromatic beam can be interpreted.

The main advantage of single diffraction is that the reactor beam is used directly without going through the monochromatizing process. Hence, a more intense beam is available for diffraction.

This study also indicates that it may be possible to correlate the Maxwellian pattern of a given sample with grain size.

C. Sodium Chloride (NaCl) Single Crystal. In this study, the NaCl single crystal was used to obtain the Maxwellian spectrum of the reactor neutrons, and this information was subsequently used to determine the planes responsible for diffracting neutrons in the samples being

investigated. The experimental Maxwellian curve from the (200) planes of the NaCl single crystal was compared with calculated curves for three cases: reflected beam directly proportional to 1) the Maxwellian velocity distribution; 2) the Maxwellian flux distribution from a perfect crystal; and 3) the Maxwellian flux distribution from a real crystal whose reflectivity is given by Eq. (58). Although the perfect crystal formula, Eq. (1) or Eq. (2), has been used to fit the Maxwellian curve^{11,12}, it is believed that the third method of computation using Eq. (59) is more correct because it is applicable to a real crystal rather than to a perfect crystal. On this basis, a neutron temperature of 61° is obtained for the core neutrons of the University of Maryland reactor.

D. Preferred Orientation in Grain-Oriented Materials.

The data show that preferred orientation in highly oriented materials can be conveniently determined by single diffraction techniques using neutrons. The (110) $\sqrt{001}$ -orientation of the M-5, M-6, and OTS electrical sheets has been clearly demonstrated, as well as the (100) $\sqrt{001}$ -orientation of the cube-textured samples. The X-ray patterns shown in Fig. 11 do verify the (110)-orientation of the M-5 sheet surface and the (100)-orientation of the cube-textured sheet surface, in agreement with previous findings^{26,27,28}.

E. Non-Oriented Materials. The rolling plane orien-

tations of materials classified as non-oriented have also been determined and compared in two samples: M-19 and M-22. However, it is doubtful if transmission diffraction measurements on these samples can give significant results because they are weakly oriented. Hence, it is possible that of the main orientations along the three directions of the sample (rolling plane, rolling direction, and cross-rolling direction), only that in the rolling plane can be determined.

F. General Conclusions. From this study, the following general conclusions can be drawn:

- a) Preferred orientation in rolled metallic sheets can be determined using single diffraction of neutrons;
- b) The techniques employed in this study work best with highly oriented materials, especially those with relatively large grains;
- c) The best results are obtained by reflection diffraction;
- d) Transmission diffraction is also possible although the counting statistics are not as good as those obtained by reflection. However, both types of diffraction (reflection and transmission) are required for a complete determination of preferred orientation;
- e) Edge-on diffraction has not been attempted. However, information obtained in this manner is not necessary for the complete determination of preferred orientation.

tation; essentially the same information can be obtained by taking reflection and transmission measurements at different inclinations of the sample's zenith angle with respect to the neutron beam;

f) Data obtained so far indicate that a complete pole figure can be drawn by taking rocking curves at different inclinations of the sample to the neutron beam.

C. Recommendations. The following program for future work on improving the experimental apparatus is recommended:

a) The neutron diffractometer can be improved by:
1) providing a sample holder which can be rotated in small increments of azimuth and zenith angles⁶⁴; and 2) making it possible for the counter to rotate azimuthally through 180° instead of just 90° , although this will probably require an entirely new goniometer. The first modification should make the detailed plotting of pole figures a very simple, though still a time-consuming, procedure. With the second modification, additional reflecting planes can be observed, such as the (222) planes in iron which are presently outside the range of the goniometer.

b) More compact shielding using borated materials should be provided. This will be necessary if the reactor power is brought up to 100KW.

H. Proposed Future Studies.

a) Further work on preferred orientation determina-

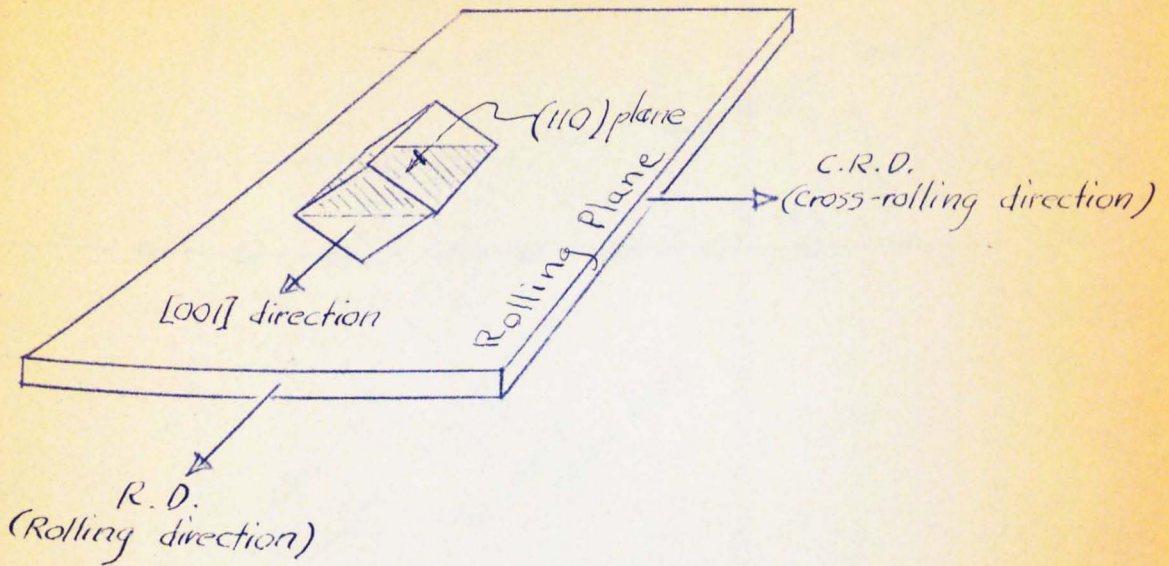
tion by single diffraction still need to be done: 1) Complete pole figures of some of the materials already available should be made. A comparison of the $\langle 100 \rangle$ and $\langle 110 \rangle$ pole figures of the "cube-on-edge" and cube-textured samples should provide useful, as well as interesting, information. 2) By reducing the neutron beam collimator width and improving the collimation from sample to detector, the slight shift of the Maxwellian peak due to extinction could be studied more carefully; this might be able to provide information on sample grain size which can be correlated with other methods. For such a study, improving the angular resolution of the apparatus by increasing the distance from sample to detector would be desirable. 3) A thorough investigation of the effect of sample thickness on the Maxwellian curve might lead to a better understanding of extinction effects. 4) The 48% nickel-iron alloys require further investigation, particularly to verify their cube-texture.

b) Preferred orientation studies on metals other than electrical sheets should also be undertaken; double crystal diffraction techniques should provide more information on materials which are weakly oriented than can be obtained with single diffraction, particularly where several components are present.

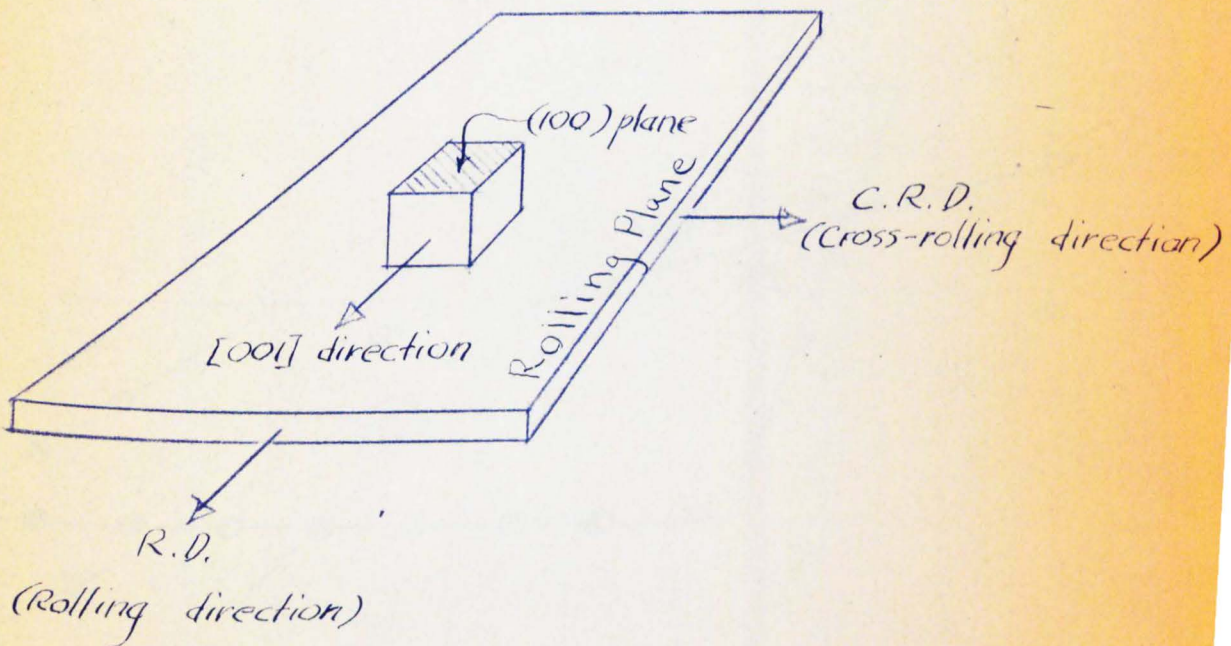
c) Diffraction techniques can be applied to non-metallic materials such as rubber and plastics; but it

is believed that double diffraction may be required.

d) The effect of stresses on neutron diffraction patterns can be investigated.



The "Cube-on-edge" Orientation



The "Cube-textured" Orientation

Fig. 1. The "Cube-on-edge" and "Cube-textured" Orientations.

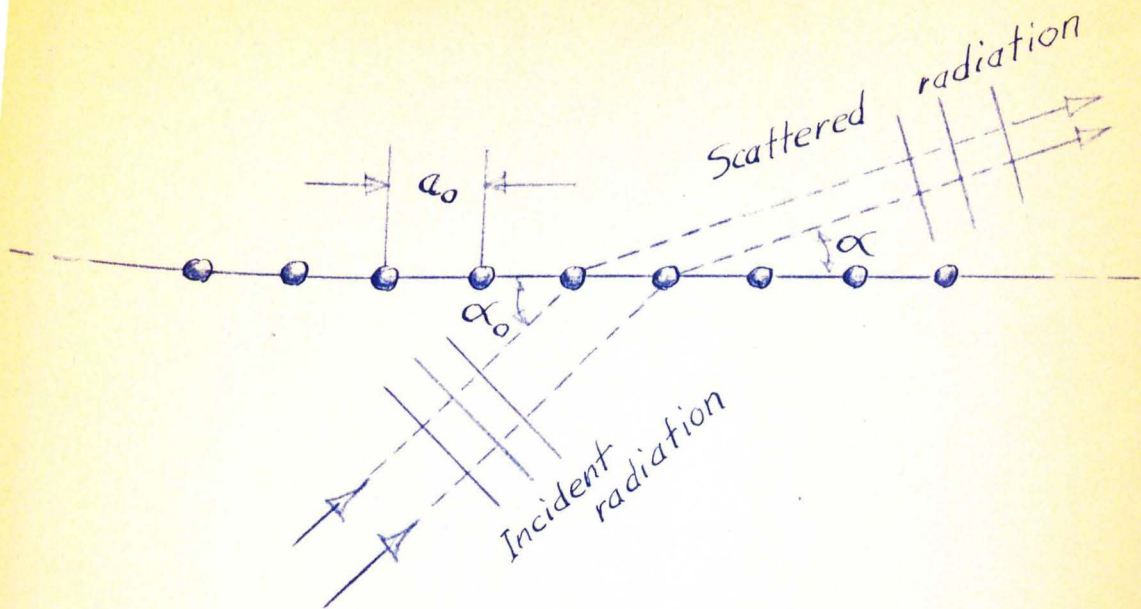


Fig. 2. One-dimensional Lattice of Scatterers

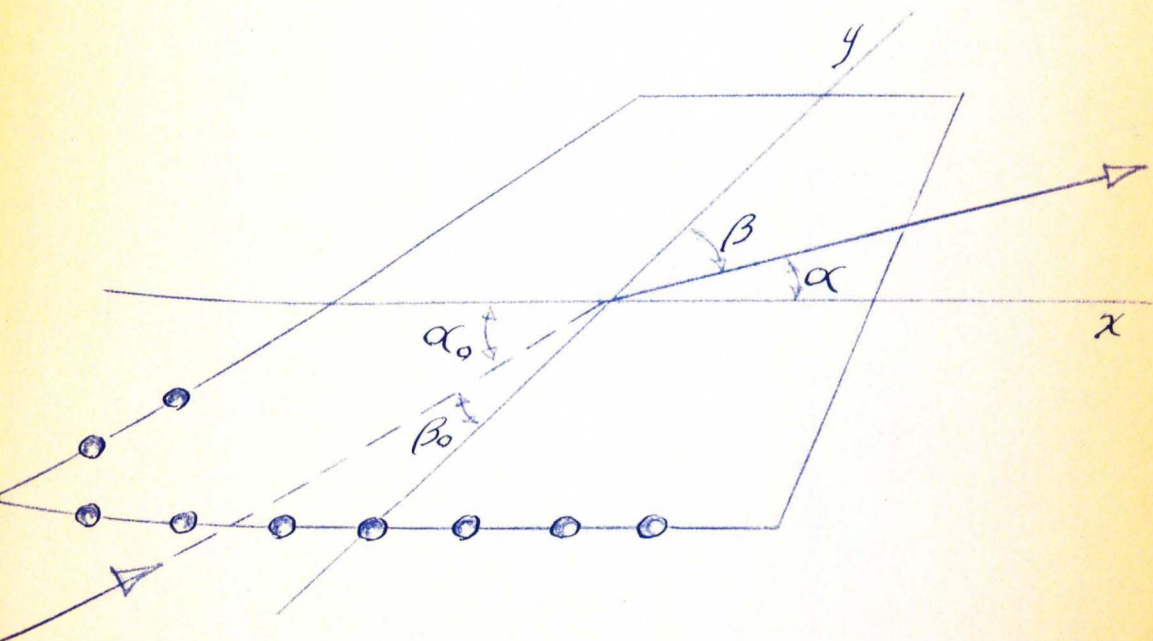
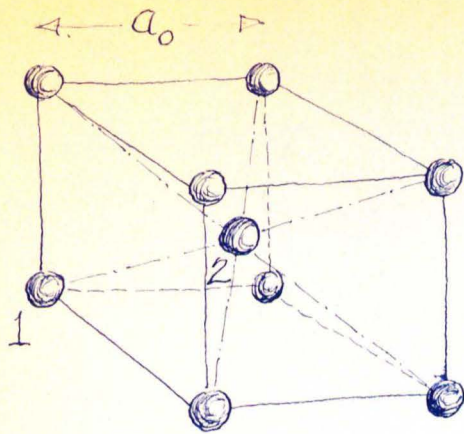


Fig. 3. Two-dimensional Lattice of Scatterers



Atom positions

1) $0, 0, 0$

2) $\frac{a_0}{2}, \frac{a_0}{2}, \frac{a_0}{2}$

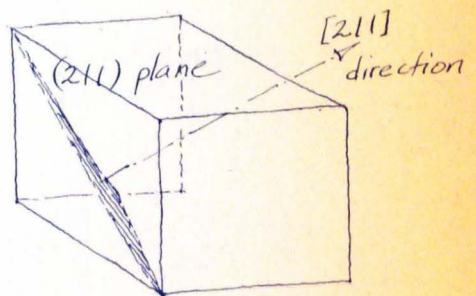
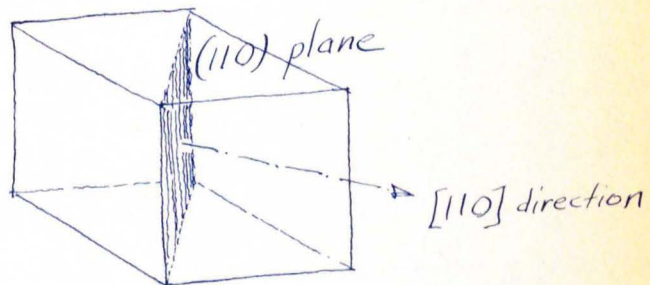
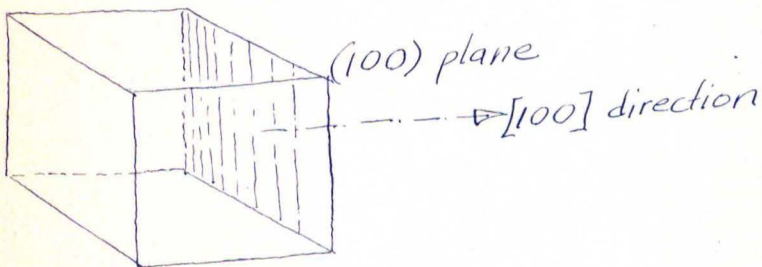
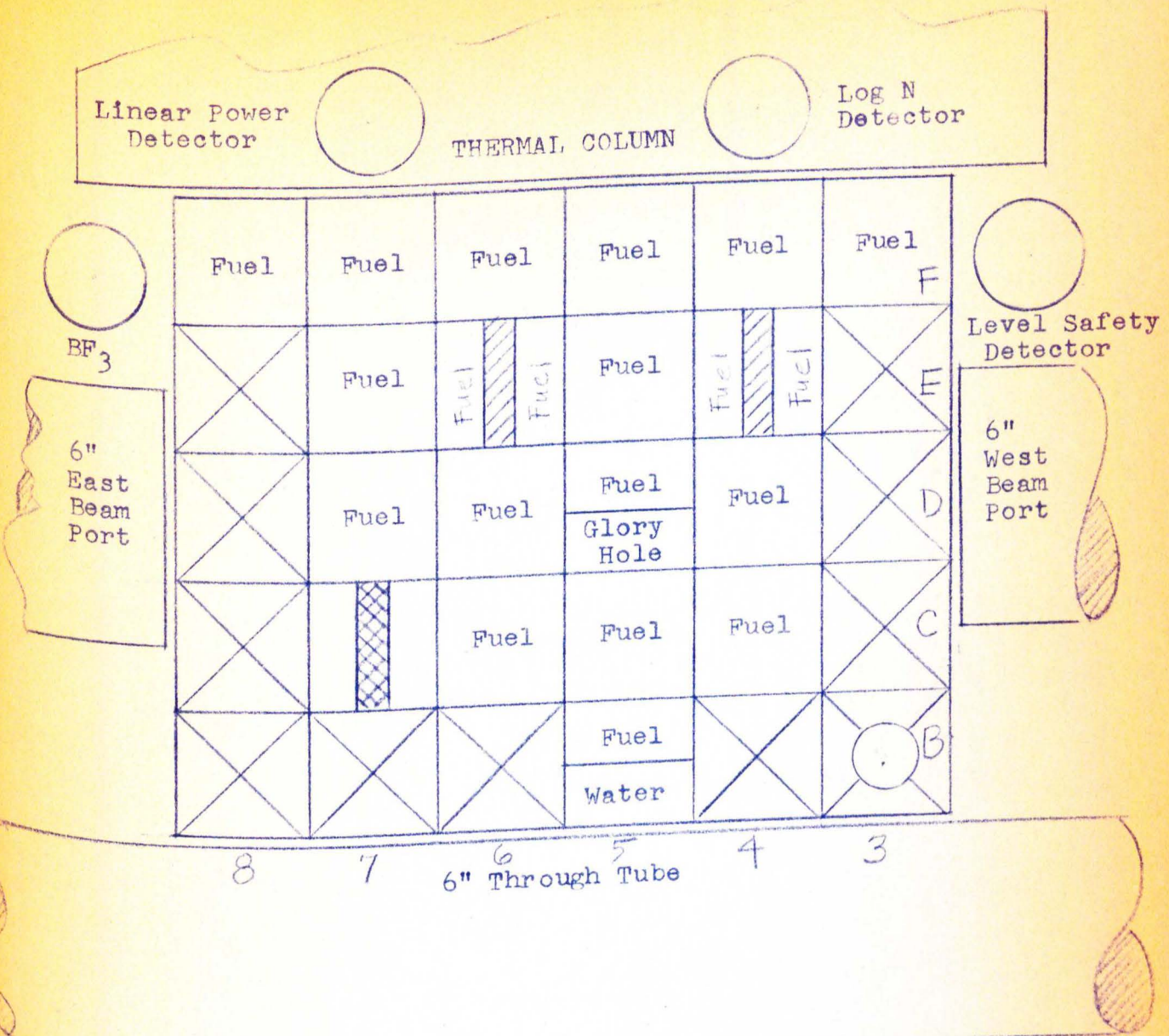
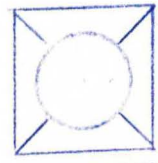


Fig. 4. The Body-centered-cubic Unit Cell.



 Shim-safety Control Rod

 Regulating Rod

 Neutron Source in Graphite

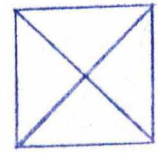
 Graphite Reflector

Fig. 5. University of Maryland Reactor Core Arrangement

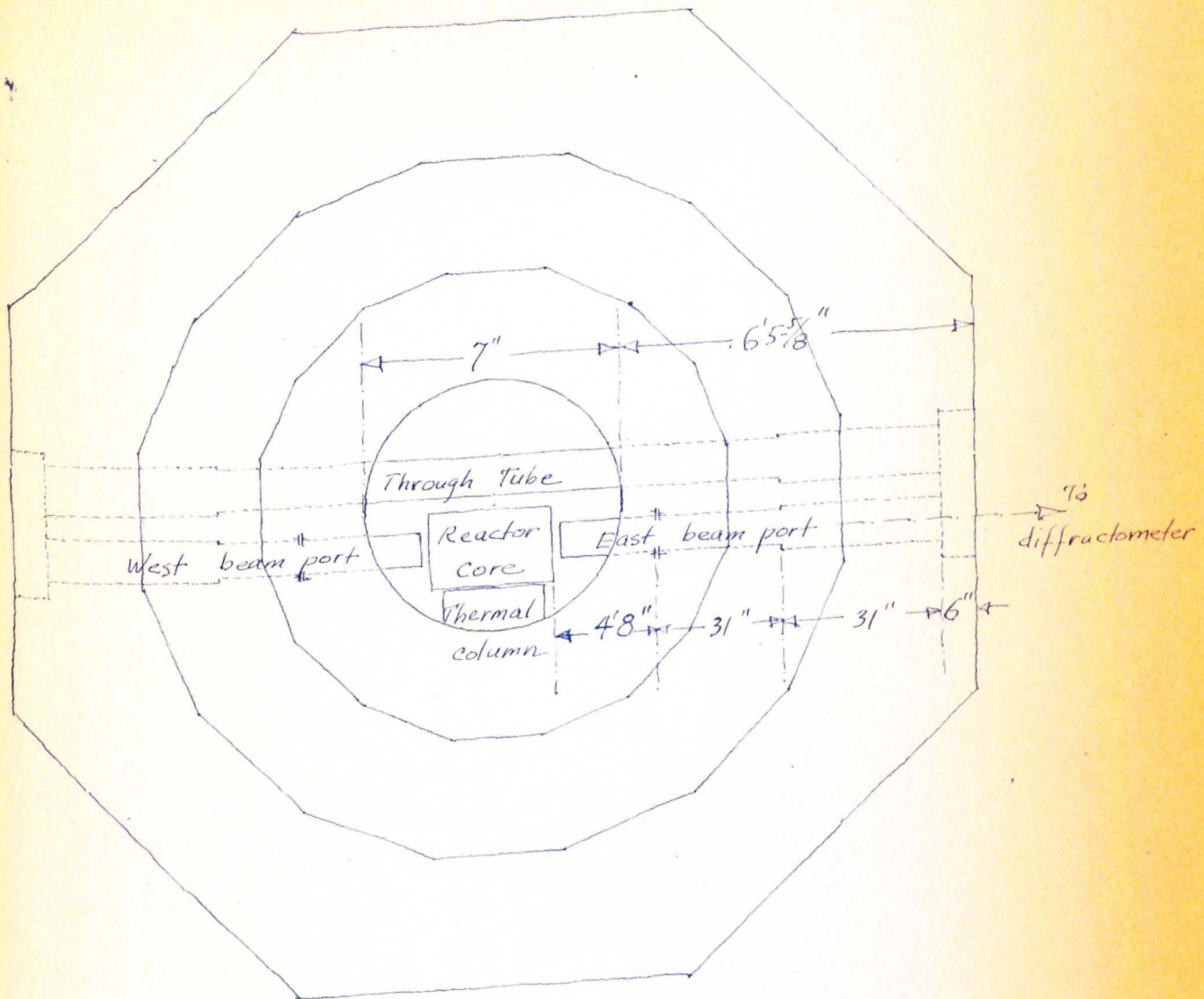


Fig. 6. Plan View of the Reactor Showing Positions of Beam Ports and Through Tube.

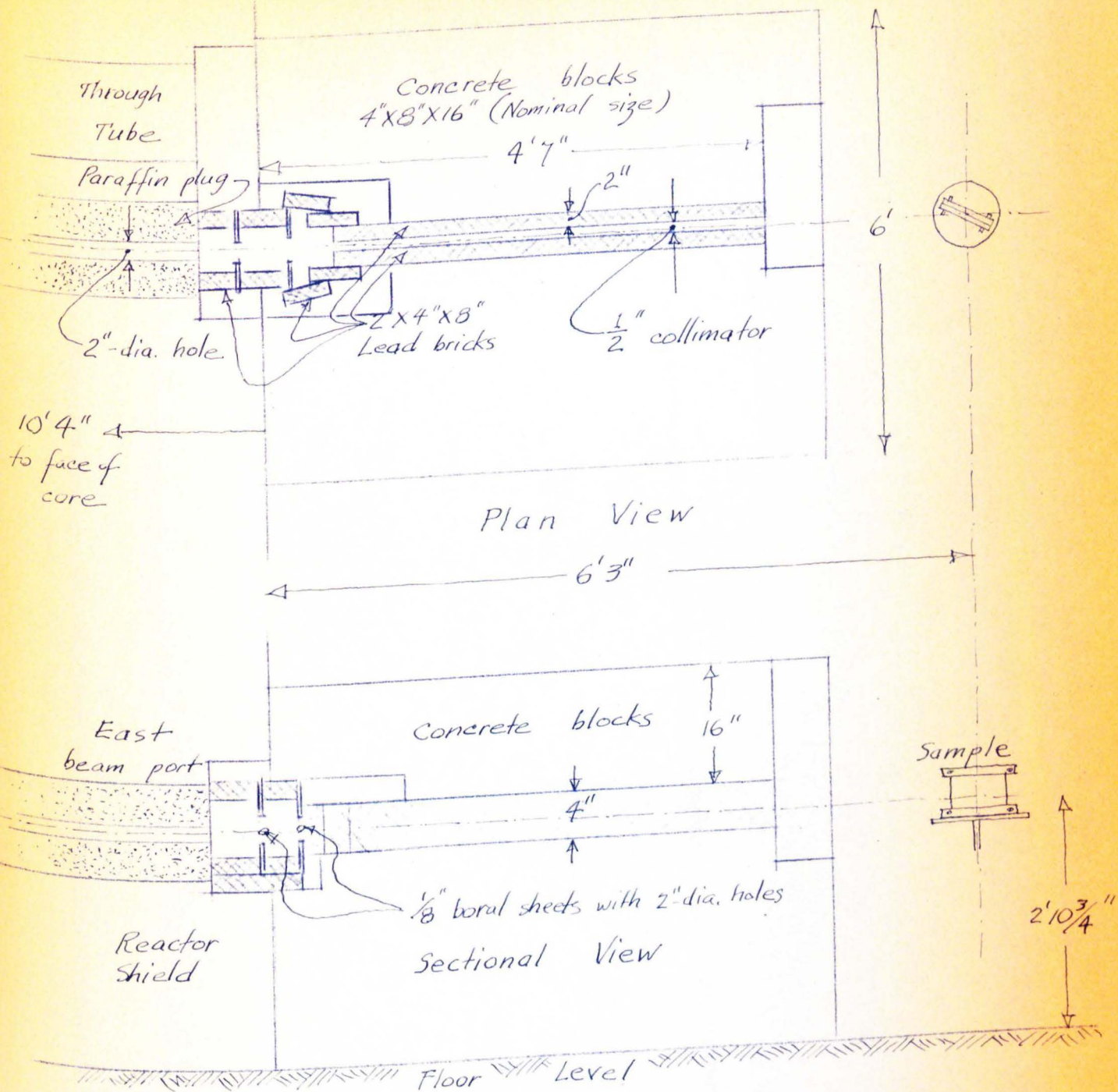


Fig. 7. The Neutron Beam Collimator.

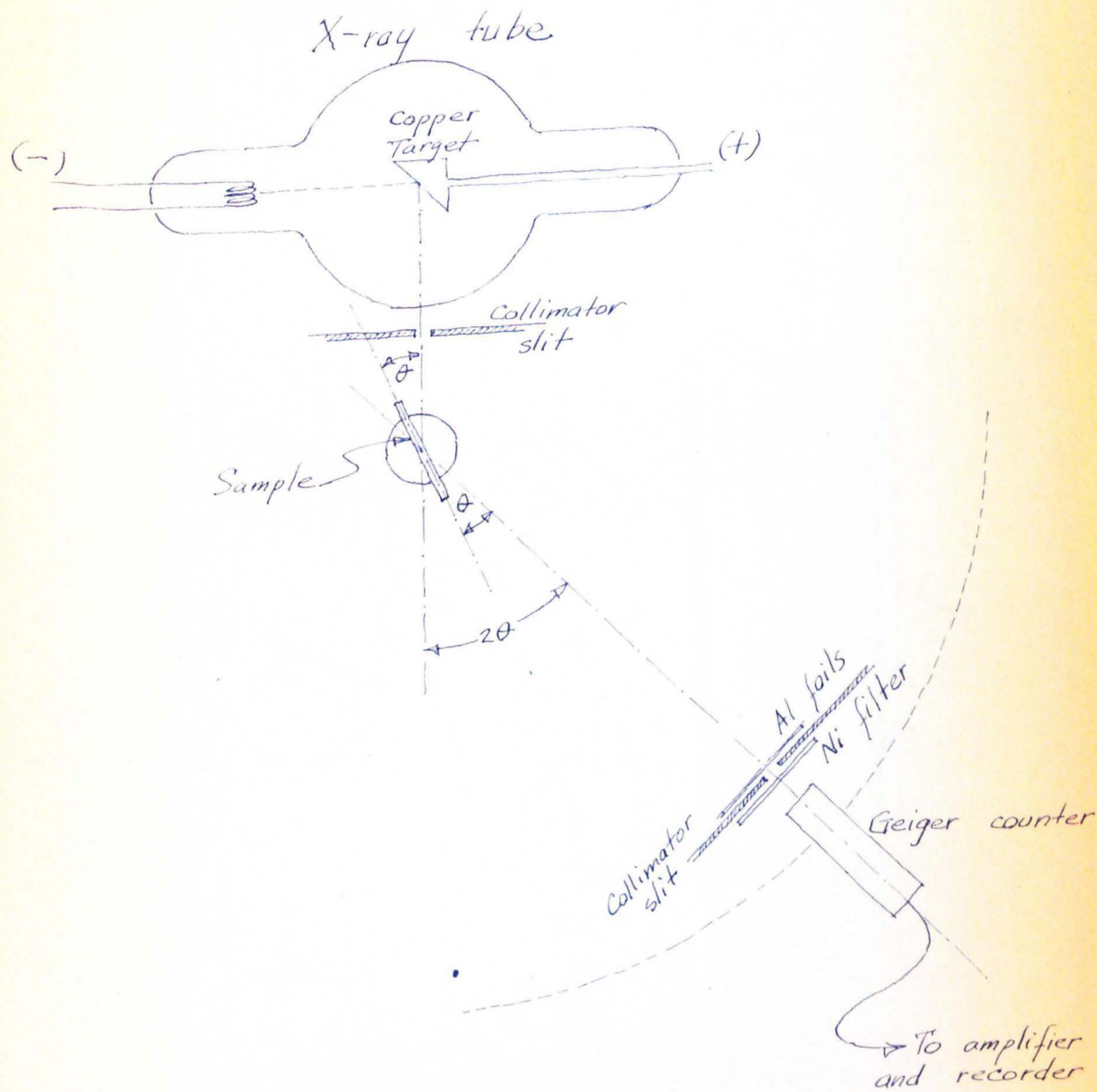


Fig. 9. Schematic Diagram of the X-Ray Spectrometer.

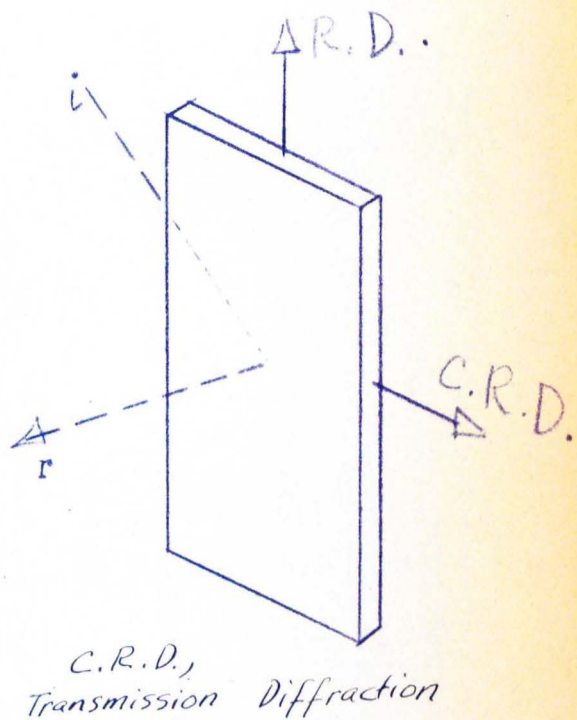
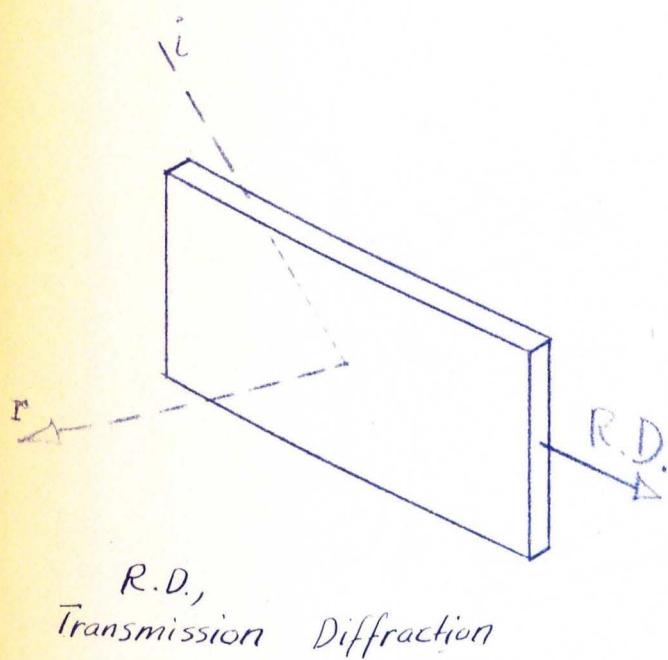
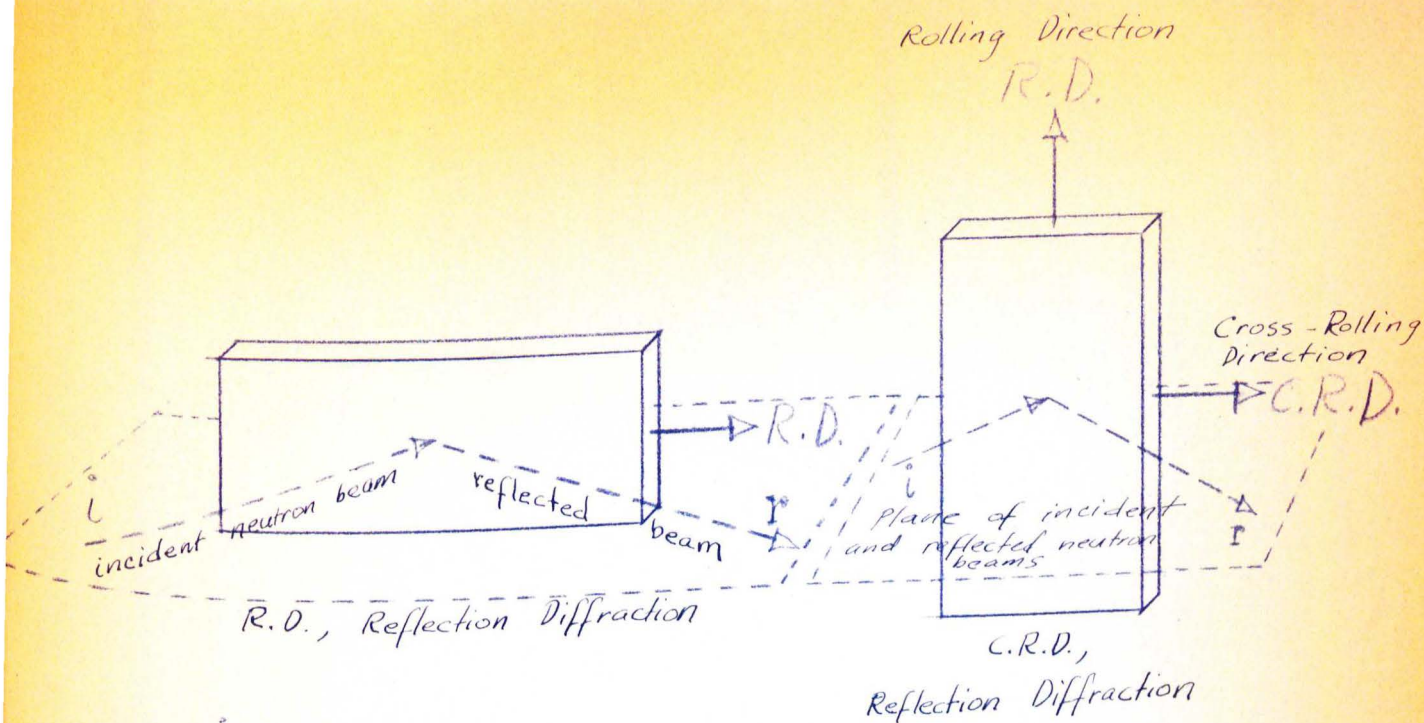


Fig. 10. Diagram Showing Sample Positions.

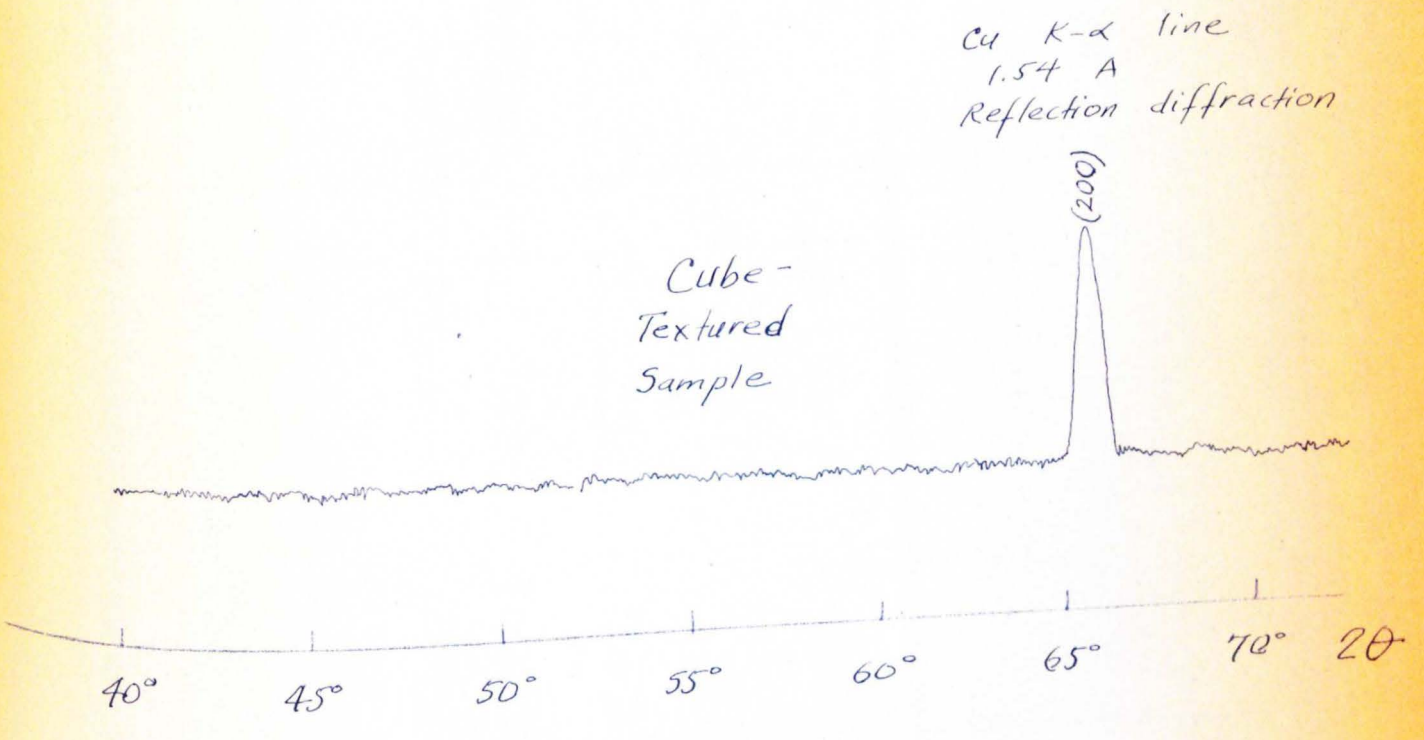
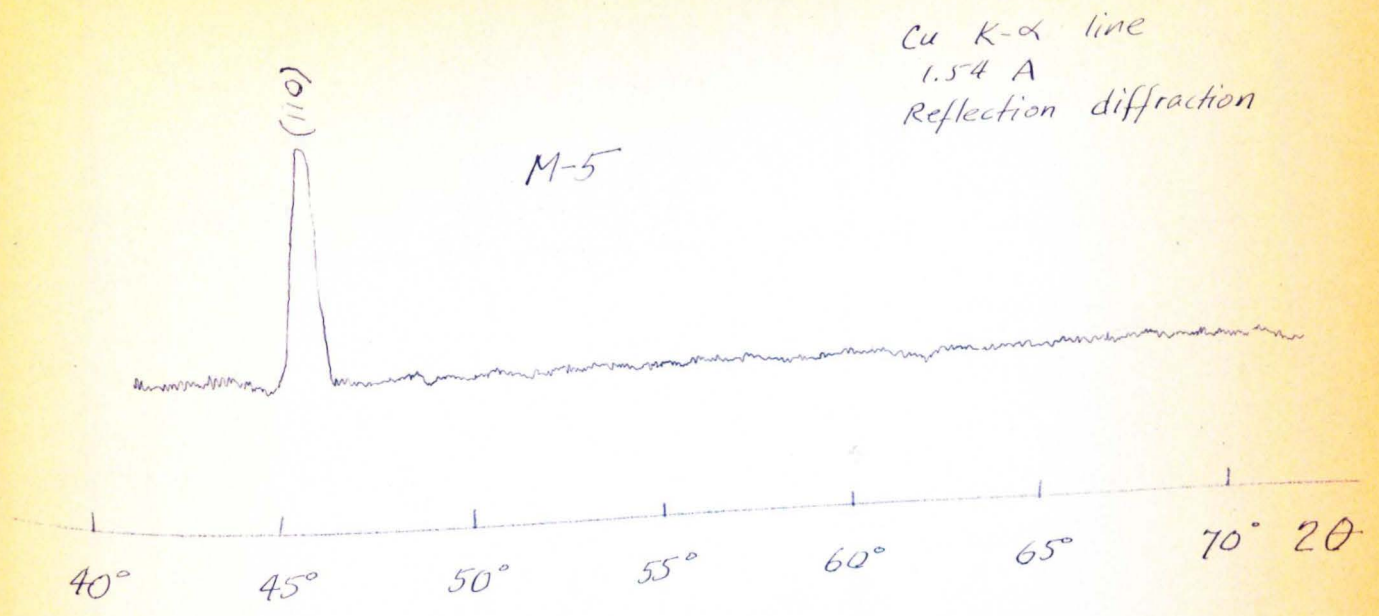


Fig. 11. X-Ray Diffraction Patterns of "Cube-on-edge" M-5 and "Cube-textured" Sample

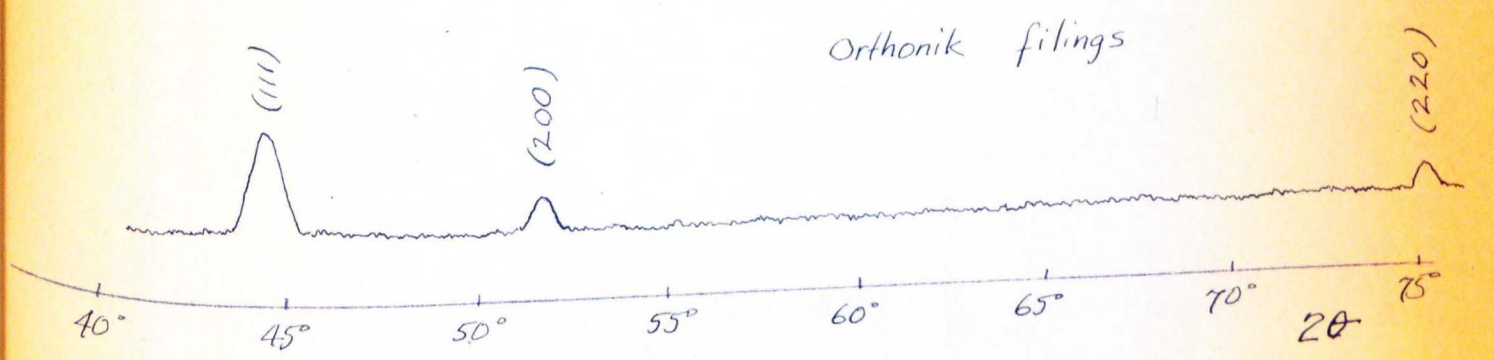
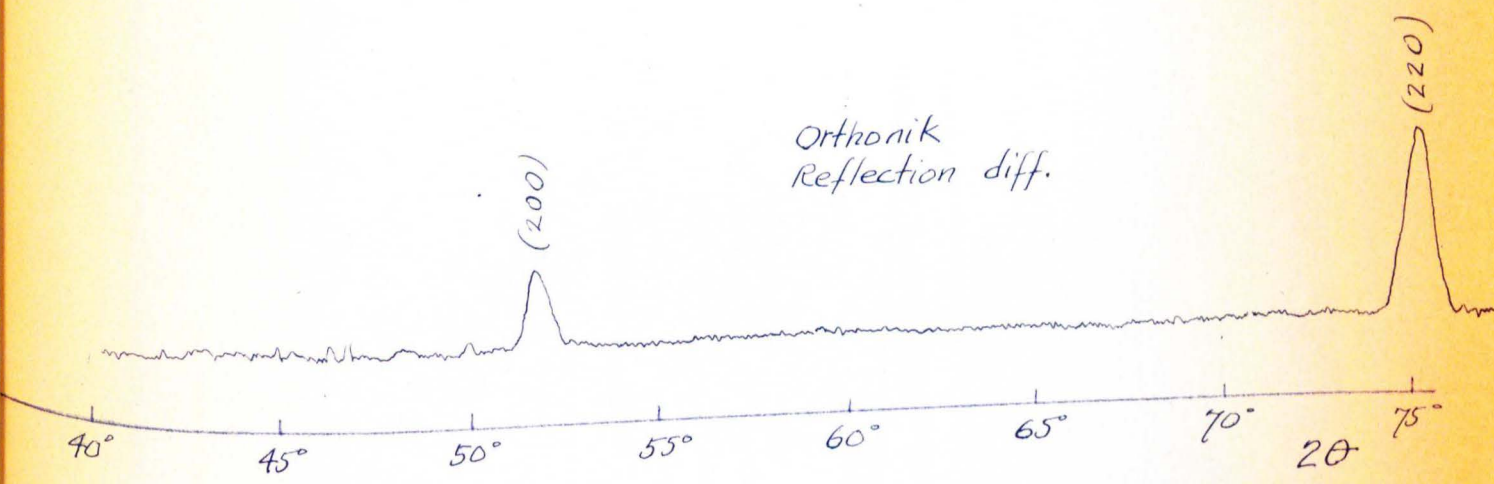
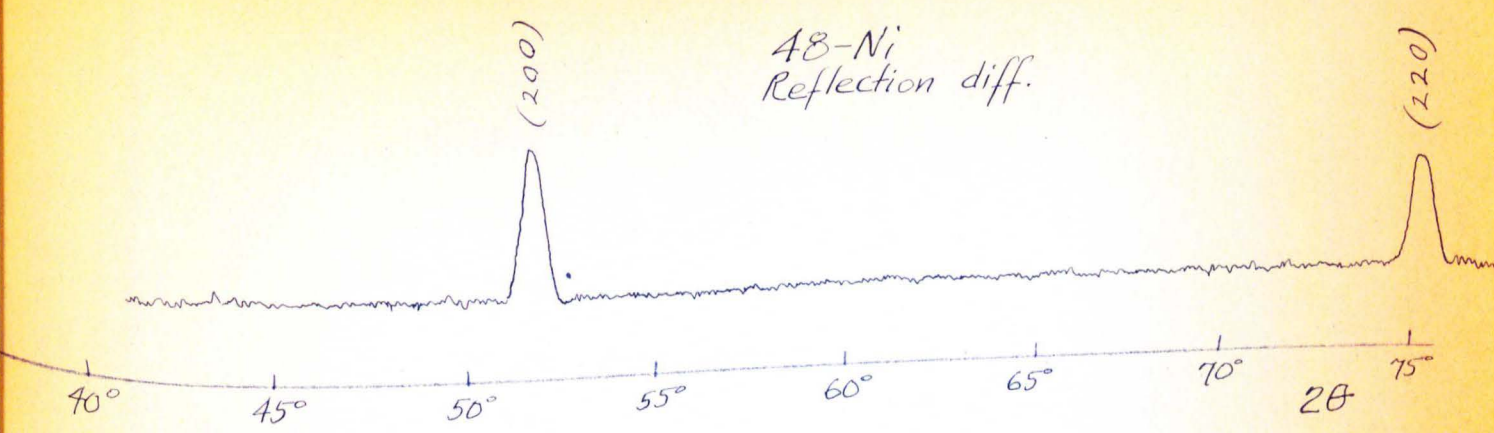


Fig.12. X-Ray Diffraction Patterns of 48-Ni and Orthonik Nickel-Iron Alloys.

NaCl Single Crystal
 Rocking Curve at $2\theta' = 60^\circ$ ($\theta = 13.5^\circ$)

1.0 KW

$$\phi = \phi' - 30^\circ$$

(At $\phi = 0$, angle of incidence
 of neutron beam = angle
 of reflection)

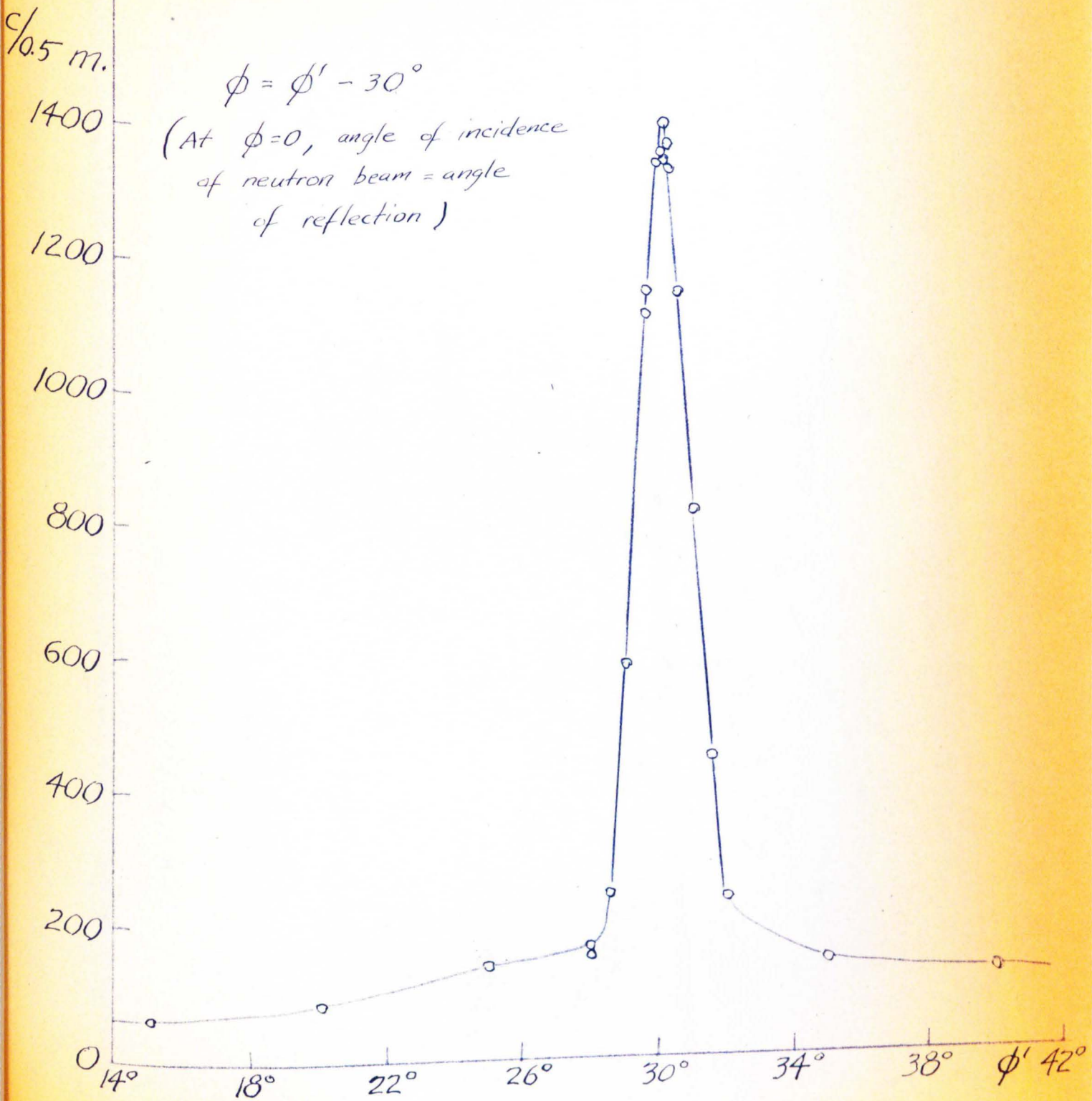
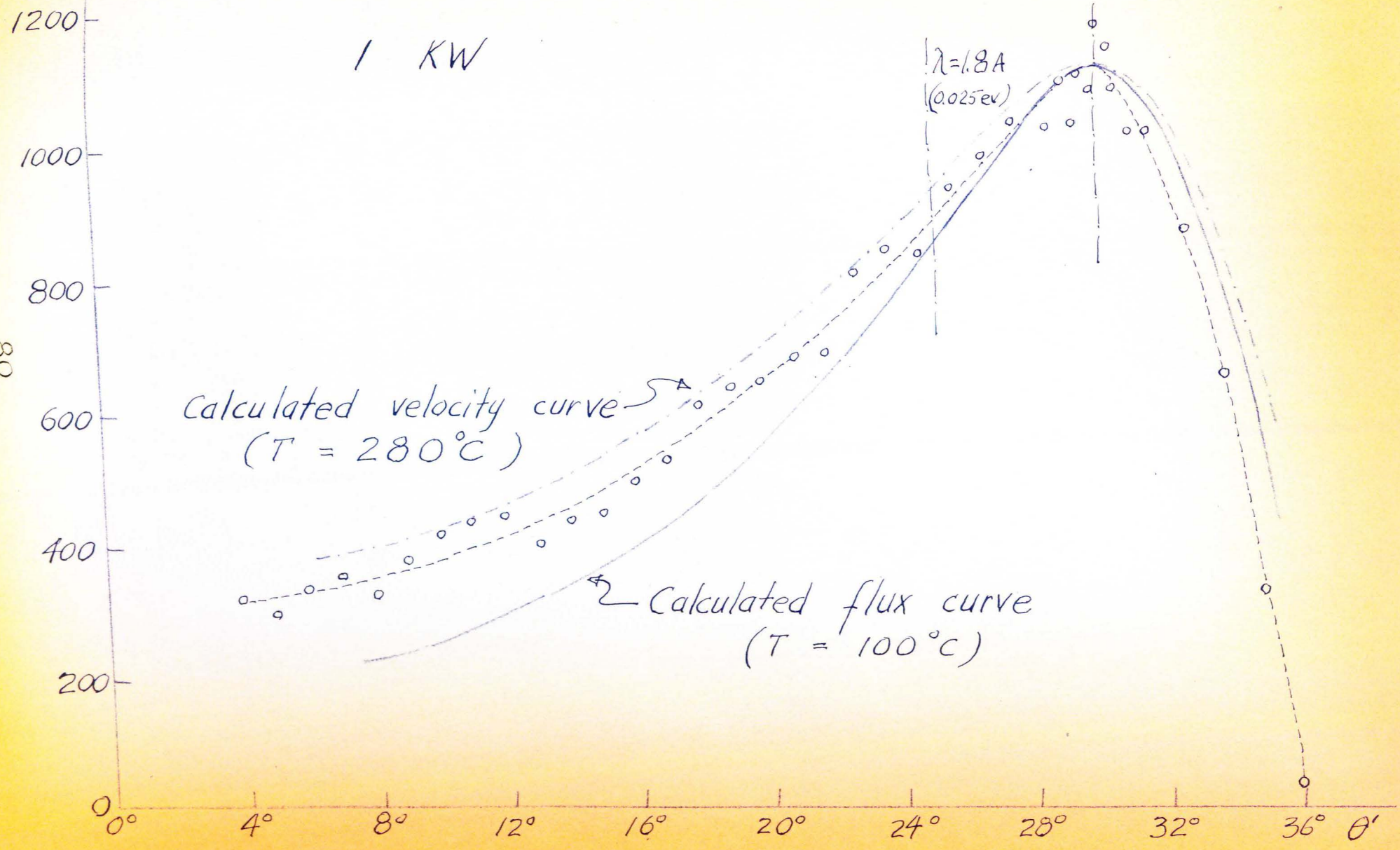


Fig. 13. NaCl Single Crystal Rocking Curve at $2\theta' = 60^\circ$ ($\theta = 13.5^\circ$).

90.5 m

Fig. 14. NaCl Single Crystal
Maxwellian Curve

1 KW



NaCl Single Crystal

Maxwellian Curve

(Calculated curve based on real crystal formula)

Eq. (59)

$c/0.5m.$

1600

1400

1200

1000

800

600

400

200

0 5° 10° 15° 20° 25° 30° 35° θ'

1.0 KW

Calculated curve based on Eq. (59)

$T = 61^\circ$

Fig. 15. NaCl Single Crystal Maxwellian Curve
(Calculated curve based on real crystal formula).

c/0.5 m

M-5, 4 Sheets, C.R.D.

9.0 KW

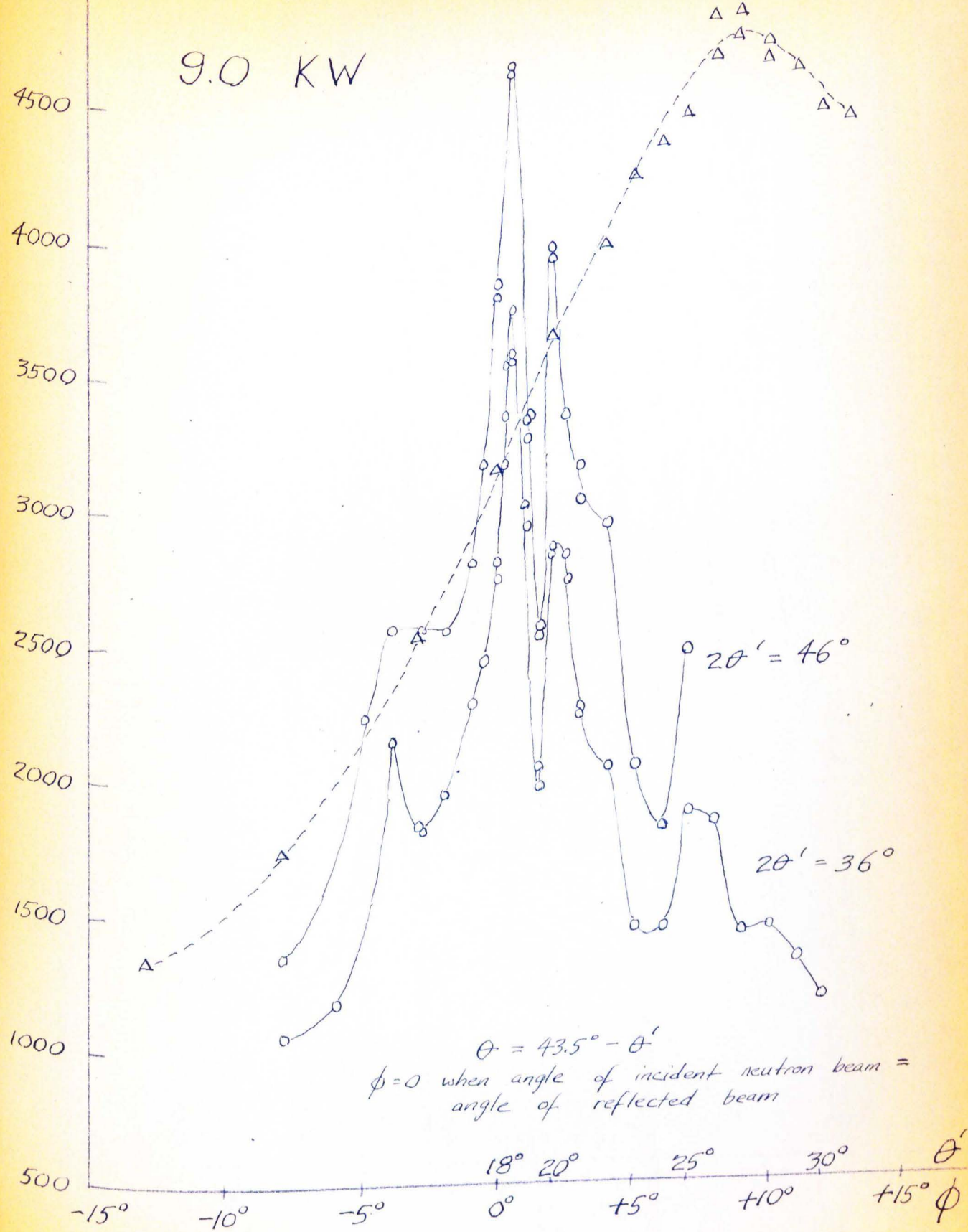


Fig. 16. M-5, 4 Sheets, Cross-Rolling Direction (C.R.D.)

M-5, 4 Sheets, C.R.D.

$$2\theta' = 46^\circ$$

c/0.5m

4500

4000

3500

3000

2500

2000

1500

1000

500

-15°

-10°

-5°

0°

+5°

+10°

ϕ

+15°

5°

10°

15°

20°

25°

30°

35°

ϕ'

Fig. 17, M-5, 4 sheets, C.R.D.

M-5, 4 Sheets, C.R.D.

9.0 KW

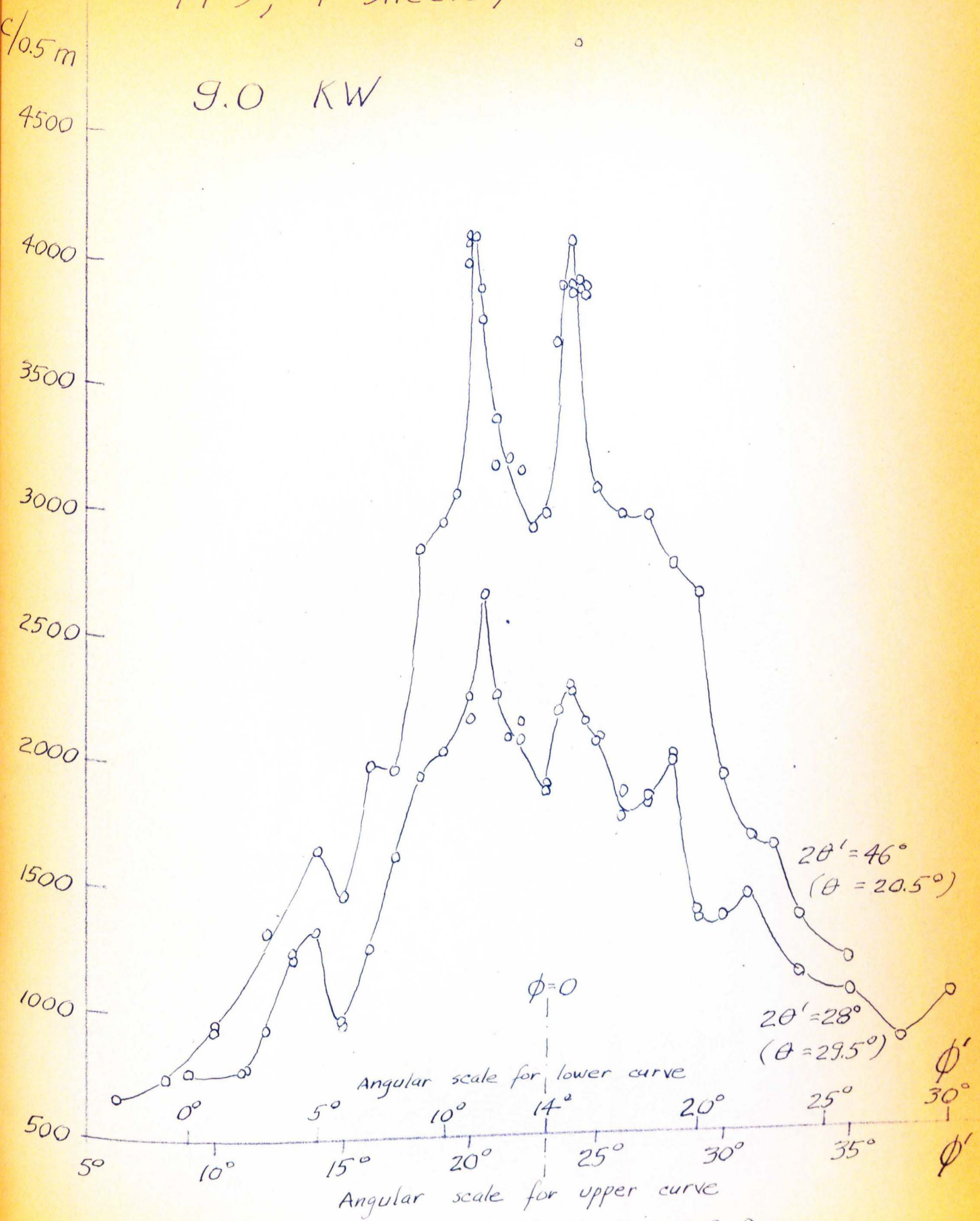


Fig. 18, M-5, 4 Sheets, C.R.D.

M-5, 4 Sheets, R.D.

c/0.5m

9.0 KW
 $2\theta' = 46^\circ$

8000

7000

6000

5000

4000

3000

2000

1000

0 -10° -5° 0° $+5^\circ$ $+10^\circ$ $+15^\circ$ ϕ
 10° 15° 20° 25° 30° 35° 40° ϕ'

Fig. 19. M-5, 4 Sheets, Rolling Direction, (R.D.)

M-5, 4 sheets, 3" X 3"

Rocking Curves, $2\theta' = 46^\circ$

9.0 KW, Reflection Diffraction

c/0.5 m

6000

5000

4000

3000

2000

1000

0

0°

5°

10°

15°

20°

25°

30°

θ'

35°

R.D.

C.R.D.

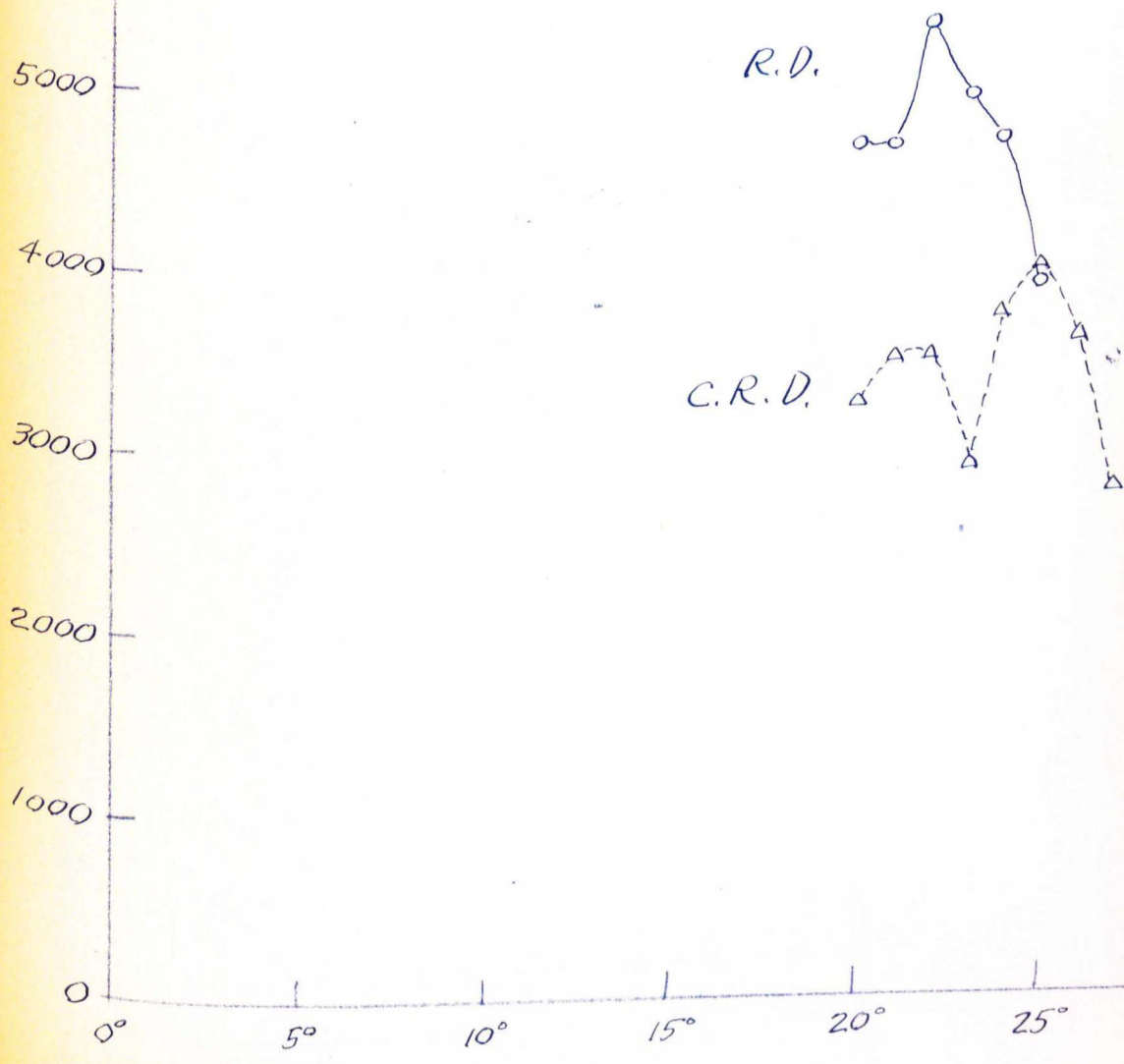


Fig. 20. M-5, 4 Sheets, 3" X 3", Rocking Curves

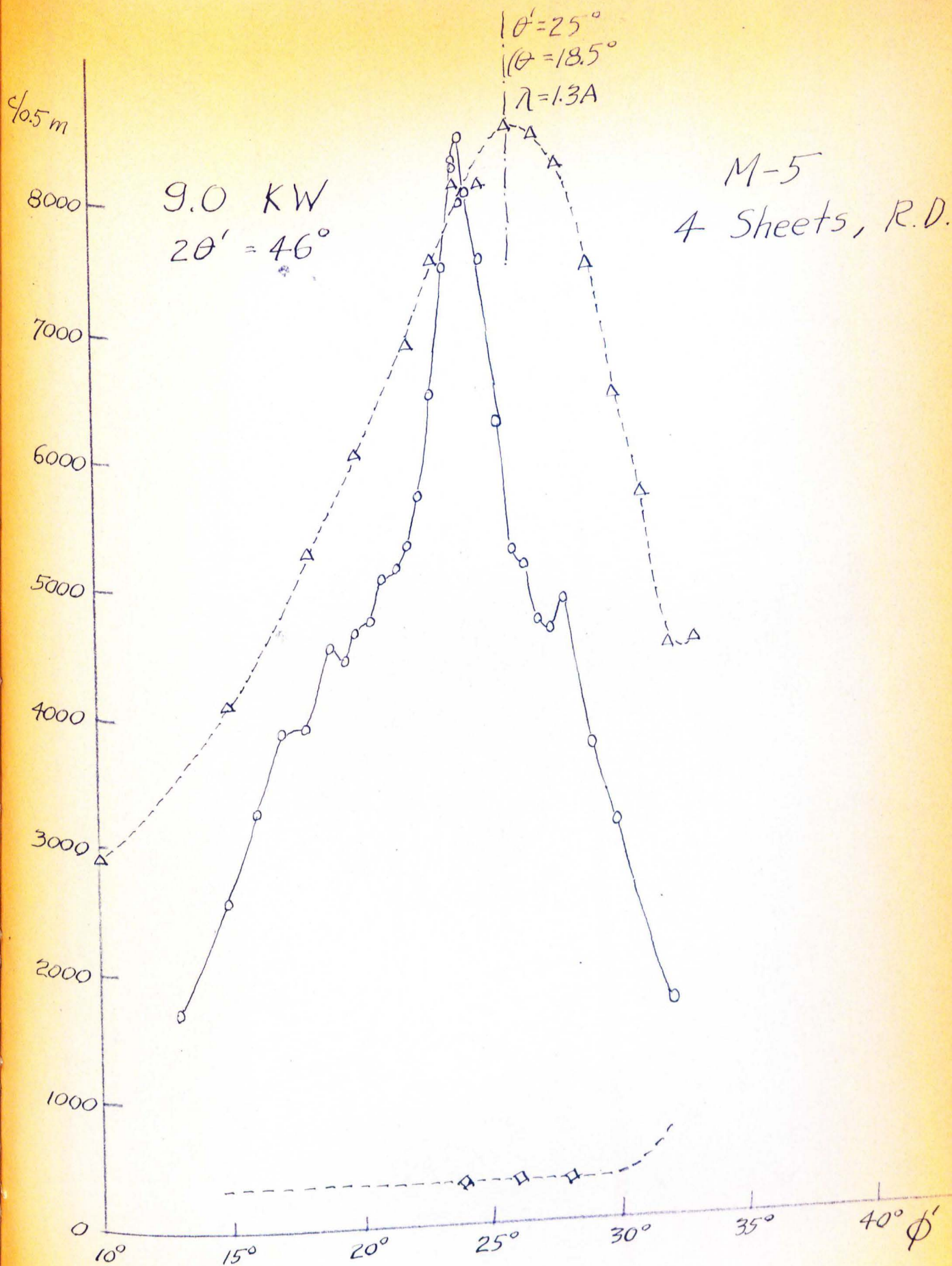


Fig. 21, M-5, 4 Sheets, R.D.

M-5, 1 Sheet, R.D.

$2\theta' = 46^\circ$

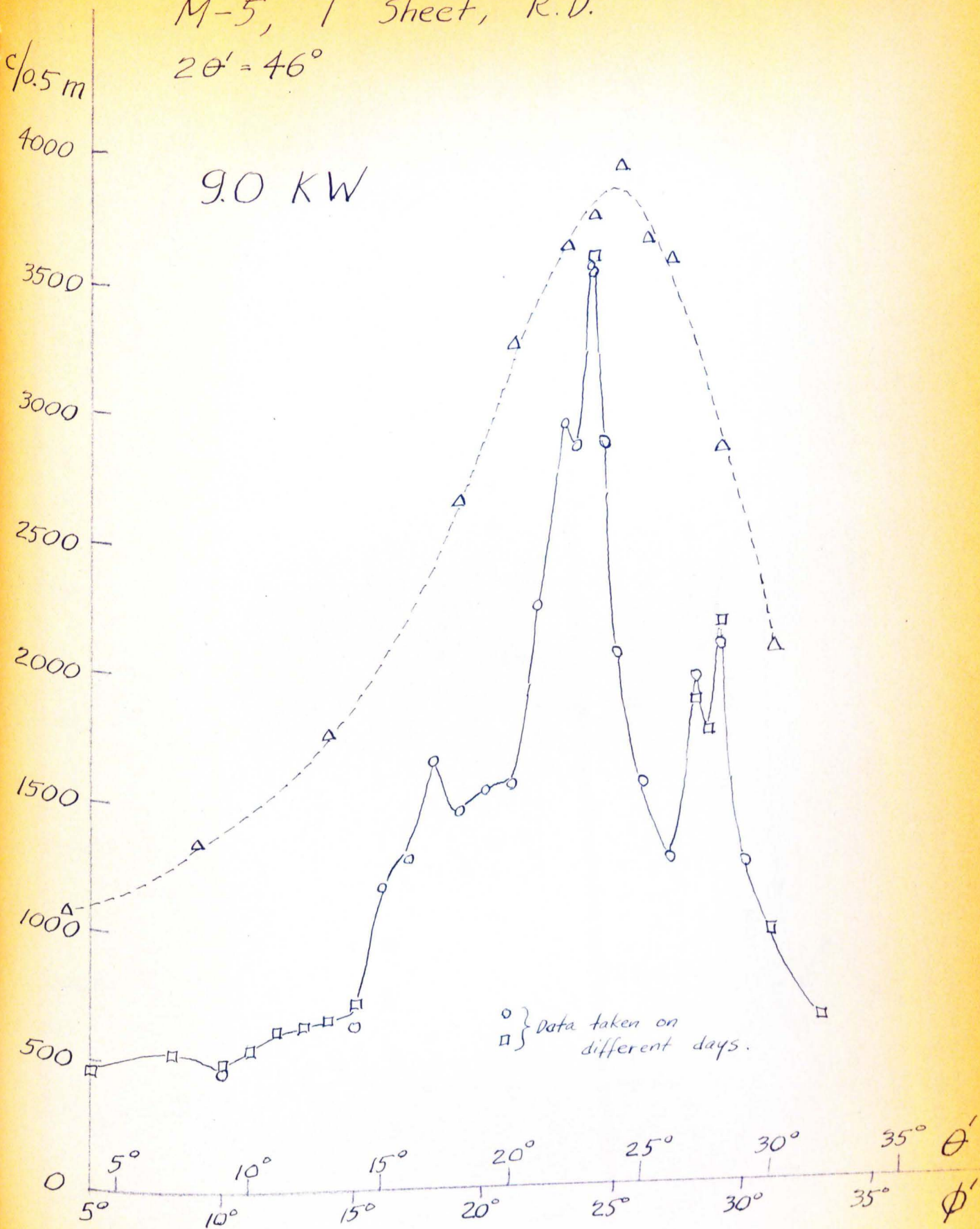


Fig. 22, M-5, 1 Sheet, R.D.

M-5, R.D.
1 & 2 Sheets

$2\theta' = 46^\circ$
9.0 KW

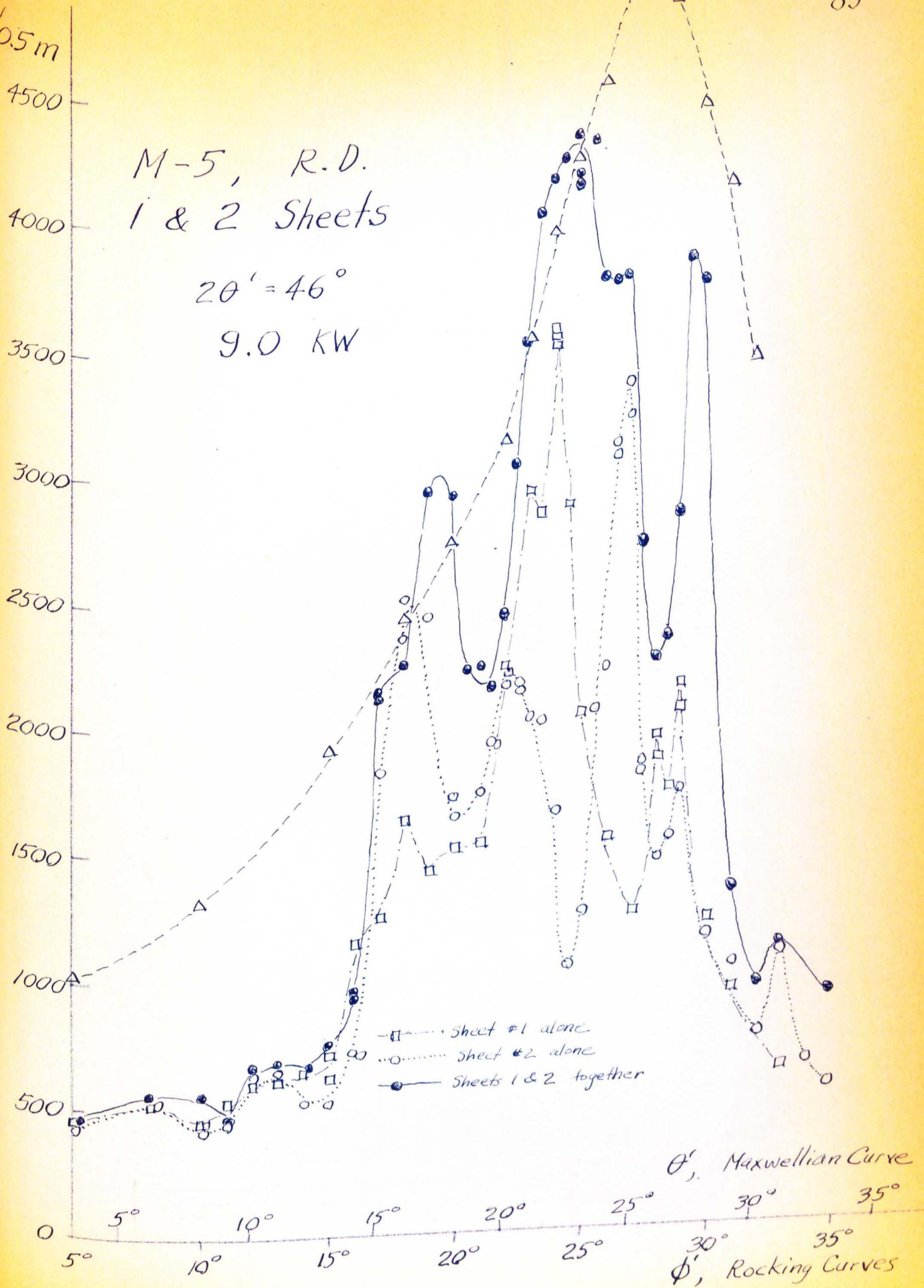


Fig. 23, M-5, 1 & 2 Sheets, R.D.

M-5, 1 & 8 sheets, R. D.
Transmission Diffraction

9.0 KW

$2\theta' = 33^\circ$

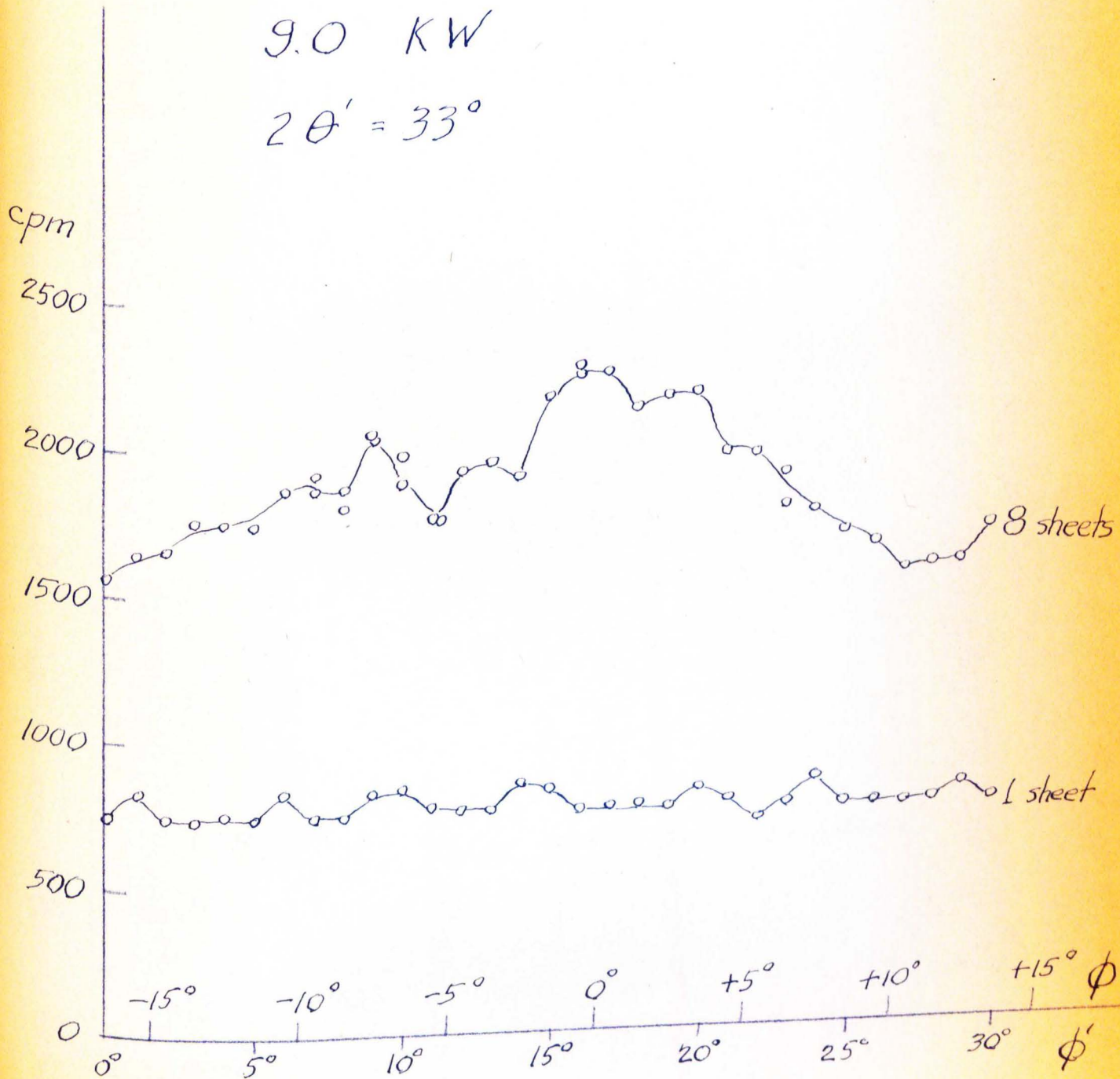


Fig. 24, M-5, 1 & 8 sheets, R. D., Transmission Diffraction

MAXWELLIAN CURVES

M-5, 8 SHEETS, TRANSMISSION DIFFRACTION

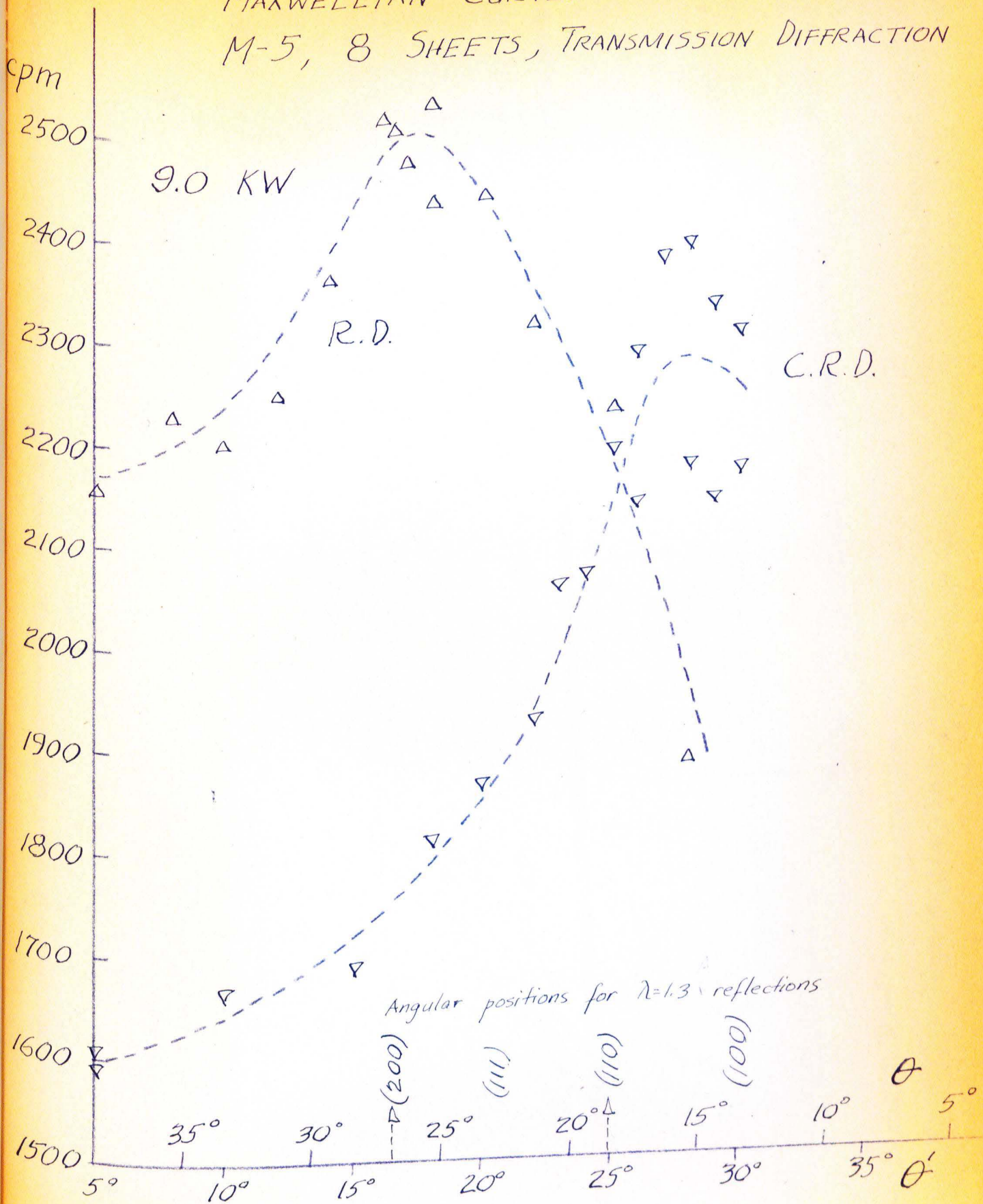


Fig. 25. Maxwellian Curves, M-5, 8 Sheets, Transmission Diffraction

cpm

MAXWELLIAN CURVES
M-5, 8 sheets
Transmission Diffraction

9.0 KW

C.R.D.

2600

2400

2200

2000

1800

1600

1400

1200

1000

800

5°

10°

15°

20°

25°

30°

35°

θ'

R.D.

(Corrected for Geometrical Effect)

Fig. 26. Maxwellian Curves, M-5, 8 Sheets, Transmission Diffraction, Corrected for Geometrical Effect.

M-6, 1 sheet, R.D.

Rocking Curves

9.0 KW

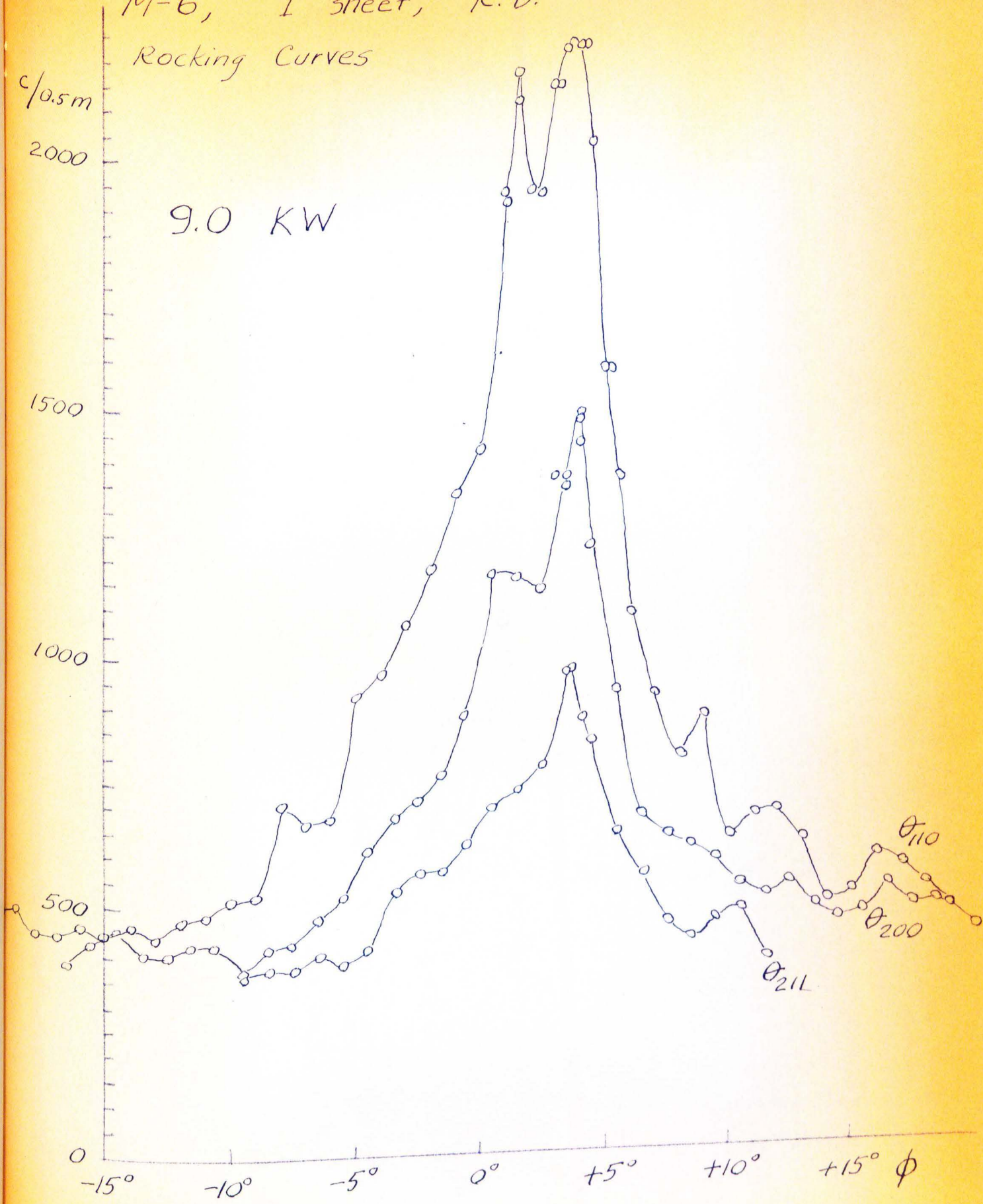


Fig. 27. M-6, 1 sheet, R.D., Rocking Curve.

"LAUE CURVE"

M-6, 1 sheet, R.D.

Reflection Diffraction

9.0 KW

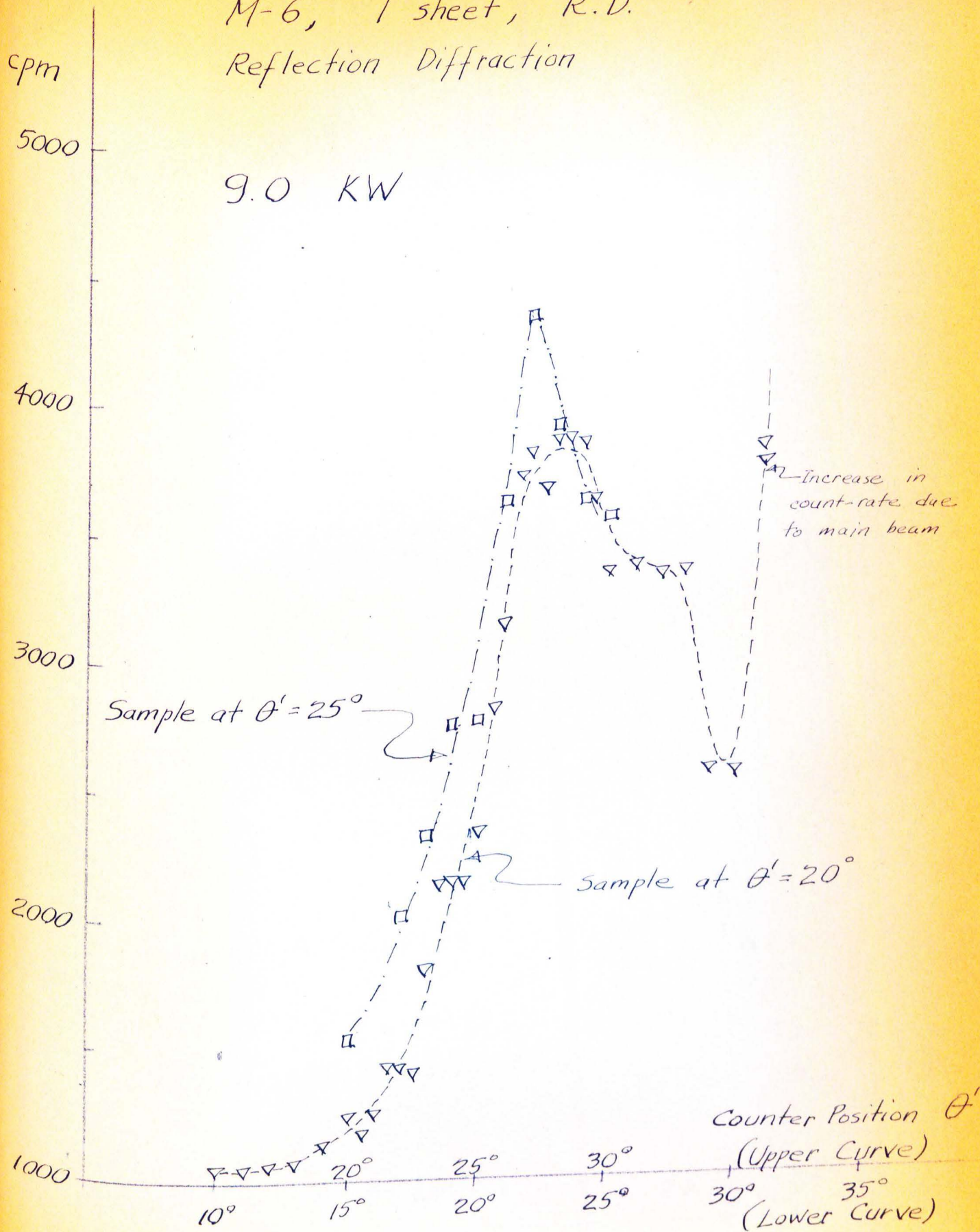


Fig. 28. "Laue Curve," M-6, 1 Sheet, R.D., Reflection Diffraction

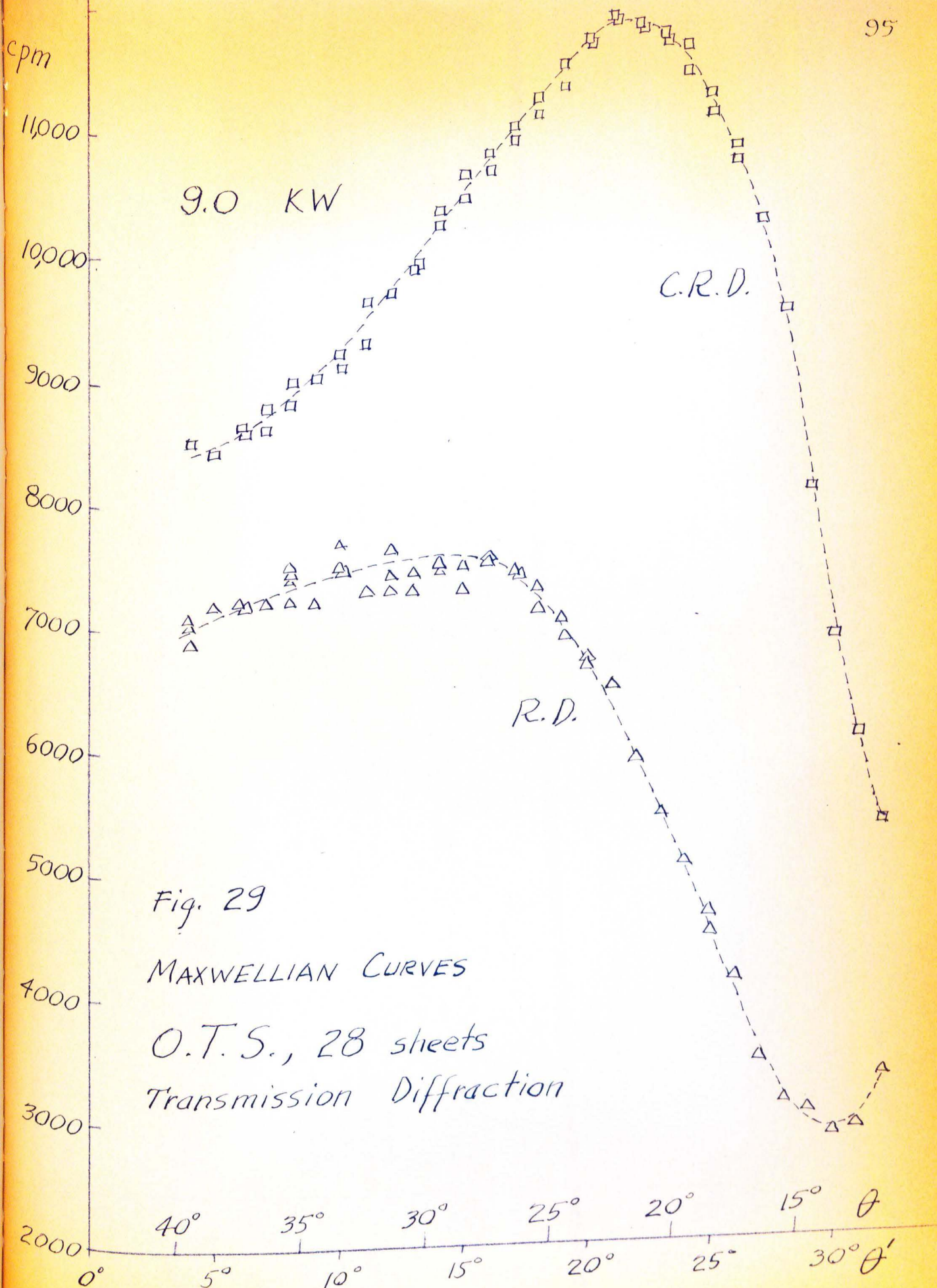


Fig. 29. Maxwellian Curves, OTS, 28 sheets, Transmission Diffraction

$c/2m$

1 Sheet OTS
Reflection Diffraction
MAXWELLIAN CURVES
9.0 KW

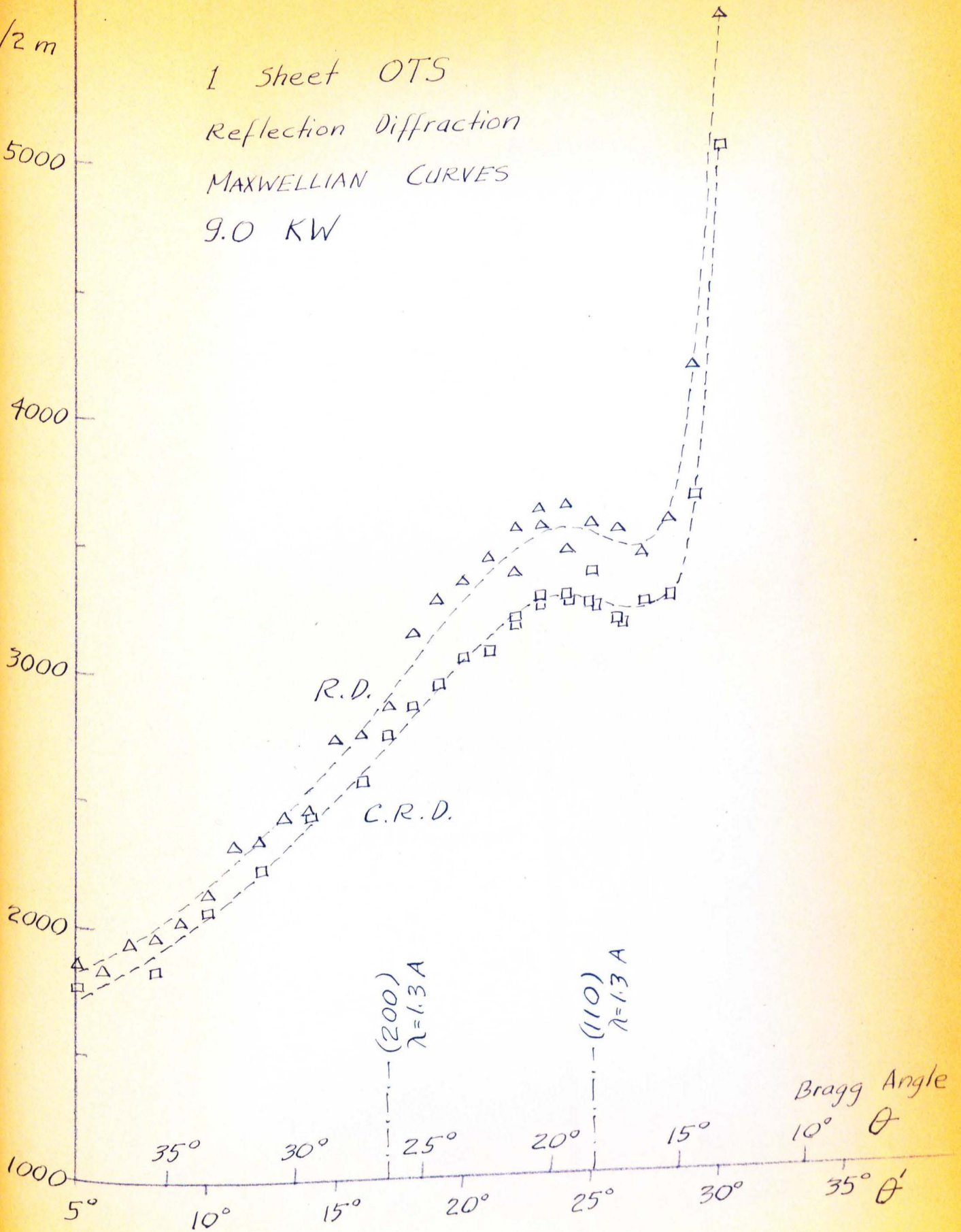


Fig. 30. Maxwellian Curves, 1 Sheet OTS, Reflection Diffraction

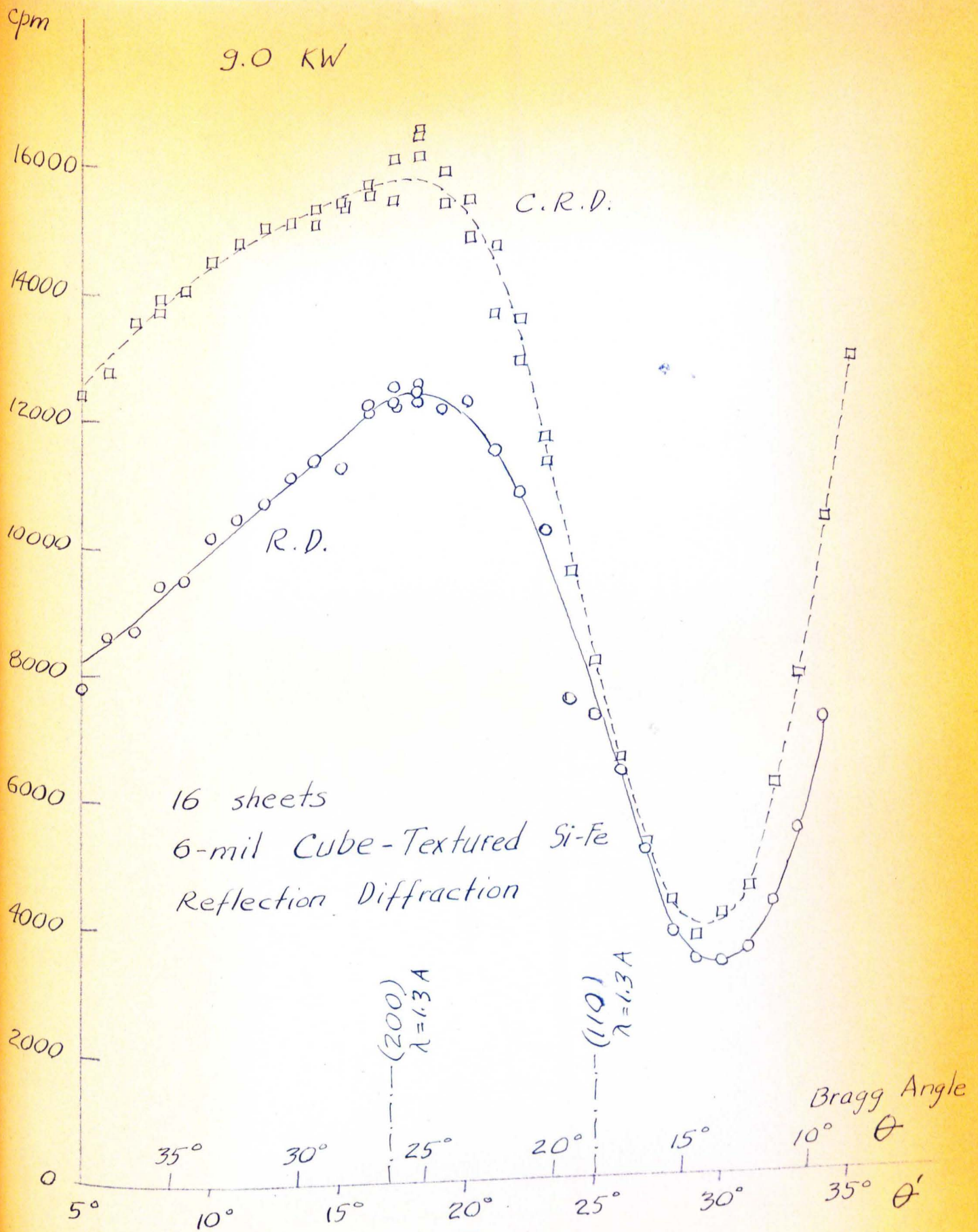


Fig. 31. 16 Sheets, 6-mil Cube-Textured Silicon-Iron, Reflection Diffraction

cpm
18,000

9.0 KW

16 sheets 6-mil
Cube-Textured Si-Fe
Reflection Diffraction
C.R.D.

Rocking Curves at: $2\theta' = 19^\circ$,
 $2\theta' = 33^\circ$,
 $2\theta' = 50^\circ$

or, $\theta_{211} = 34^\circ$

$\theta_{200} = 27^\circ$

$\theta_{110} = 18.5^\circ$

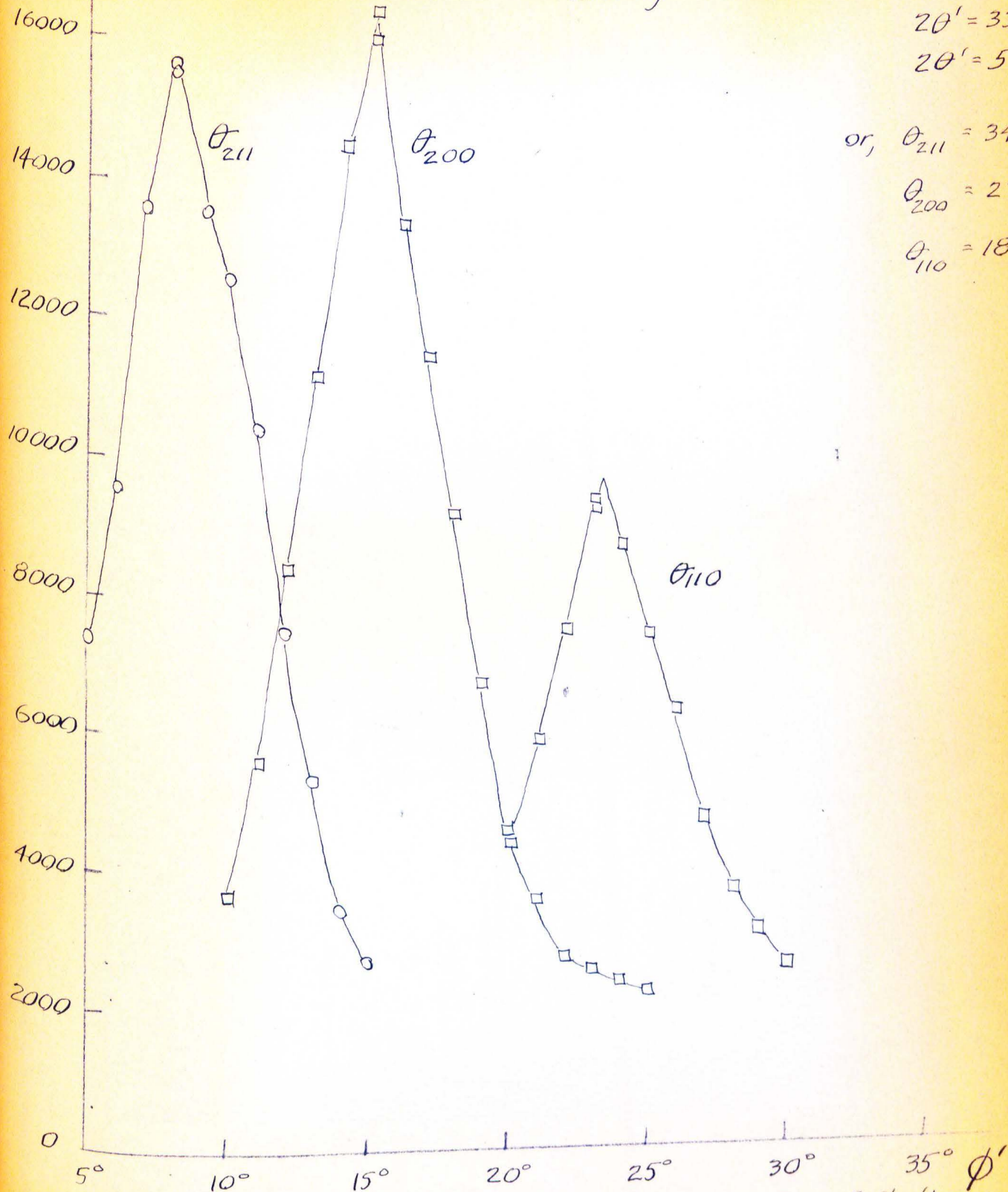


Fig. 32. 16 Sheets, 6-mil Cube-Textured Silicon-Iron, Reflection Diffraction, Rocking curves at $2\theta' = 19^\circ$, 33° , and 50°

cpm

16 sheets 6-mil
Cube - Textured Si-Fe
Transmission Diffraction

c/0.5 m

Maxwellian Curves

9.0 KW

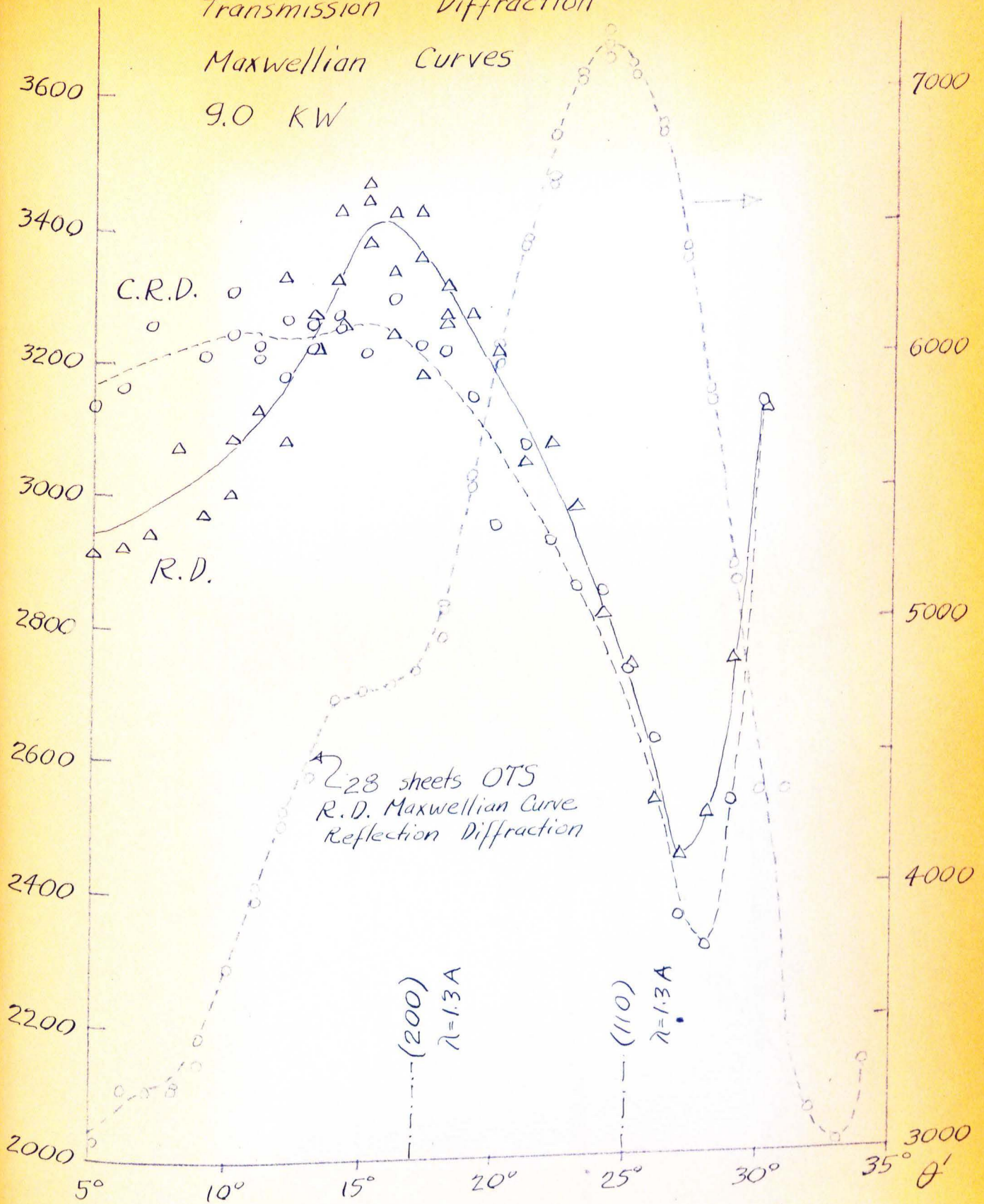
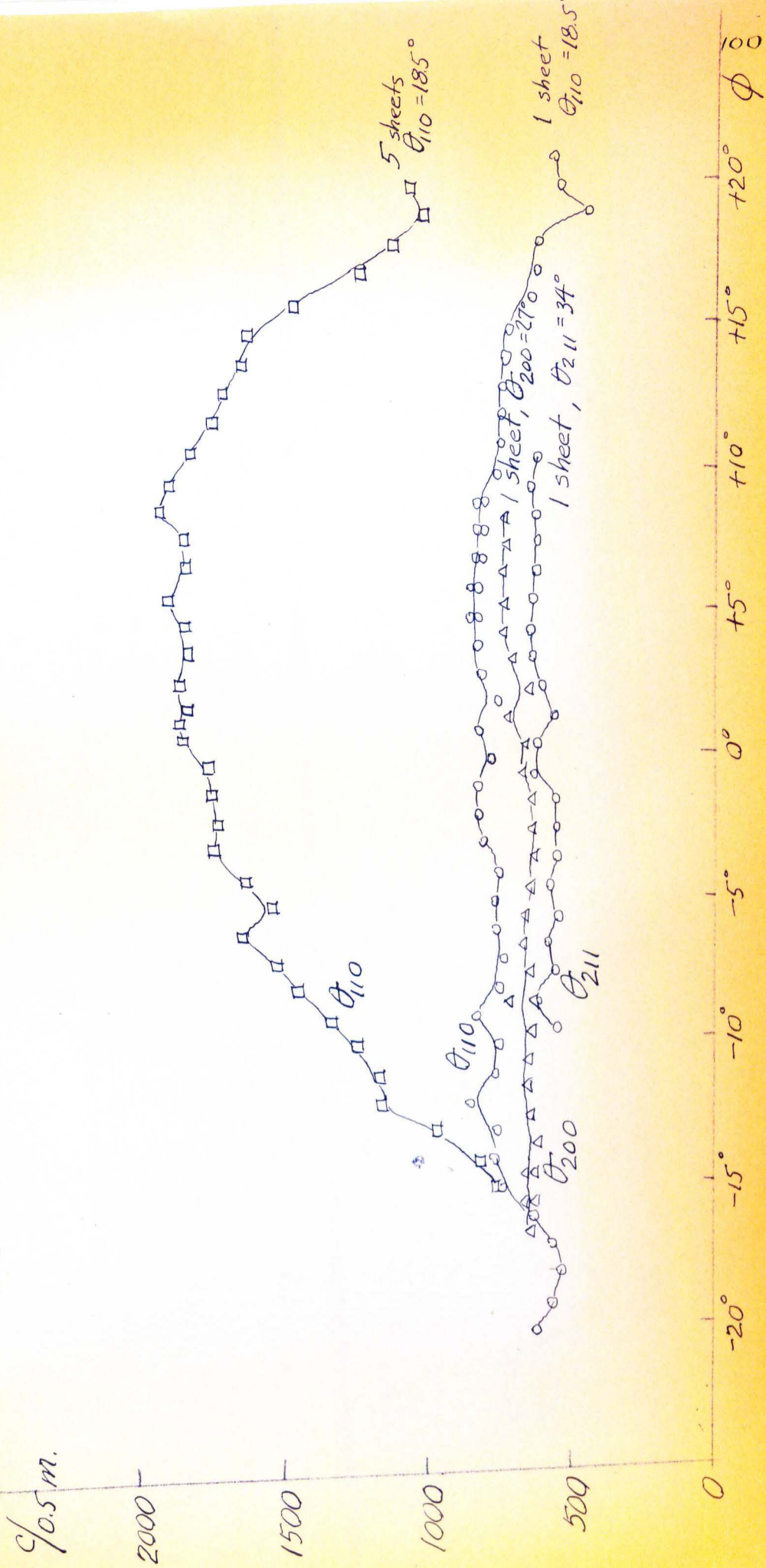


Fig. 33. 16 sheets 6-mil Cube-Textured Silicon-Iron
Transmission Diffraction, Maxwellian Curves

Fig. 34

M-22, 1 & 5 sheets, R.D.
Reflection Diffraction

9.0 KW



MAXWELLIAN CURVES

M-22, 5 sheets; M-19, 5 sheets

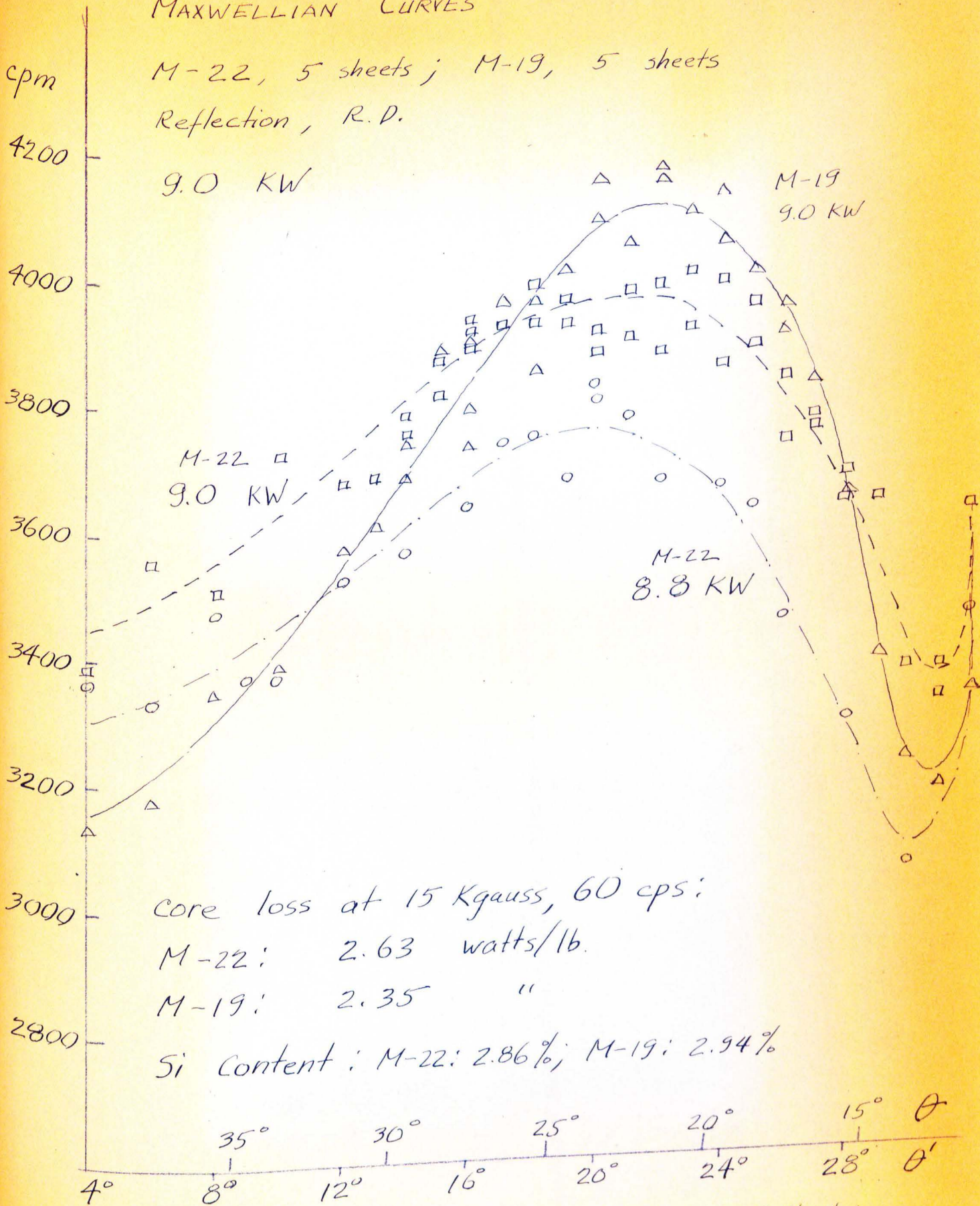
Reflection, R.D.

9.0 KW

M-19
9.0 KW

M-22
9.0 KW

M-22
8.8 KW



core loss at 15 Kgauss, 60 cps:

M-22: 2.63 watts/lb.

M-19: 2.35 "

Si Content: M-22: 2.86%; M-19: 2.94%

Fig. 35. Maxwellian Curves, M-22, 5 sheets; M-19, 5 sheets;
Reflection Diffraction, R.D.

MAXWELLIAN CURVES
 48-Ni & ORTHONIK
 Reflection, R.D.
 9.0 KW

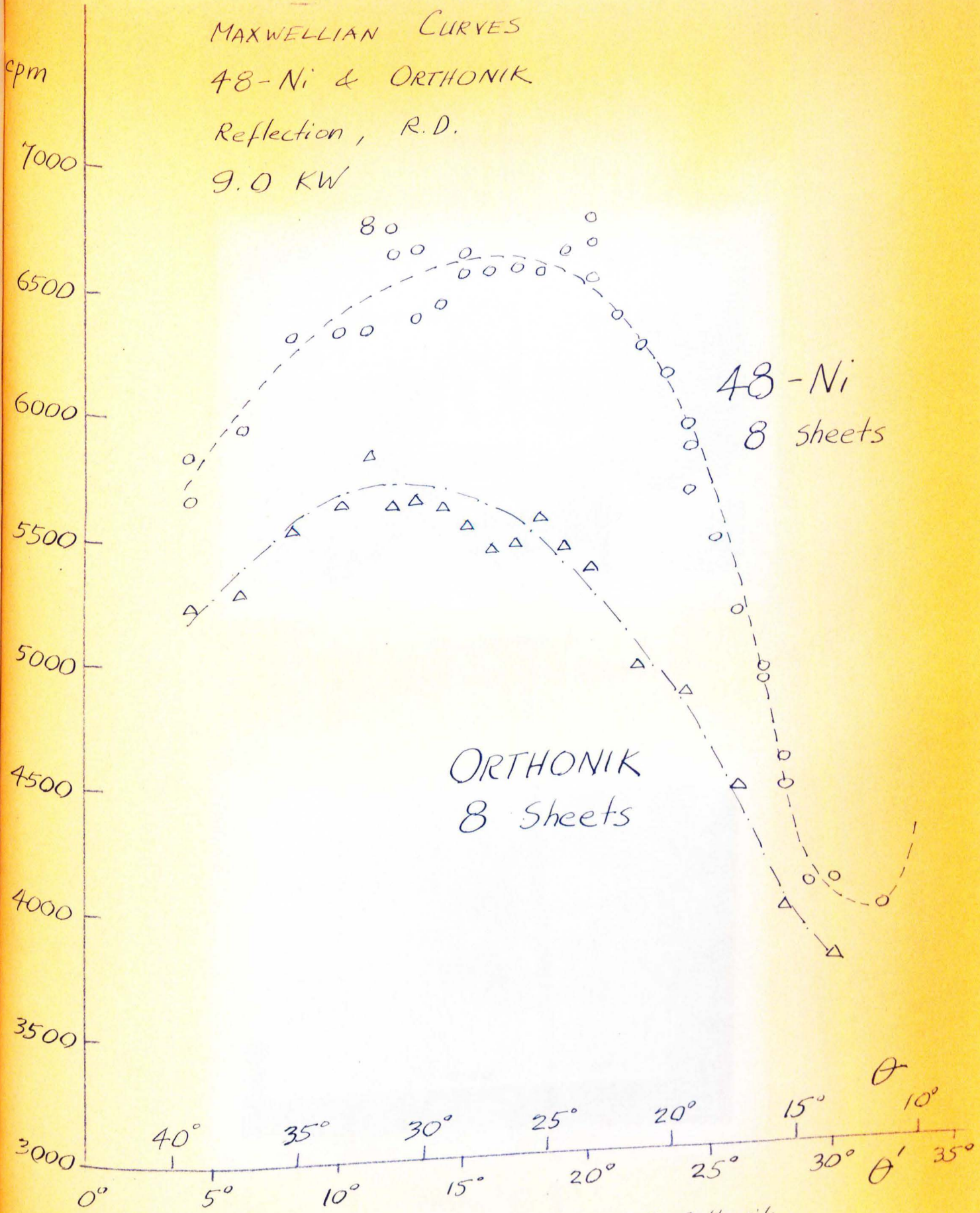


Fig. 36. Maxwellian Curves, 48-Ni & Orthonik
 Reflection Diffraction, R.D.

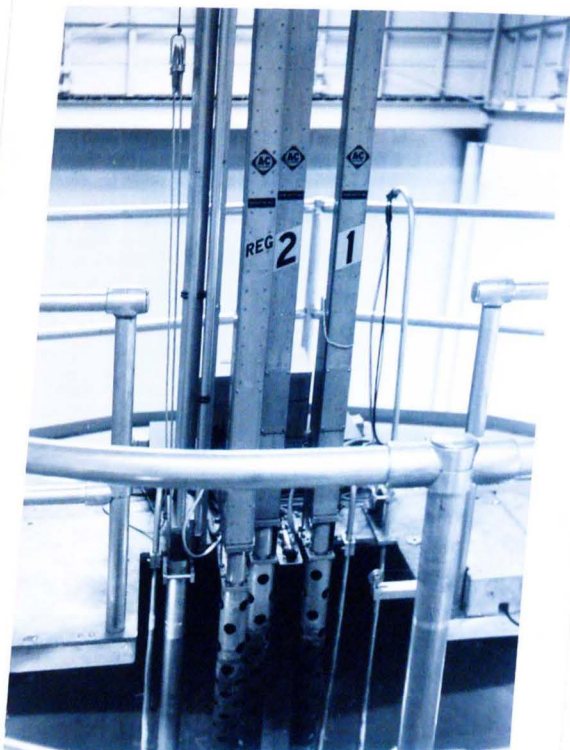
APPENDIX A



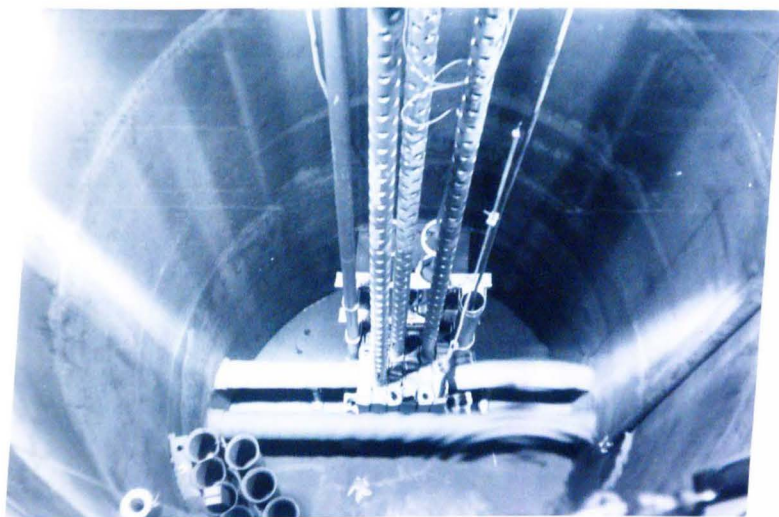
Photograph 1
The Reactor Control Console



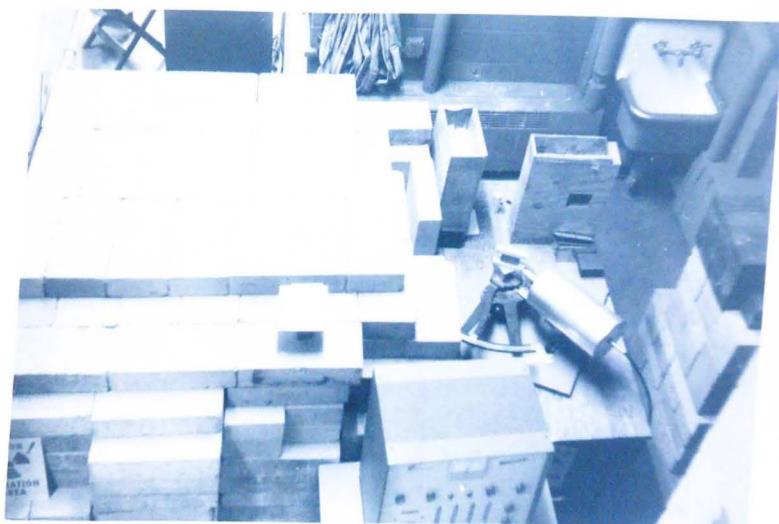
Photograph 2
The University of Maryland Nuclear Reactor



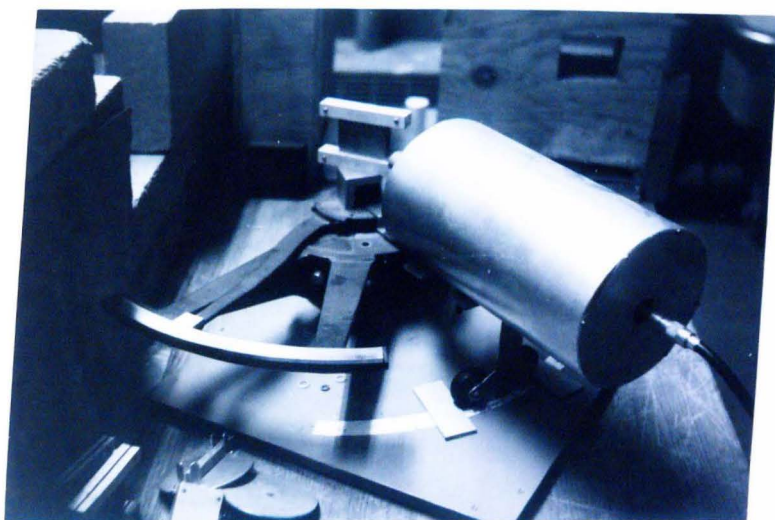
Photograph 3
The Control Rod Drives



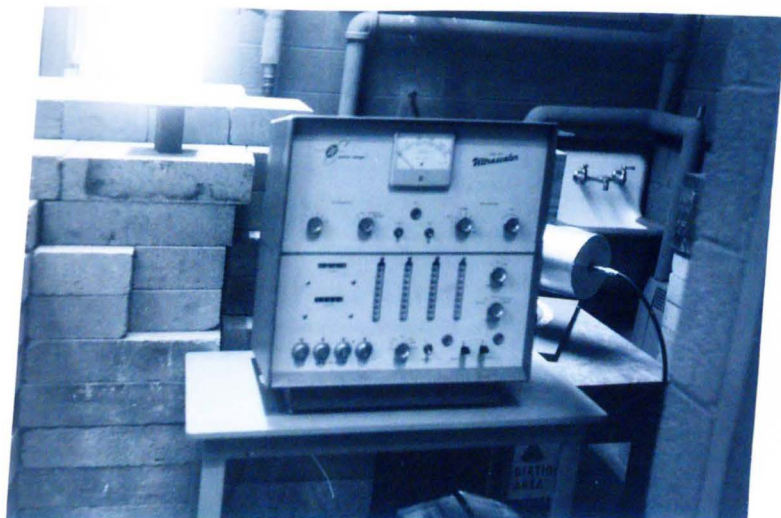
Photograph 4
The Reactor Core



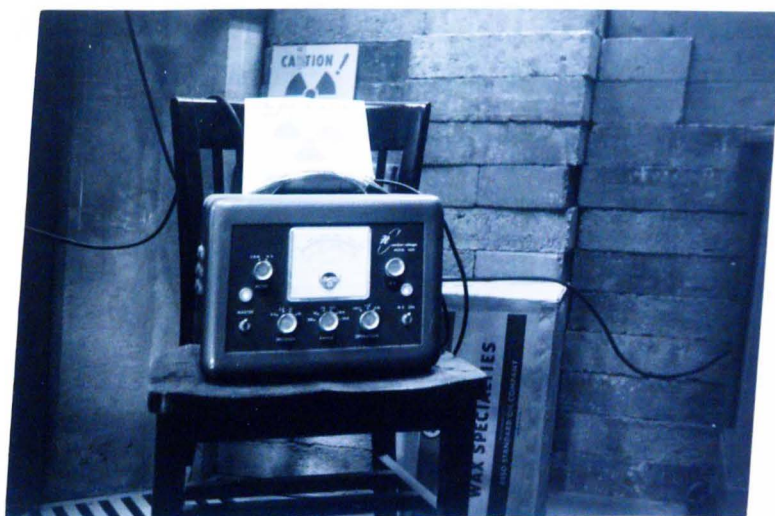
Photograph 5
Concrete-block Shielding and Diffractometer



Photograph 6
The Diffractometer (Goniometer)
Showing BF₃ Detector

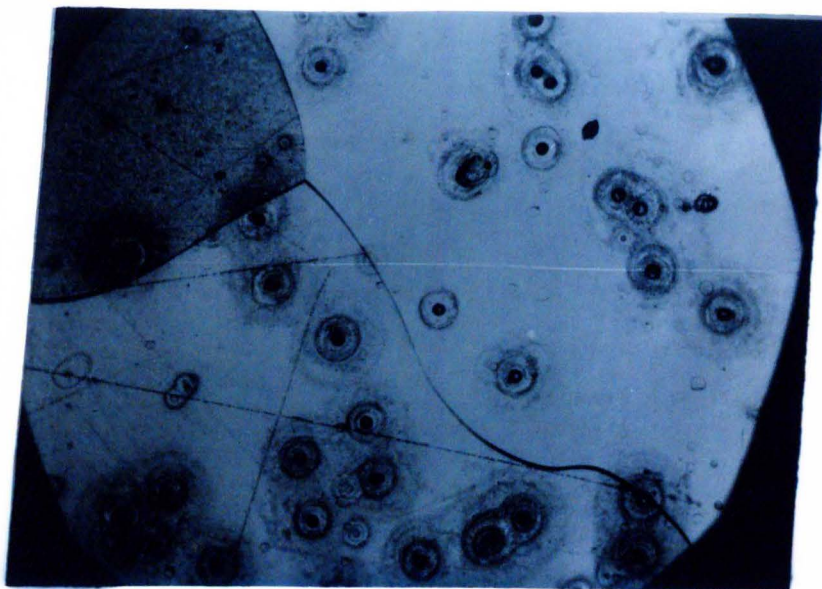


Photograph 7
The Nuclear Chicago Ultrascaler

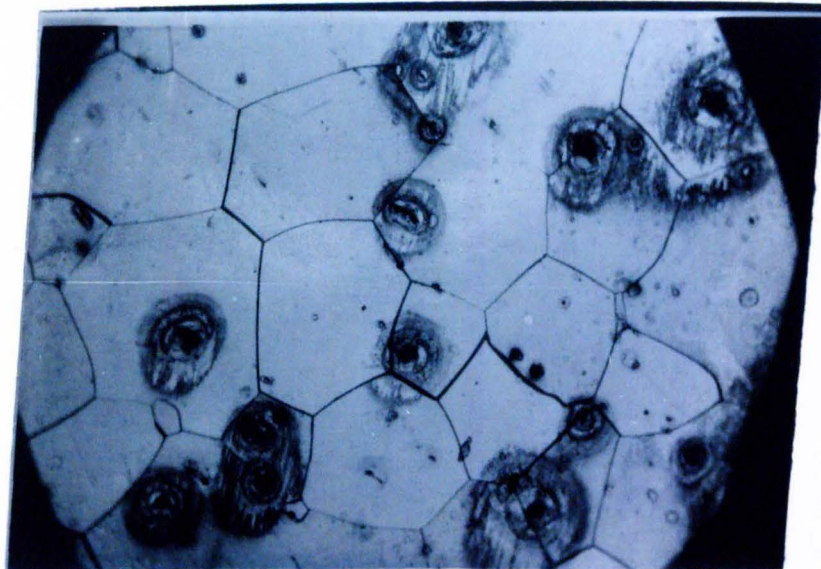


Photograph 8
The Nuclear Chicago Radiation Monitor

APPENDIX B



Photomicrograph 1
M-5, 100X



Photomicrograph 2
M-22, 100X

REFERENCES

1. W. Boas, Physics of Metals and Alloys, John Wiley & Sons, Inc., New York (1947).
2. C. S. Barrett, Structure of Metals, 2nd Ed., McGraw-Hill Book Co., Inc., New York (1952).
3. D. P. Mitchell and P. N. Powers, Phys. Rev., 50, 486 (1936).
4. J. R. Dunning, G. B. Pegram, F. A. Fink, D. P. Whitehall, and E. Segre, Phys. Rev., 48, 704 (1935).
5. O. Halpern, M. Hamermesh, and M. H. Johnson, Phys. Rev., 59, 981 (1941).
6. M. D. Whitaker and H. G. Beyer, Phys. Rev., 55, 1101 (1939).
7. M. D. Whitaker and H. G. Beyer, Phys. Rev., 57, 976 (1940).
8. F. C. Nix, H. G. Beyer, and J. R. Dunning, Phys. Rev., 58, 1036 (1940).
9. F. C. Nix and G. F. Clement, Phys. Rev., 68, 159 (1945).
10. W. H. Zinn, Phys. Rev., 71, 752 (1947).
11. M. L. Goldberger and F. Seitz, Phys. Rev., 71, 294 (1947).
12. W. J. Sturm, Phys. Rev., 71, 757 (1947).
13. E. Fermi and L. Marshall, Phys. Rev., 71, 666 (1947).
14. D. J. Hughes, Neutron Optics, Interscience Publishers, Inc., New York (1954).
15. E. Fermi, W. J. Sturm, and R. G. Sachs, Phys. Rev., 71, 589 (1947).
16. C. G. Schull and E. O. Wollan, Phys. Rev., 81, 527 (1951).

17. R. D. Lowde, *Nature*, 167, 243 (1951).
18. G. E. Bacon and R. D. Lowde, *Acta Cryst.*, 1, 303 (1948).
19. E. O. Wollan and C. G. Schull, *Proc. Int. Conf. Peaceful Uses of Atomic Energy*, 2, 66 (1955).
20. A. W. McReynolds, *Proc. Int. Conf. Peaceful Uses of Atomic Energy*, 2, 93 (1955).
21. S. S. Sidhu, L. Heaton, and M. H. Mueller, *Proc. 2nd U. N. Int. Conf. Peaceful Uses of Atomic Energy*, 14, 212 (1958).
22. J. M. Hastings, N. Elliott, L. M. Corliss, and W. C. Hamilton, *Proc. 2nd U. N. Int. Conf. Peaceful Uses of Atomic Energy*, 14, 228 (1958).
23. J. Laniesse, P. Meriel, and M. Englander, *J. Nuclear Materials*, 2, 69 (1960).
24. E. Gumlich, *Trans. Faraday Soc.*, 8, 98 (1912).
25. N. P. Goss, *Trans. Am. Soc. Metals*, 23, 511 (1935).
26. W. E. Ruder, *Trans. Am. Soc. Metals*, 23, 533 (1935).
27. R. M. Bozorth, *Trans. Am. Soc. Metals*, 23, 1107 (1935).
28. J. T. Burwell, *Trans. AIME*, 140, 353 (1940).
29. B. F. Decker and D. Harker, *J. Applied Physics*, 22, 900 (1951).
30. C. G. Dunn, *Acta Met.*, 1, 163 (1953).
31. J. E. May and D. Turnbull, *Trans. AIME*, 212, 769 (1958).
32. E. V. Walker and J. Howard, *J. Iron & Steel Inst.*, 194, 96 (1960).
33. W. Morrill, *Metal Progress*, 78, 84 (1960).
34. J. L. Walter and W. R. Hibbard, Jr., *Trans. AIME*, 212, 731 (1958).
35. R. M. Bozorth, *Rev. Modern Physics*, 19, 29 (1947).

36. H. J. Williams, *Phys. Rev.*, 52, 747 (1937).
37. The International Nickel Co., Inc., Nickel Alloy Steels, 2nd Ed., N. Y., N. Y. (1947).
38. G. Sachs and J. Spretnak, *Trans. AIME*, 140, 359 (1940).
39. W. S. Spring, *Iron Age*, 163, 70 (March 31, 1949).
40. W. E. Seymour and D. Harker, *Trans. AIME*, 188, 1001 (1950).
41. M. F. Littman, *Communications and Electronics*, 1, 220 (1952).
42. M. F. Littmann, *J. Metals*, 8, 593 (1956).
43. G. Phragmen, *J. Iron & Steel Inst.*, 123, 465 (1931).
44. A. J. Bradley, A. H. Jay, and A. Taylor, *Phil. Mag.*, 23, 545 (1937).
45. E. S. Greiner, J. S. Marsh, and B. Stoughton, The Alloys of Iron and Silicon, McGraw-Hill Book Co., New York and London (1933).
46. A. L. Sutton and W. Hume-Rothery, *Phil. Mag.*, 46, 1295 (1955).
47. A. H. Compton and S. K. Allison, X-Rays in Theory and Experiment, 2nd Ed., D. Van Nostrand Co., Inc., Princeton, N. J. (1935).
48. W. H. Zachariasen, Theory of X-Ray Diffraction in Crystals, John Wiley & Sons, Inc., N. Y., Chapman & Hall, Ltd., London (1945).
49. D. J. Hughes, Pile Neutron Research, Addison-Wesley Publishing Co., Inc. (1953).
50. G. E. Bacon and J. Thewlis, *Proc. Roy. Soc. London, Series A*, 196, 50 (1949).
51. C. G. Darwin, *Phil. Mag.*, 43, 800 (1922).
52. M. J. Buerger, Crystal-structure Analysis, John Wiley & Sons, Inc., New York (1960).

53. G. E. Bacon, Neutron Diffraction, 2nd Ed., Oxford (1962).
54. W. W. Gerken, "Measurement of neutron Energy Effects Using Multiple Threshold Detectors," Ph. D. Thesis, University of Maryland (1963).
55. J. O. Cermak, "Indium Foil Determination of the Thermal Neutron Flux Distribution in the University of Maryland Swimming Pool Reactor," Master's Thesis, University of Maryland (1962).
56. Allis-Chalmers Manufacturing Co., "Initial Criticality and Full-power Operation of the University of Maryland Reactor," Washington, D. C., (April, 1961).
57. W. J. Price, Nuclear Radiation Detection, McGraw-Hill Book Co., Inc., N. Y. (1958).
58. W. L. Bragg, C. G. Darwin, R. W. James, Phil. Mag., 1, 897 (1926).
59. K. Lonsdale, Crystals and X-Rays, D. Van Nostrand Co., Inc., New York (1949).
60. G. W. Wiener and K. Detert, J. Metals, 10, 507 (1958).
61. J. L. Walter, W. R. Hibbard, Jr., H. C. Fiedler, H. E. Grenoble, R. H. Pry, and P. G. Frischmann, J. Metals, 10, 509 (1958).
62. J. L. Walter, W. R. Hibbard, H. C. Fiedler, H. E. Grenoble, R. H. Pry, and P. G. Frischmann, J. Appl. Physics., 29, 363 (1958).
63. G. Wiener, P. A. Albert, R. H. Trapp, and M. F. Littmann, J. Appl. Phys., 29, 366 (1958).
64. B. F. Decker, E. T. Asp, and D. Harker, J. Appl. Phys., 19, 388 (1948).

VITA

Name: Manuel Romulo Eugenio

Permanent Address: 2570 Bautista St., Singalong Subdivision
Manila, Philippines

Degree and date to be conferred: Ph. D., 1963

Date of birth: June 10, 1929

Place of birth: Tarlac, Philippines

Secondary education: De La Salle High School, Manila,
Philippines
March, 1946

| Collegiate institutions attended | Date | Degree | Date of Degree |
|----------------------------------|---------|-----------|----------------|
| Mapua Institute of Technology | 1946-47 | - | - |
| University of the Philippines | 1947-51 | B. S. | April 1951 |
| De La Salle College | 1951-53 | B.S.Ch.E. | March 1953 |
| Oklahoma State University | 1955-56 | M. S. | June 1959 |

Major: Nuclear Engineering

Minor: Chemical Engineering

Publications:

1. "The Effect of Pulsation on Liquid-Liquid Mass-Transfer resistances," ANL-5874 (1958).
2. P. G. Afable, C. Nuguid, and M. Eugenio, " The Prospects for Nuclear Power in the Philippines," World Power Conf., Madrid (1959).

Positions held:

1. Chemist, Philippine Refining Co., Manila, Philippines (1953-55)
2. Resident Student Associate, Argonne National Lab., Argonne, Ill. (1956-57)
3. Scientist, Philippine Atomic Energy Commission, Manila, Philippines (1958-)